UNIVERSIDADE ESTADUAL PAULISTA
"JÚLIO DE MESQUITA FILHO"
Campus de Ilha Solteira

SÃO PAULO STATE UNIVERSITY "JÚLIO DE MESQUITA FILHO"

FACULTY OF ENGINEERING
ILHA SOLTEIRA CAMPUS

VIVIANE CASSOL MARQUES

AN INVESTIGATION INTO WAYS OF SUBSTRUCTURING FOR A VIBRATORY SYSTEM WITH RUBBER ISOLATORS

Ilha Solteira
2017

UNIVERSIDADE ESTADUAL PAULISTA
"JÚLIO DE MESQUITA FILHO"
Campus de Ilha Solteira

VIVIANE CASSOL MARQUES

AN INVESTIGATION INTO WAYS OF SUBSTRUCTURING FOR A VIBRATORY SYSTEM WITH RUBBER ISOLATORS

Thesis presented to the Faculty of Engineering - UNESP - Ilha Solteira, to obtain the title of Doctor of Mechanical Engineering.

Knowledge area: Solid Mechanics

Prof. Dr. Michael John Brennan
Orientator

Ilha Solteira
2017

FICHA CATALOGRÁFICA
Desenvolvido pelo Serviço Técnico de Biblioteca e Documentação

M357i

Marques, Viviane Cassol.
An investigation into ways of substructuring for a vibratory system with rubber isolators / Viviane Cassol Marques. -- Ilha Solteira: [s.n.], 2017
121 f. : il.

Tese (doutorado) - Universidade Estadual Paulista. Faculdade de Engenharia de Ilha Solteira. Área de conhecimento: Solid Mechanics, 2017

Orientador: Michael John Brennan
Inclui bibliografia

1. Substruração. 2. Amortecedor de borracha. 3. Mobilidades.

UNIVERSIDADE ESTADUAL PAULISTA

Câmpus de Ilha Solteira

CERTIFICADO DE APROVAÇÃO

TÍTULO DA TESE: An investigation into ways of substructuring for a vibratory system with rubber isolators

AUTORA: VIVIANE CASSOL MARQUES
ORIENTADOR: MICHAEL JOHN BRENNAN

Aprovada como parte das exigências para obtenção do Título de Doutora em ENGENHARIA MECÂNICA, área: MECANICA DOS SÓLIDOS pela Comissão Examinadora:

Prof. Dr. MICHAEL JOHN BRENNAN
Departamento de Engenharia Mecânica / Faculdade de Engenharia de Ilha Solteira

Prof. Dr. AMARILDO TABONE PASCHOALINI
Departamento de Engenharia Mecânica / Faculdade de Engenharia de Ilha Solteira

Prof. Dr. JOÃO ANTONIO PEREIRA
Departamento de Engenharia Mecânica / Faculdade de Engenharia de Ilha Solteira

Prof. Dr. ARCANJO LENZI
Engenharia Mecânica / Universidade Federal de Santa Catarina

DOUTOR LEOPOLDO PISANELLI RODRIGUES DE OLIVEIRA
Departamento de Engenharia Mecânica / ESCOLA DE ENGENHARIA DE SÃO CARLOS-USP

Ilha Solteira, 12 de dezembro de 2017

”Das Utopias

Se as coisas são inatingíveis... Ora!
Não é motivo para não querê-las...
Que tristes os caminhos, se não fora
A presença distante das estrelas!”

Mário Quintana

ACKNOWLEDGEMENT

I would like to express my especial thanks and gratitude to my teacher and tutor Mr. Michael John Brennan, who encourage me and gave me all the necessary guidance and support to successfully complete this thesis, with him I came to know about so many new things, I am really thankful.

Secondly I Would like to thank God, because my faith help me to continue with focus to finish the thesis.

Finally, but no less important I would like to thank my parents and my husband for all the support and patience in the difficult times., and to my little boy Valentin who came to our lives during this stressful time to help mammy to maintain the calm and the desire to finish this so important project in my life.

RESUMO

Grandes estruturas, como aviões, navios e até mesmo sistemas de refrigeração, que possuem muitos componentes podem ser substruturados, com o intuito de agilizar e facilitar o cálculo da transmissão vibratória entre seus componentes. Existem diversas formas e domínios em que esta substruração pode ser realizada, sendo a utilizada nesta tese a substruturação no domínio da frequência utilizando para o cálculo as mobilidades medidas nos pontos de acoplamento dos componentes. Esta tese se concentra na substruturação de sistemas dinâmicos que possuem áreas flexíveis de contato como o que ocorre no acoplamento de amortecedores de borracha em sistemas vibratórios, sendo que para estes casos foi verificado que os métodos de substruturação mais usuais não apresentaram bons resultados para frequências superiores a primeira frequência natural do sistema completo, mesmo quando utilizados vários pontos de acoplamento no amortecedor de borracha. Utilizando o cálculo do comprimento de onda em diferentes materiais, neste caso o aço e a borracha, foi possível determinar uma relação entre a distância dos pontos de acoplamento e o comprimento de onda em que a metodologia de substruturação apresenta resultados acurados. Devido a estas limitações dos métodos de substruração, quando acoplamentos flexíveis existem nos subsistemas considerados, uma nova forma de substruração foi apresentada a qual mostrou resultados muito melhores, especialmente quando comparados com os resultados do sistema completo quando substruturado no acoplamento flexível.

Palavras-Chave: Substruração. Amortecedor de borracha. Mobilidades.

ABSTRACT

Large structures, such as airplanes, ships and even refrigeration systems, which have many components, can be substructured in order to speed up and facilitate the process of calculating the vibratory transmission between the system components. There are several methods and domains in which the substructuring can be done. In this thesis the substructuring method in the frequency domain is chosen to do the calculations, with the mobilities measured at the coupling points of the components. This thesis focuses on the substructuring of dynamic systems that have flexible distributed connections, such as those which occur in the coupling with rubber isolators in vibratory systems. For these cases, the most usual substructuring methods are shown not to give good results for frequencies higher than the first natural frequency of the complete system, even when several coupling points are used for the rubber isolator. Using the calculation of the flexural wavelength in different materials, in this case steel and rubber, it is possible to determine a relationship between the distance of the coupling points within the isolator and the wavelengths of the component materials, at which the substructuring methodology gives accurate results. Due to these limitations of current substructuring methods, when soft flexible couplings exist in the subsystems, a new substructuring approach is presented, and is shown to really improve the results, especially when compared to the when the complete system is substructured at the flexible coupling.

Key-words: Substructuring. Rubber isolator. Mobilities.

LIST OF FIGURES

LIST OF TABLES

LIST OF ABBREVIATIONS

DOF	*Degree-of-freedom*
TPA	*Transfer Path Analysis*
TP	*Transfer Path*
CMS	*Component Mode Systhesis*
FRF	*Frquency Response Function*
FBS	*Frequency Based Substructuring*
QZS	*Quasi-zero Stiffness*
FEM	*Finite Element Method*

LIST OF SYMBOLS

$\mathbf{B}$	*Compatibility condition Matrix*
$\mathbf{C}$	*Damping Matrix*
$\mathbf{K}$	*Stiffness Matrix*
$\mathbf{L}$	*Interface degrees of freedom localization Matrix*
$\mathbf{M}$	*Mass Matrix*
$\mathbf{R}$	*Substructuring individual reduction Matrix*
$\mathbf{Z}$	*Dynamics stiffness Matrix*
$\mathbf{f}$	*External Force Vector*
$\mathbf{g}$	*Connecting Force Vector*
$\mathbf{q}$	*Unique set off degree of freedom Vector*
$\mathbf{r}$	*Residual force Vector*
$\mathbf{u}$	*Displacement and Rotation DOF vector*
C	*Damping coefficient*
E	*Young Modulus*
F	*Force*
I	*Momento of inertia*
K	*Stiffness coefficient*
Z	*Impedance*
Y	*Mobility*

b	*Width*
d	*Distance between the connection points*
g	*Interface force*
h	*Thickness*
k	*Stiffness*
k	*Wavenumber*
l	*Length*
m	*Mass*
u	*Velocity*
$\boldsymbol{\alpha}$	*Interface generalized coordinates Vector*
$\boldsymbol{\lambda}$	*Interface force Vector*
$\boldsymbol{\eta}$	*Reduction Matrix*
ρ	*Densiy*
ζ	*Damping ratio*
ϕ	*Mode shape*
ω	*Radial frequency*
η	*Loss Factor*
λ	*Flexural wavelength*

SUMMARY

1 INTRODUCTION

Substructuring builds on the idea that a complex problem, that might not be solvable directly, or would take a long time to solve, can be decomposed into subcomponents which can be solved quickly and then assembled back into the original structure.

In structural dynamics, and with computational methods in mechanics in general, another way to increase the speed of the analysis even further is to reduce the set of degrees of freedom (DOFs) for each substructure. From this smaller set of DOFs, an approximate model is obtained for each substructure, and finally the substructures are coupled to form a reduced model of the original structure. An example of this is the refrigeration system investigated, by Marques (2010), in which only one degree of freedom was used to represent each substructure.

Marques (2010) used the transfer path methodology to solve de substructured system and, as will be discussed in this work, there is a numerous ramifications of this methodology, some examples are the operational transfer path analysis show by Klerk and Ossipov (2010), and a comparison of this methodologies applied to a electric vehicle is presented by A. Diez-Ibarbia et al. (2017). Another transfer path methodology called link-preserving decoupling method can be used to couple the substructured system and an example of application is shown by Keersmaekers (2015).

The subcomponents do not have to be analytical models, but can be experimentally acquired models. A complex structure which consists of many parts, for example a car shown in Auweraer et al. (2007), or a wind turbine shown by Manzato et al. (2015), can be disassembled into its components. For these parts, or substructures, it is possible to create models from various experiments. These experimental models can then be coupled to give the solution for the full structure, which is denoted experimental substructuring, Matthew et al. (2011) show an example of this methodology. Of particular interest in this thesis is the coupling of experimental models with analytical models, which is often called experimental-analytical dynamic substructuring. Van der Seijs et al. (2015) and Rixen (2016) show some uses of this methodology in their works. This makes it possible to build experimental models from substructures that are too complex, or would be too expensive to model, and couple them to simpler substructures which can easily be modeled analytically.

1.1 MOTIVATION

During the master degree project of the author, measurements were made of sound power radiated by a compressor, model Embraco EMIe30HER - 220V / 50-60Hz. This compressor was connected to a refrigeration system, model Consul CRC12A, and it was found that at low frequencies, there was a strong interaction between the compressor and the cooling system, which meant that the refrigerator system amplifies the sound power when compared to the compressor alone.

In Figure 1 a comparison of the sound power level of the refrigeration system and the compressor alone is shown, in which the noise can be divided into two parts, one containing low and medium frequencies and one that comprises higher frequencies. The range of 100 Hz to 2 kHz contains 76% of the total noise, where 5% of this is radiated only by the compressor, which means that the remaining noise in this band represents the interaction between the compressor and the cooling system. At higher frequencies, practically all noise generated by the compressor is directly radiated by the fridge (MARQUES, 2010).

Figure 1 - Compressor contribution to the radiated noise by the refrigeration system.

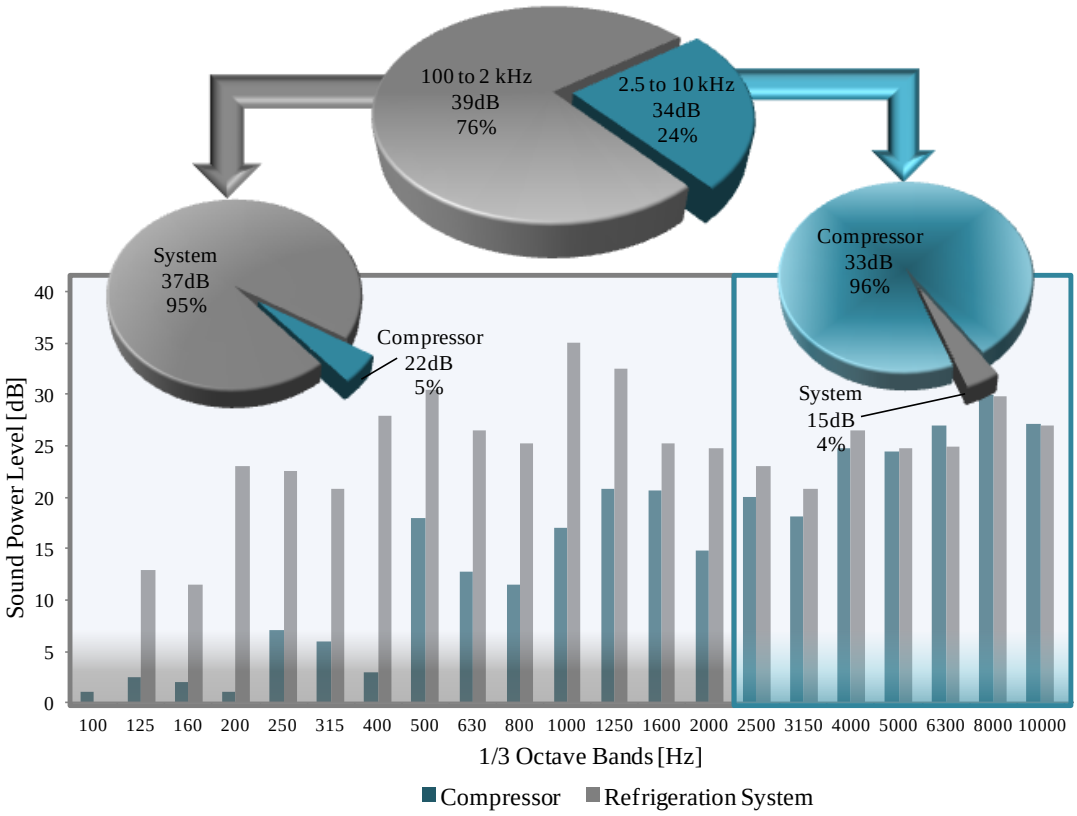

Source: Marques (2010).

It is difficult to determine which coupling between the components of the system has greater influence on the radiated noise by the refrigerator. In order to quantify these values, Marques (2010) used the Transfer Path Analysis (TPA) method to determine the contribution of some energy transfer paths. The TPA method used involves measuring the mobilities and impedances in the coupling points considered and the sound pressure transfer functions from the refrigeration system to a dummy head considered as a listener. The components are then coupled together using the mobility coupling and the auralization techniques to obtain the sound pressure level of each transfer path (TP) considered. More details of the calculations can be found in Marques (2010).

Now, considering the refrigeration system shown in Figure 2, an approximate model of the cooling system was substructured in the following transfer paths, using only one degree of freedom at the connection points to couple the substuctures. The transfer paths considered in the work, are shown in Figure 2. They are four in number and the descriptions of the subcomponents are as follows:

Transfer Path 1 - Base plate of the compressor - isolators - base plate of the system - radiated noise to the listener position;

Transfer Path 2 - Compressor suction tube - system suction tube - radiated noise;

Transfer Path 3 - Compressor discharge tube - system discharge tube - radiated noise;

Transfer Path 4 - Direct compressor noise radiation to the listener position.

Figure 2 - Representation of the transfer paths considered in the fridge system.

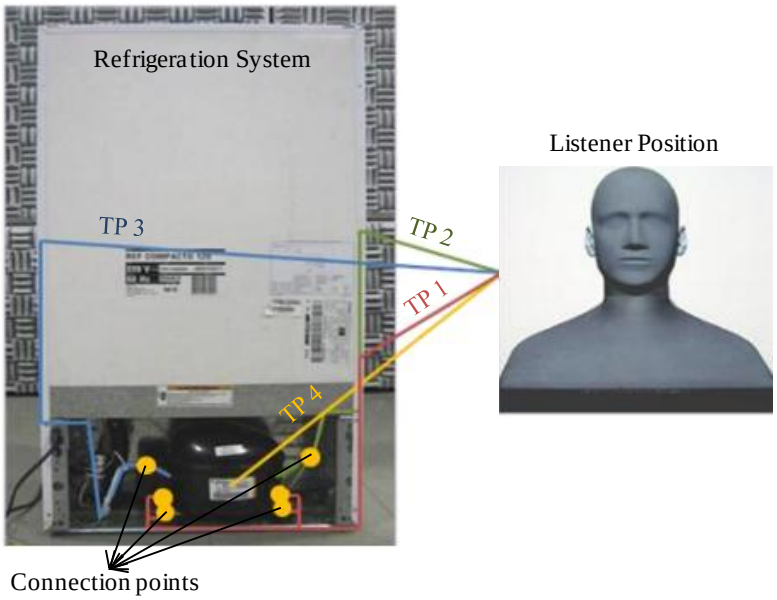

Source: Marques (2010).

Figure 3 shows the contribution of each transfer path considered, and the estimated total noise, it can be seen that the vibrational energy that passes through the isolators dominates at low frequencies while the suction and discharge tubes contribute more at medium frequencies. The direct radiation from the compressor dominates from the 2500Hz band where the resonance frequencies of the compressor shell starts (MARQUES, 2010).

Figure 3 - Contribution of each transfer path.

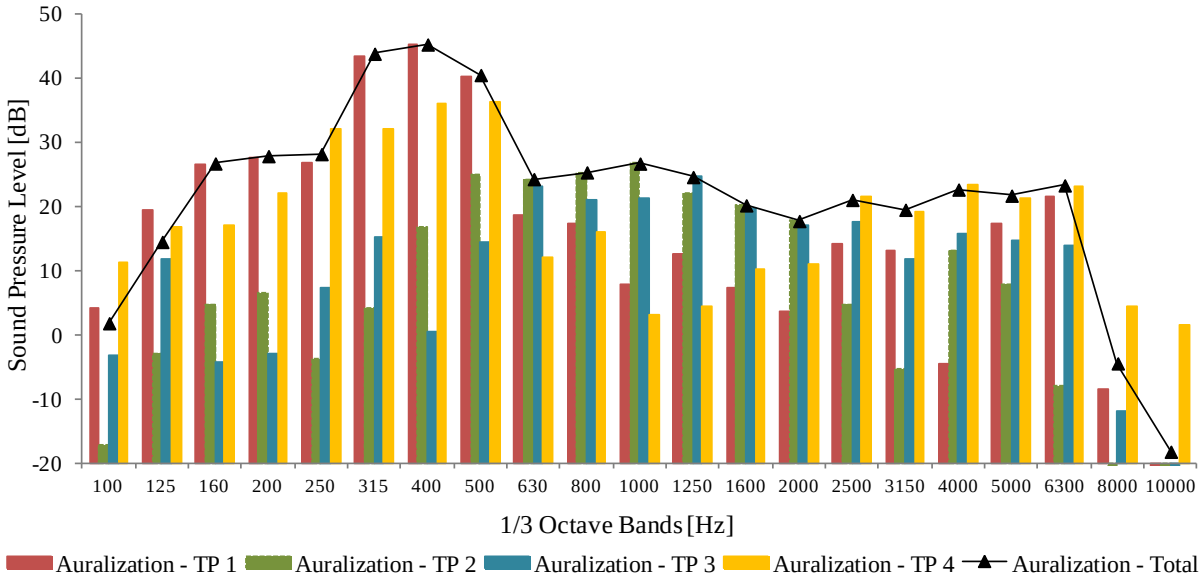

Source: Marques (2010).

Figure 4 shows the comparison between the calculated total noise and the measured total noise of the refrigeration system. It is possible to see that the major differences between the calculated and measured values are at low frequencies, which may indicate that there is a problem in transfer transfer path 1, where the rubber isolators are part of this energy transfer path.

Figure 4 - Comparison between the total noise measured and auralized.

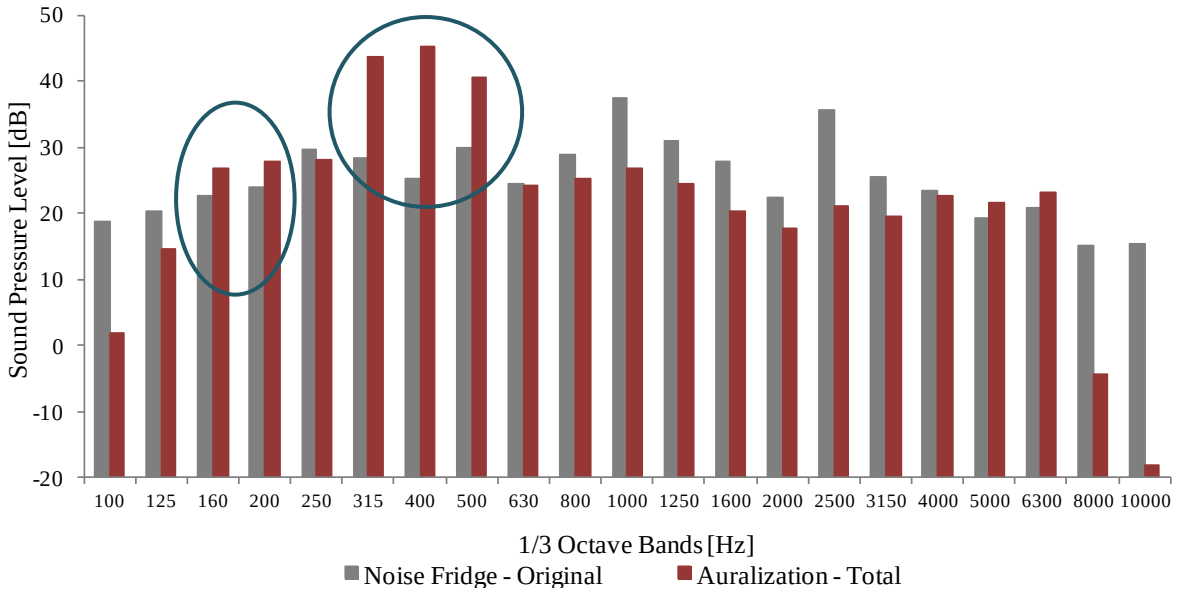

Source: Marques (2010).

In the work of Marques (2010), the connection of the points of contact were modelled considering only one degree-of-freedom and not the six degrees-of-freedom that actually exist in all connection points. Moreover, possible non-linearities existing in the cooling system, such as geometrical non-linearities in rubber isolators were not considered.

As it will be shown in the Chapter 3 of this thesis, the non-linearities in the isolators, for small displacements are small, so the main principle that will be investigated in this work is the forms of substructuring of vibratory systems with isolators.

1.2 LITERATURE REVIEW

This section presents a brief literature review of substructuring and the domains in which the analysis can be done. Further literature related to the basic principles of mounting with isolators, their static and dynamic characterization, as well as finite element principles and its application to real models, is discussed.

1.2.1 Substructuring

Dynamic substructuring is the process by which individual components are analyzed or tested separately and then combined to predict the response of the built-up structure, (Manzato et al., 2015). According to Klerk et al. (2008), there are some important advantages of using a substructured system instead of using global methods where the entire problem is handled at the same time.

1) It allows the evaluation of the dynamic behavior of structures that are too large or complex to be analyzed as a whole. For experimental analysis, this is true for large and complex systems such as aircraft. For numerical models, this holds when the number of degrees of freedom is such that solution techniques cannot obtain results in a reasonable time.

2) By analyzing the subsystems, local dynamic behavior can be recognized more easily than when the entire system is analyzed. Thereby, dynamic substrucuring allows identification of local problems as well as efficient local optimization. Also, dynamic substructuring allows the elimination of local subsystem behavior which has no significant impact on the assembled system. This results in a simple representation of the component's dynamics (e.g., an effective mass criteria) and, consequently, an additional reduction of analysis time.

3) Dynamic substructuring allows the possibility of combining modeled parts (discretized or analytical) and experimentally identified components.

4) It allows sharing and combining substructures from different project groups.

Klerk et al. (2008), give three classifications of dynamic substructuring that use three distinct domains. The component mode synthesis (CMS) method, where the substructures are reduced to a modal domain, and the coupling, or synthesis is between these reduced systems, as explained in Craig (2000) and Craig and Kurdila (2006). The second approach is a frequency based one, where the frequency response functions (FRFs) of the substructures are coupled. This method is commonly denoted FRF-based substructuring (FBS), i.e., it works in the frequency domain, (Manzato et al., 2015). The third method is direct coupling. In this case, the coupling is in the physical domain.

Figure 5 shows a representation of these three domains, considering that in the physical domain, the structure is characterized by its mass, stiffness, and damping

distributions. In the frequency domain a structure is represented by its frequency response functions. In the modal domain, the dynamic behavior of a structure is interpreted as a combination of modal responses.

Figure 5 – Representation of system dynamics in the three domains.

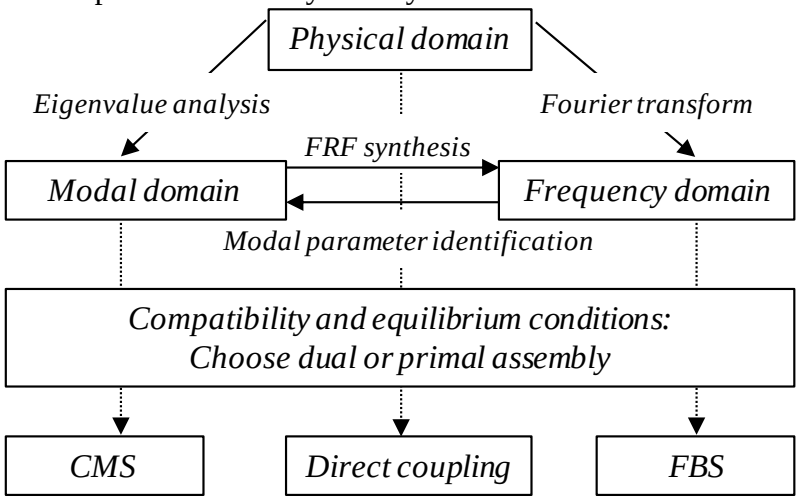

Source: Klerk et al. (2008).

Independent of the coupling method used in the analysis of a structure, there are two conditions that must be satisfied at the connection points between the substructures:

1) Compatibility of the substructure displacements at the interface – the so-called compatibility condition.

2) Force equilibrium on the substructure interface degrees-of-freedom – the so-called equilibrium condition.

At the interface, the dynamics of the substructures can be represented by their displacements or forces and a primal or dual respectively assembled system of equations is obtained, as shown schematically in Figure 5.

The differences between the coupling methods in the three distinct domains and a review of each one is given in Chapter 2. In this thesis, a frequency based substructuring is adopted, using mobility or impedance coupling methods.

1.2.2 Mounting with isolators

A vibration isolator is defined by the ISO standard 2041:1990 as “a support, usually resilient,... designed to attenuate the transmission of vibration in a frequency range”. This resilient element is used in a large range of applications, such as compressors, cars and ships, for example (Tao et al., 2000), in which a design optimization of a marine engine-mount is shown. It is also used in bridges, buildings and innumerous applications, where it is desirable to reduce the transmission of vibration generated by a source to the receiver structure.

A vibration isolator generally comprises a resilient element attached to a mounting plate at each end. Resilient elements include rubbers, elastomers, polymers, metal springs, corks, felts and air bags, (Dickens, 2002). In this thesis, a rubber isolator connecting two vibratory subsystems, is considered.

Rubber is an elastomeric material that generally has a small plastic deformation, high elongation (small Young's modulus, and are capable of sustaining deformation) and high retraction velocity. This definition is used for natural rubber as well as synthetic ones (Mott and Roland, 2009).

Another characteristic of rubber isolators is that they are resilient. This means that when they experience a deformation, they accumulate energy without rupture and with small plastic deformation. Rubber isolators also have internal damping, do not suffer from corrosion, do not require lubrification and, when submitted to large deformations, do not obey the Hooks law (Harris, 1976).

The behavior of the rubber varies with temperature. At low temperatures, the molecules are relatively inactive, resulting in a higher stiffness, as the relative movement between them is low. There is low intermolecular friction and, consequently, there is low damping (Istvan and Beranek, 2006).

At high temperatures, the molecules move with more facility, resulting in a low stiffness, and as the interaction between the molecules is low, there is low energy dissipation through the intermolecular friction. Finally, at medium temperatures, the interaction between the molecules is intermediate, and the Young's modulus is intermediate, but with a high loss factor.

Figure 6 shows a example of this dependency for the Young's modulus, E or G, and loss factor, η, for a elastic material with a variation in the temperature and frequency.

Figure 6 – Variation of the Young's modulus and loss factor with the temperature and frequency.

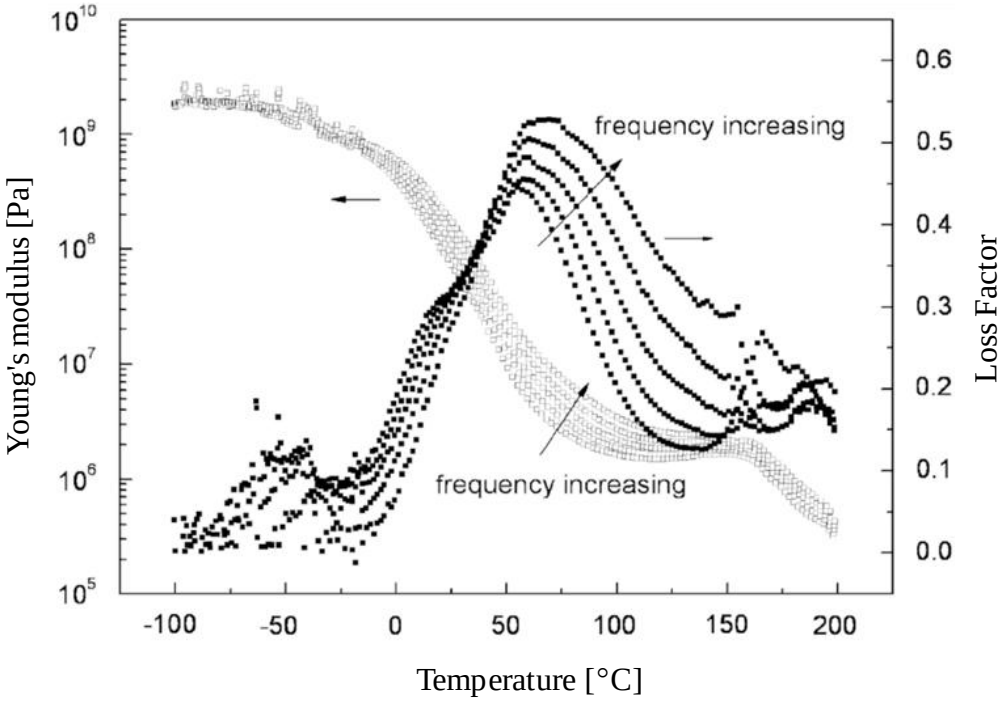

Source: Sun et al. (2008).

To determine the Young's modulus of the rubber isolator used in this thesis, a static test of the sample was performed. However, as the effectiveness of a vibration isolator is determined by its dynamic properties, and the dynamic properties of the structures to which it is attached, as described by Dickens and Norwood, (2001), dynamic tests were also carried out, including determination of the loss factor of the isolators.

A vibration isolator can be dynamically described in terms of four-pole parameters, which relate the force and velocity on the side of the isolator to the force and velocity on the other side, as shown by Molloy, (1957). A more complete article describing the dynamic and static tests for rubber isolators was presented by Snowdon, (1979). Li et al., (2007) demonstrated the use of the four-pole parameter in acoustics, for the transmission loss calculation in mufflers. To carry this out, it is necessary substitute the variables of force by pressure and velocity by volume velocity. Other examples of applications of four-pole parameters are given by Barbieri and Lima (2004) and Andersen (2008).

1.2.2.1 Geometric Non-linearities in isolators

As already mentioned a rubber isolator is often used to isolate undesirable vibrations, which is a problem for many systems. All the examples cited thus far considered linear isolators. A linear vibration isolator is effective if its natural frequency is lower than the excitation frequency. However, in case of severe disturbances, such as shock, impact or random vibration, the spectrum of excitation may have low frequency components (Ibrahim, 2008), which prove to be problematic.

Consider an ideal case where a mass m is supported by a linear spring k on a rigid base. Isolation only occurs above the frequency of $\sqrt{2k/m}$, which is $\sqrt{2}$ times the natural frequency of the system. It can be seen that for a lower spring stiffness, there is a large frequency range of vibration isolation. However, a low stiffness, results in a large static deformation of the system (CARRELLA et al., 2007). In order to overcome this disadvantage, non-linear springs have been used to obtain a high static stiffness, small static displacement, small dynamic stiffness and consequently a low natural frequency (Kovacic et al., 2008).

A non-linear spring can be formed by an arrangement of linear springs positioned in an oblique form. According to Carrella et al. (2009), with the appropriate choice of geometry and stiffness of the spring arrangement, a zero dynamic stiffness can be obtained. This mechanism is called quasi-zero stiffness (QZS).

Because of the benefits of non-linearities, many isolators used in practice are designed to work in their non-linear range. Some studies concerning this are described by Ibrahim (2008), and Wang et al. (2005). Interest in non-linear isolators is growing as shown by Richards and Singh, (2000) and Kim and Singh, (2001). Among the studies conducted recently about non-linear isolators, are Stenti et al., (2010) and Lu et al., (2013). Many studies have also been conducted to determine the non-linear properties of an isolator. Examples of methodologies to determine these non-linear properties are given by Mallik et al. (1999) and Richards and Singh (2001). In this thesis, the amplitude of vibration is considered to be low, so that the rubber isolators and the subsystems connected to the isolators can be considered linear. This facilitates the use of substructuring methods.

1.2.3 Finite Elements Models

The ideas and theory that today is known as finite element method (FEM) emerged from the beginning of twenty century. According to Huebner (1982) the FE method was used for the first time by Clough in 1960 in the study of plane elasticity for stress analysis in aircraft. From the work of Clough in the earlier sixties, the finite element method was used extensively for linear stress analysis, deflection and vibration in several engineer areas, as shown by Clough (1990).

The basic principle of decomposing an object into subcomponents, solving them, and assembling them again is used in the finite element method, where the subcomponents are called elements. This decomposition brings with it not only simplicity, but also speed, as it allows for parallel computing, which increases the speed of the analysis, (Klerk et al., 2008).

The finite element method divides a continuous system with infinite degrees of freedom into a discrete system with finite degrees of freedom. Linearly independent basis functions that are related to each degree of freedom are used to represent this discrete system (Azevedo, 2003). When solved, these functions give the eigenvalues and eigenvectors of the system.

From the eigenvalues, it is possible to calculate the natural frequencies of the structure. The eigenvectors, which are also calculated from the basis functions, provide the vibration modes of the structure, which show how the nodes of the elements move at the natural frequencies of the structure. The set of elements (and nodes) in which the structure is divided is called the structure mesh (Bittencourt, 2010).

There is hope that coupling between experimental and analytical models will decrease the cost of analyzing complex mechanical systems such as cars, airplanes, rocket launchers and wind turbines, if some parts can be modeled by, for example by Finite Elements (FE) whilst other parts can be experimentally acquired models. Some examples of FE applications are given by Wang et al., (2010), Wang and Inman, (2013) and Yang and Yau, (2015). Thus, substructuring also offers the possibility for companies to share confidential data in the form of reduced models.

1.3 OBJECTIVES

The objectives of this thesis are:

- To investigate the dynamic substructuring approach, using the frequency domain methodology, applied to a vibratory system with flexible distributed connections, such as rubber isolator.

- To determine the influence of the flexural wavelength in different materials, for example, a soft one and a hard one, when they are coupled in a dynamic system. Of particular interest is the accuracy of solution for this system if there are several points of connection.

- To determine if the proposed method of substructuring can improve the results for a coupled vibratory system, similar to that of a compressor-isolator-fridge system.

1.4 CONTRIBUTIONS TO KNOWLEDGE

- The limitations of substructuring methods for systems with distributed rather than point connections have been shown.

- A new approach to substructuring systems with soft distributed connections has been proposed and validated using numerical models that are adjusted using experimental data.

1.5 OUTLINE OF THE THESIS

Following this Introduction, Chapter 2 illustrates the methods of substructuring dynamic systems and applies the methodologies in the frequency domain to two simple vibratory examples. Chapter 3 analyses a rubber isolator distributed connection when a translational force is applied to a system formed by a mass, isolator and a beam. The transfer

path substructuring methodology is used to calculate the solution for the complete system. In Chapter 4 a new approach to substructuring a system with soft distributed connections is proposed and the system is analysed using transfer path methodology. Chapter 5 contains the conclusions of the thesis and some recommendations for further work.

2 PRINCIPLES OF SYSTEM DYNAMIC SUBSTRUCTURING

2.1 INTRODUCTION

In many engineering applications there are vibratory systems in which it is convenient to consider a complex engineering structure as an assembly of simpler components or substructures. According to Manzato et al. (2015) there is a method that helps to achieve this goal called dynamic substructuring, which is a process in which individual components are analyzed or tested separately and then combined to determine the response of the built-up structure. The aim of this chapter is to review the methods for substructuring in vibratory systems and to present two examples of substructuring using coupling methods in the frequency domain.

2.2 SUBSTRUCTURING METHODS

When a structural system, for example a vehicle, an airplane or any other large, complex structural system needs to be analyzed to determine its response to dynamic excitation, some form of substructure coupling method is usually employed. In this section the classification of dynamic substructuring methods is discussed, considering three distinct domains.

2.2.1 Coupling in the Physical Domain

In the physical domain, a system is represented by its mass, damping and stiffness matrices that could be obtained from a mechanical and geometrical model. The equations of motion in the physical domain for a dynamic subsystem *a* may be written as (KLERK et al., 2008)

$$\mathbf{M}^{(a)}\ddot{\mathbf{u}}^{(a)}(t)+\mathbf{C}^{(a)}\dot{\mathbf{u}}^{(a)}(t)+\mathbf{K}^{(a)}\mathbf{u}^{(a)}(t)=\mathbf{f}^{(a)}(t)+\mathbf{g}^{(a)}(t) \quad (1)$$

where $\mathbf{M}^{(a)}$, $\mathbf{C}^{(a)}$ and $\mathbf{K}^{(a)}$ are the mass, damping and stiffness matrices of substructure *a*. $\mathbf{u}^{(a)}$ denotes its vector of degrees-of-freedom (DOF), that can contain displacements and rotations, $\mathbf{f}^{(a)}$ is the external force vector, and $\mathbf{g}^{(a)}$ is the vector of connecting forces with the other substructures. These connecting forces are associated with a compatibility condition. Considering that the system is linear and time invariant, the equation of motion of *n* substructures that are to be coupled can be rewritten in block-diagonal matrix form as

$$\mathbf{M}\ddot{\mathbf{u}}(t)+\mathbf{C}\dot{\mathbf{u}}(t)+\mathbf{K}\mathbf{u}(t)=\mathbf{f}(t)+\mathbf{g}(t) \tag{2}$$

with

$$\mathbf{M} \triangleq diag\left(\mathbf{M}^{(1)},\ldots,\mathbf{M}^{(n)}\right)=\begin{pmatrix}\mathbf{M}^{(1)} & \cdots & . \\ \vdots & \ddots & \vdots \\ . & \cdots & \mathbf{M}^{(n)}\end{pmatrix}$$

$$\mathbf{C} \triangleq diag\left(\mathbf{C}^{(1)},\ldots,\mathbf{C}^{(n)}\right)$$

$$\mathbf{K} \triangleq diag\left(\mathbf{K}^{(1)},\ldots,\mathbf{K}^{(n)}\right)$$

$$\mathbf{u}(t) \triangleq \begin{Bmatrix}\mathbf{u}^{(1)} \\ \vdots \\ \mathbf{u}^{(n)}\end{Bmatrix}, \qquad \mathbf{f}(t) \triangleq \begin{Bmatrix}\mathbf{f}^{(1)} \\ \vdots \\ \mathbf{f}^{(n)}\end{Bmatrix}, \qquad \mathbf{g}(t) \triangleq \begin{Bmatrix}\mathbf{g}^{(1)} \\ \vdots \\ \mathbf{g}^{(n)}\end{Bmatrix}$$

The compatibility condition can be expressed by

$$\mathbf{B}\mathbf{u}(t)=0 \tag{3}$$

The $\mathbf{B}$ matrix operates on the interface degrees of freedom, and represents the compatibility condition state in that any pair of matching interface degrees of freedom $u^{(k)}$ and $u^{(l)}$ must have the same displacement. This means that $u^{(k)}-u^{(l)}=0$. The equilibrium condition is expressed by

$$\mathbf{L}^{T}\mathbf{g}(t)=0 \tag{4}$$

The matrix $\mathbf{L}$ is the matrix that localizes the interface degrees of freedom of the substructures, and $\mathbf{L}^{T}$ is the transposed matrix of $\mathbf{L}$. The expression states that when the connection forces are summed, their resultant must be equal to zero, it means that $g^{(k)}+g^{(l)}=0$. Now the total system can be described as

$$\begin{cases} \mathbf{M}\ddot{\mathbf{u}}(t)+\mathbf{C}\dot{\mathbf{u}}(t)+\mathbf{K}\mathbf{u}(t)=\mathbf{f}(t)+\mathbf{g}(t) & \text{(5a)} \\ \mathbf{B}\mathbf{u}(t)=0 & \text{(5b)} \\ \mathbf{L}^T\mathbf{g}(t)=0 & \text{(5c)} \end{cases}$$

Equation (5), shows a connection between any number of substructures with any number of arbitrary couplings. Using this set of equations, the coupled system can be obtained in either a primal or a dual way. More details of this are given in appendix A.

Classically, finite element models, for example, are assembled in a primal formulation manner, where a unique set of interface degrees of freedom is defined as

$$\mathbf{u}(t)=\mathbf{L}\mathbf{q}(t) \tag{6}$$

Because of the choice of this unique set $\mathbf{q}(t)$ and considering Equation (5), the system is now described as

$$\begin{cases} \mathbf{M}\mathbf{L}\ddot{\mathbf{q}}(t)+\mathbf{C}\mathbf{L}\dot{\mathbf{q}}(t)+\mathbf{K}\mathbf{L}\mathbf{q}(t)=\mathbf{f}(t)+\mathbf{g}(t) & \text{(7a)} \\ \mathbf{L}^T\mathbf{g}(t)=0 & \text{(7b)} \end{cases}$$

Pre-multiplying the equilibrium equation by $\mathbf{L}^T$ and knowing that $\mathbf{L}^T\mathbf{g}(t)=0$, so the primal assembled system is reduced to

$$\tilde{\mathbf{M}}\ddot{\mathbf{q}}(t)+\tilde{\mathbf{C}}\dot{\mathbf{q}}(t)+\tilde{\mathbf{K}}\mathbf{q}(t)=\tilde{\mathbf{f}}(t) \tag{8}$$

where

$$\begin{cases} \tilde{\mathbf{M}} \triangleq \mathbf{L}^T\mathbf{M}\mathbf{L} \\ \tilde{\mathbf{C}} \triangleq \mathbf{L}^T\mathbf{C}\mathbf{L} \\ \tilde{\mathbf{K}} \triangleq \mathbf{L}^T\mathbf{K}\mathbf{L} \\ \tilde{\mathbf{f}} \triangleq \mathbf{L}^T\mathbf{f} \end{cases}$$

For a dual assembly formulation, the full set of global degrees-of-freedom is kept and the system equations are obtained by satisfying the interface equilibrium by

$$\mathbf{g}(t)=-\mathbf{B}^T\lambda(t) \tag{9}$$

where, λ corresponds to the interface force, that acts in opposite directions for any pair of dual interface degrees of freedom. Due to the construction of the **B** matrix, and the equilibrium condition, Equation (1), is thus written as

$$\mathbf{L}^T\mathbf{g}(t) = -\mathbf{L}^T\mathbf{B}^T\lambda(t) = 0 \tag{10}$$

Consequently, the system of Equation (5) is now described as

$$\begin{cases} \mathbf{M}\ddot{\mathbf{u}}(t) + \mathbf{C}\dot{\mathbf{u}}(t) + \mathbf{K}\mathbf{u}(t) + \mathbf{B}^T\lambda(t) = \mathbf{f}(t) \\ \mathbf{B}\mathbf{u}(t) = 0 \end{cases} \tag{11}$$

2.2.2 Coupling in the Modal Domain

In the early 1970's, dynamic substructuring ideas were first developed by Hurty et al. (1971). In this paper, they developed the techniques for the dynamic analysis of large structures that involves the division into substructures or components. These techniques make use of component displacement modes to synthesize global systems of generalized coordinates and, for that reason, they have come to be known as modal synthesis or component mode techniques.

According to Craig (2000), component-mode synthesis involves two basic steps:

- Definition of sets of component modes;

- Coupling of component modes to form a reduced-order system model.

Figure 7 shows a flow chart that illustrates the relationship of substructure analysis to substructure testing.

Figure 7 – Model-Reduction tasks

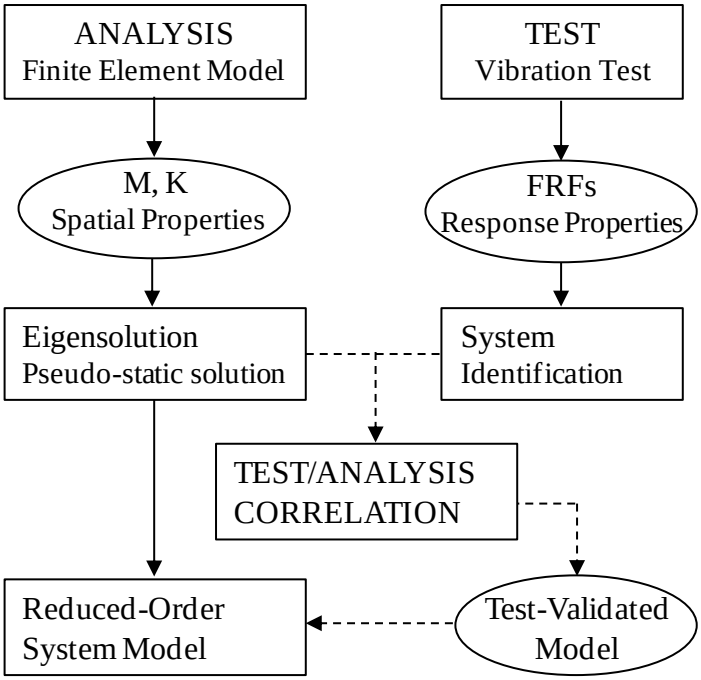

Source: Craig (2000).

The component-mode synthesis (CMS) method usually includes a modal analysis of the substructure, from which the modal vectors are obtained. These are used to reduce the equations of motions from the physical to the modal domain (Klerk et al., 2008). The reduced model generates a new set of generalized coordinates. More details about how to choose the reduced model can be found in the works of Hurty et al., (1971) and Craig, (2000).

Now, considering the vector of generalized coordinates, $\boldsymbol{\eta}(t)$, and the reduction matrix, $\mathbf{R}$, that is a block-diagonal matrix with the substructures' individual reduction matrices, then

$$\mathbf{u}(t) \simeq \mathbf{R}\boldsymbol{\eta}(t) \tag{12}$$

where $\mathbf{R} \triangleq diag[\mathbf{R}^1, \ldots, \mathbf{R}^n]$. Substituting Equation (12) into the equilibrium Equation (1) results in

$$\mathbf{M}^{(a)}\mathbf{R}\ddot{\boldsymbol{\eta}}^{(a)}(t) + \mathbf{C}^{(a)}\mathbf{R}\dot{\boldsymbol{\eta}}^{(a)}(t) + \mathbf{K}^{(a)}\mathbf{R}\boldsymbol{\eta}^{(a)}(t) = \mathbf{f}^{(a)}(t) + \mathbf{g}^{(a)}(t) + \mathbf{r}^{(a)}(t) \tag{13}$$

where $\mathbf{r}^{(a)}(t)$ is a residual force introduced due to the reduction of the system model, which is necessary to fully represent the real system. The reduced equilibrium equations are obtained by imposing the condition that the residual force must be zero in the reduced space, i.e.,

$\mathbf{R}^{(a)T}\mathbf{r}^{(a)}(t)=0$. So, according to Klerk et al., (2008) the reduced decoupled equations of motion are

$$\mathbf{M}_m\ddot{\boldsymbol{\eta}}(t)+\mathbf{C}_m\dot{\boldsymbol{\eta}}(t)+\mathbf{K}_m\boldsymbol{\eta}(t)=\mathbf{f}_m(t)+\mathbf{g}_m(t) \tag{14}$$

where

$$\begin{cases}\mathbf{M}_m \triangleq \mathbf{R}^T\mathbf{M}\mathbf{R}\\ \mathbf{C}_m \triangleq \mathbf{R}^T\mathbf{C}\mathbf{R}\\ \mathbf{K}_m \triangleq \mathbf{R}^T\mathbf{K}\mathbf{R}\\ \mathbf{f}_m \triangleq \mathbf{R}^T\mathbf{f}\\ \mathbf{g}_m \triangleq \mathbf{R}^T\mathbf{g}\end{cases}$$

in which the subscript *m* denotes matrices in the modal domain.

When the subsystems are coupled, it is necessary that the compatibility and force equilibrium equations are valid as discussed in the previous section. So, these equations need to be rewritten in the modal domain as well. For generalized coordinates, the compatibility condition is written as

$$\mathbf{B}_m\boldsymbol{\eta}(t)=0 \tag{15}$$

where

$$\mathbf{B}_m \triangleq \mathbf{B}\mathbf{R}$$

$$\boldsymbol{\eta}(t)=\mathbf{L}_m\mathbf{q}(t)$$

Here $\mathbf{q}$ is the unique set of generalized coordinates of the assembled system and the matrix $\mathbf{L}_m$ is the localization matrix associated with the generalized coordinates. Considering the reduced model, the coupling condition can be written as

$$\begin{cases}\mathbf{M}_m\ddot{\boldsymbol{\eta}}(t)+\mathbf{C}_m\dot{\boldsymbol{\eta}}(t)+\mathbf{K}_m\boldsymbol{\eta}(t)=\mathbf{f}_m(t)+\mathbf{g}_m(t) & \text{(16a)}\\ \mathbf{B}_m\boldsymbol{\eta}(t)=0 & \text{(16b)}\\ \mathbf{L}^T{}_m\mathbf{g}_m(t)=0 & \text{(16c)}\end{cases}$$

Using Equations (16), it is possible to assemble the structures using the primal or dual formulation. Starting with the primal formulation, in which a unique set of interface DOFs is chosen, it is possible rewrite Equation (16) for this set of coordinates to give

$$\begin{cases} \mathbf{M}_m\mathbf{L}_m\ddot{\mathbf{q}}(t)+\mathbf{C}_m\mathbf{L}_m\dot{\mathbf{q}}(t)+\mathbf{K}_m\mathbf{L}_m\mathbf{q}(t)=\mathbf{f}_m(t)+\mathbf{g}_m(t) & (17a) \\ \mathbf{B}_m\mathbf{L}_m\xi(t)=0 & (17b) \\ \mathbf{L}^T{}_m\mathbf{g}_m(t)=0 & (17c) \end{cases}$$

From Equation (17b) it is important to note that $\mathbf{L}_m = null(\mathbf{B}_m)$, so this is zero. Now multiplying the other equation by $\mathbf{L}^T{}_m$ and noting that $\mathbf{L}^T{}_m\mathbf{g}_m(t)$ must be zero, the primal system of equations of the coupled structure is

$$\tilde{\mathbf{M}}_m\ddot{\mathbf{q}}(t)+\tilde{\mathbf{C}}_m\dot{\mathbf{q}}(t)+\tilde{\mathbf{K}}_m\mathbf{q}(t)=\tilde{\mathbf{f}}_m(t) \tag{18}$$

where

$$\begin{cases} \tilde{\mathbf{M}}_m \triangleq \mathbf{L}_m{}^T\mathbf{M}_m\mathbf{L}_m \\ \tilde{\mathbf{C}}_m \triangleq \mathbf{L}_m{}^T\mathbf{C}_m\mathbf{L}_m \\ \tilde{\mathbf{K}}_m \triangleq \mathbf{L}_m{}^T\mathbf{K}_m\mathbf{L}_m \\ \tilde{\mathbf{f}}_m \triangleq \mathbf{L}_m{}^T\mathbf{f}_m \end{cases}$$

The dual formulation is obtained by imposing that the interface forces in the generalized coordinates are given by

$$\mathbf{g}_m(t) = -\mathbf{B}_m\alpha \tag{19}$$

where α is a Lagrange multiplier associated with the interface generalized coordinates. The force equilibrium is now

$$\mathbf{L}_m{}^T\mathbf{B}_m\alpha = 0 \tag{20}$$

and the dual equations of motion assembled system for generalized coordinates is now given by

$$\begin{cases} \mathbf{M}_m\ddot{\boldsymbol{\eta}}(t)+\mathbf{C}_m\dot{\boldsymbol{\eta}}(t)+\mathbf{K}_m\boldsymbol{\eta}(t)+\mathbf{B}_m{}^T\alpha=\mathbf{f}_m(t) & (21a) \\ \mathbf{B}_m\boldsymbol{\eta}(t)=0 & (21b) \end{cases}$$

2.2.3 Coupling in the Frequency Domain

In this thesis a frequency based substructuring is used, and three methodologies related to this are illustrated in this section. The first one uses the matrices of system properties, and

the primal and dual formulation are presented, as with the physical and modal domain methods.

The second methodology shows the mobility or impedance method, in this case, the transfer and driving point motilities and impedances are used to couple the substructures. Finally, the transfer path analysis is presented. In this case the transfer path is calculated using the subsystem admittance method.

2.2.3.1 Using system property matrices

Considering that the mechanical subsystems are linear, time invariant and in steady state it is possible transform the equations of motions as well as the coupling conditions from the physical domain to the frequency domain using the Fourier transform (Klerk et al., 2008).

Applying the Fourier transform to Equations (5a, b, c), results in

$$\begin{cases} \mathbf{Z}(\omega)\mathbf{u}(j\omega) = \mathbf{f}(\omega) + \mathbf{g}(\omega) & \text{(22a)} \\ \mathbf{B}\mathbf{u}(\omega) = 0 & \text{(22b)} \\ \mathbf{L}^T\mathbf{g}(\omega) = 0 & \text{(22c)} \end{cases}$$

where **u**, **f**, **g** represent the complex amplitude vector of the harmonic response and the forces, **Z** is the block-diagonal matrix containing the dynamic stiffness matrices of the substructures, and is given by

$$\mathbf{Z}(j\omega) \triangleq -\omega^2\mathbf{M} + j\omega\mathbf{C} + \mathbf{K} \tag{23}$$

Now, to obtain a primal formulation, the interface compatibility is imposed by choosing a unique set of interface degrees of freedom, $\mathbf{q}$, as

$$\tilde{\mathbf{Z}}(\omega)\mathbf{q}(j\omega) = \tilde{\mathbf{f}}(\omega) \tag{24}$$

where

$$\begin{cases} \tilde{\mathbf{Z}} \triangleq \mathbf{L}^T\mathbf{Z}\mathbf{L} \\ \tilde{\mathbf{f}} \triangleq \mathbf{L}^T\mathbf{f} \end{cases}$$

For the dual formulation, to assemble the subsystems shown in the Equation (22), the equilibrium condition is imposed, considering the interface forces as $\mathbf{g}(\omega) = -\mathbf{B}^T \alpha(\omega)$, where α is a Lagrange multiplier associated with the interface generalized coordinates. Considering the same approach as in the coupling for the physical domain, this results in

$$\begin{cases} \mathbf{Z}(\omega)\mathbf{u}(j\omega) + \mathbf{B}\alpha(\omega) = \mathbf{f}(\omega) & \text{(25a)} \\ \mathbf{B}^T\mathbf{u}(\omega) = 0 & \text{(25b)} \end{cases}$$

2.2.3.2 Using mobility or impedance matrices

Mobilities and impedances are widely used to perform the coupling of complex systems, the basic theory and some examples are shown by Jerome (1980), Peterson and Plunt (1982), Mondot and Peterson (1987), Baars (1996), Hynnä (2002), Gardonio and Brennan (2004), Fahy and Gardonio (2007), Van der Seijs (2015) and Manzato et al. (2015). The mobility and impedance method is based on the principles of superposition and reciprocity, which are valid for linear systems (Fahy and Gardonio, 2007). This method does not use the equations of motion, as described previously, but the frequency response functions of the subsystems that can be obtained by classic analytical methods, the finite element method, experimental measurements or a combination of these. Some real systems can be modeled using lumped mechanical elements (Hynnä, 2002). Such elements are a spring, a damper and a mass, as shown in Figure 8.

Figure 8 – Linear spring, damper and mass elements

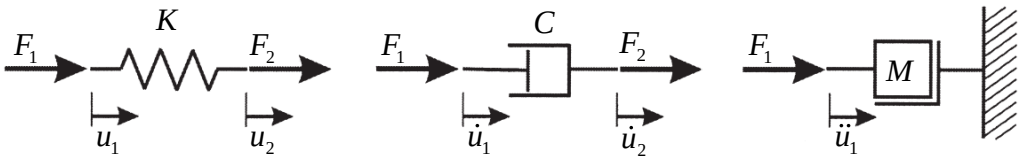

Source: Fahy and Gardonio (2007).

Consider that F_1 and F_2 are axial forces that act on the elements and u_1 and u_2 are the axial displacements. The dot over the variables denotes differentiation with respect to time. The constitutive equations for the assumed massless spring and viscous damper elements are

$$F_1 = -F_2 = K\left(u_1 - u_2\right), \quad F_1 = -F_2 = C\left(\dot{u}_1 - \dot{u}_2\right) \tag{26a}$$
(26b)

The constants *K* and *C* are the stiffness and damping coefficients. Applying Newton's second law to the mass element *M*, gives

$$F_1 = M\ddot{u}_1 \tag{27}$$

Considering that the excitation force is harmonic with the form $F(t) = \tilde{F}e^{i\omega t}$, the displacement response will be $u(t) = \tilde{u}e^{i\omega t}$, where ω is the radial frequency and $i = \sqrt{-1}$. Now, fixing one of the ends of the spring and the damper, it is possible to determine the expressions for the mechanical mobilities for all of the elements (Fahy and Gardonio, 2007), and are given by

$$\tilde{Y}_K = \frac{\dot{\tilde{u}}_1}{\tilde{F}_1}\bigg|_{\dot{\tilde{u}}_2=0} = \frac{i\omega}{K}, \qquad \tilde{Y}_C = \frac{\dot{\tilde{u}}_1}{\tilde{F}_1}\bigg|_{\dot{\tilde{u}}_2=0} = \frac{1}{C},$$
$$\tilde{Y}_M = \frac{\dot{\tilde{u}}_1}{\tilde{F}_1} = \frac{-i}{\omega M} \tag{28a,b, c}$$

The impedances of the elements are reciprocals of the expressions in Equations (28) and so are given by

$$\tilde{Z}_K = \frac{\tilde{F}_1}{\dot{\tilde{u}}_1}\bigg|_{\tilde{F}_2=0} = \frac{-iK}{\omega}, \qquad \tilde{Z}_C = \frac{\tilde{F}_1}{\dot{\tilde{u}}_1}\bigg|_{\tilde{F}_2=0} = C,$$
$$\tilde{Z}_M = \frac{\tilde{F}_1}{\dot{\tilde{u}}_1}\bigg|_{\tilde{F}_2=0} = i\omega M \tag{29a,b, c}$$

Real systems that can be represented, by multiple spring, damper and mass elements may be arranged either in parallel or series configurations. The mobility and impedance functions can be derived for equivalent mobility and impedance elements by considering the following equations for

- Parallel connection –

$$\frac{1}{\tilde{Y}_e} = \sum_{n=1}^{N} \frac{1}{\tilde{Y}_n}, \quad \tilde{Z}_e = \sum_{n=1}^{N} \tilde{Z}_n \tag{30a,b}$$

- Series connection –

$$\tilde{Y}_e = \sum_{n=1}^{N} \tilde{Y}_n, \quad \frac{1}{\tilde{Z}_e} = \sum_{n=1}^{N} \frac{1}{\tilde{Z}_n} \tag{31a,b}$$

To demonstrate an application of this modeling approach a single degree of freedom mechanical system composed of a lumped mass, spring and damper is considered, as shown in Figure 9.

Figure 9 – Single-degree-of-freedom mechanical system.

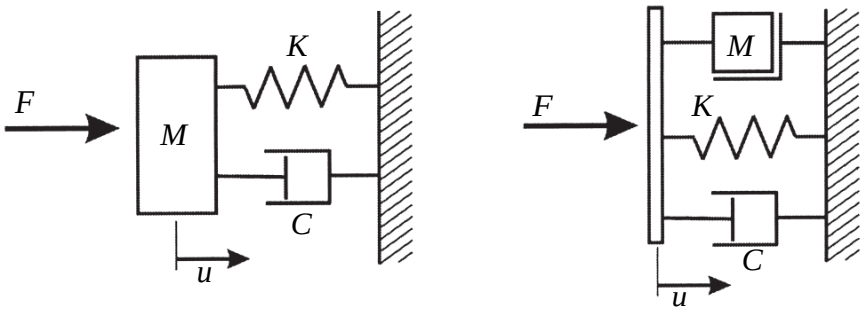

(a) Conventional Diagram (b) Mobility Diagram

Source: Fahy and Gardonio (2007).

Figure 9 (a) shows the conventional way to represent the system, and (b) shows a mobility representation. Examining the conventional diagram, it is not so clear that all the elements are connected in parallel, while this is more visible in the mobility diagram. Thus, it is important to visualize these two forms before starting the calculations.

Considering the mobility coupling of the components and considering a combination of Equations (28) and (30), the mobility function for the mechanical system is given by

$$\tilde{Y}_e = \frac{1}{i\omega M + C - iK/\omega} \tag{32}$$

The plot in Figure 10 is the modulus of the mobility function of the system shown in Figure 9. In this plot, the mobility of the mass and spring is also shown to illustrate which element

controls the dynamic behavior in each frequency range. It is possible to see that at low frequencies there is spring-like behavior, whereas at high frequencies the system exhibits mass-like behavior.

At the resonance frequency, the modulus of the mobilities of the mass and spring are the same, but with opposite signs, i.e., $Y_K = -Y_M$, therefore the mobility of the system at this frequency is only Y_C, which means that only damping controls the vibration response at the resonance frequency.

Figure 10 – Mobility function for the mechanical system presented in the Figure 9.

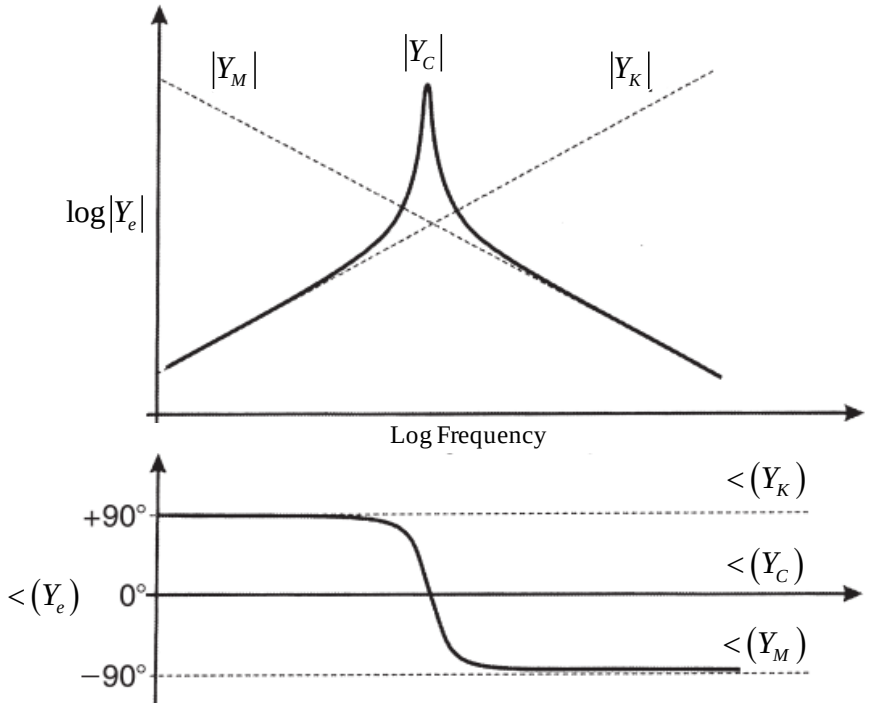

Source: Fahy and Gardonio (2007).

Now, consider that the linear system, shown in Figure 11, cannot be represented by lumped parameters so, there is a general representation using impedance and mobility matrices to represent these systems or components (Gardonio and Brennan, 2004).

Figure 11 – General linear system.

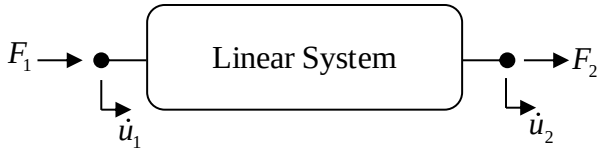

Source: Adapted from Gardonio and Brennan (2004).

The relationship between the two connections of the system, considering the impedance matrix is:

$$\begin{Bmatrix} F_1 \\ F_2 \end{Bmatrix} = \begin{bmatrix} Z_{11} & Z_{12} \\ Z_{21} & Z_{22} \end{bmatrix} \begin{Bmatrix} \dot{u}_1 \\ \dot{u}_2 \end{Bmatrix} \quad \text{or, in vector form} \quad \mathbf{f} = \mathbf{Z}\dot{\mathbf{u}} \tag{33}$$

The corresponding mobility matrix is:

$$\begin{Bmatrix} \dot{u}_1 \\ \dot{u}_2 \end{Bmatrix} = \begin{bmatrix} Y_{11} & Y_{12} \\ Y_{21} & Y_{22} \end{bmatrix} \begin{Bmatrix} F_1 \\ F_2 \end{Bmatrix} \quad \text{or, in vector form} \quad \dot{\mathbf{u}} = \mathbf{Y}\mathbf{f} \tag{34}$$

It is important to note that for lumped parameters, for example a spring, $\tilde{Z}_K = \tilde{Y}_K^{-1}$ the mobility and the impedance are reciprocal, but for the matrices this is not valid, i e., for each component of the matrices $\mathbf{Z}_{ij} \neq \mathbf{Y}_{ij}^{-1}$. This is because the matrices are derived by applying different boundary conditions. To determine each element of the impedance matrix, the point at which the force is applied is unconstrained, but all other points are constrained, it means that all other velocities are set to zero, so $Z_{ij} = \left.\frac{F_i}{\dot{u}_j}\right|_{\dot{u}_{k\neq j}=0}$. Reciprocally, for an element of the mobility matrix, the point at which a force is applied is constrained, but all other points are set free, so that $Y_{ij} = \left.\frac{\dot{u}_i}{F_j}\right|_{F_{k\neq j}=0}$ Gardonio and Brennan (2004).

Now, consider the coupling between two mechanical systems that are subsystems of a real machine, for example, as shown in the Figure 12, each one is represented as a matrix of mobilities or impedances.

Figure 12 – Coupling of two mechanical systems using impedance and mobility matrices.

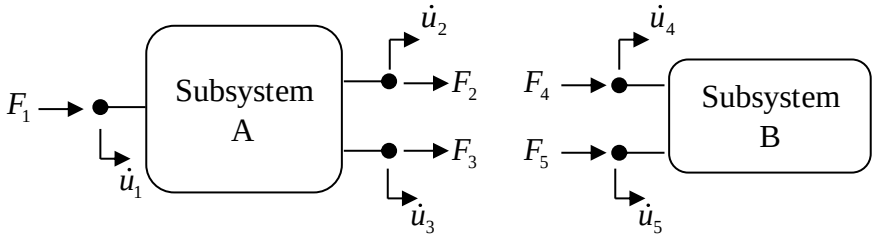

Source: Elaborated by the author.

To obtain the velocities of the coupled system it is necessary to determine the mobility matrix for both subsystems. So for the subsystem A the mobility matrix is

$$\begin{Bmatrix} \dot{u}_1 \\ \dot{u}_2 \\ \dot{u}_3 \end{Bmatrix} = \begin{bmatrix} Y_{11} & Y_{12} & Y_{13} \\ Y_{21} & Y_{22} & Y_{23} \\ Y_{31} & Y_{32} & Y_{33} \end{bmatrix} \begin{Bmatrix} F_1 \\ F_2 \\ F_3 \end{Bmatrix} \tag{35}$$

This equation could be rewritten considering the external and coupling forces as

$$\begin{Bmatrix} \dot{u}_1 \\ \dot{u}_2 \\ \dot{u}_3 \end{Bmatrix} = \begin{bmatrix} Y_{11} & Y_{12} & Y_{13} \\ Y_{21} & Y_{22} & Y_{23} \\ Y_{31} & Y_{32} & Y_{33} \end{bmatrix} \begin{Bmatrix} F_1 \\ 0 \\ 0 \end{Bmatrix} + \begin{bmatrix} Y_{11} & Y_{12} & Y_{13} \\ Y_{21} & Y_{22} & Y_{23} \\ Y_{31} & Y_{32} & Y_{33} \end{bmatrix} \begin{Bmatrix} 0 \\ F_2 \\ F_3 \end{Bmatrix} \tag{36a}$$

$$\dot{\mathbf{u}} = \mathbf{Y}_{\mathrm{A}}\mathbf{F}_1 + \mathbf{Y}_{\mathrm{A}}\mathbf{F} \tag{36b}$$

Now considering subsystem B, the mobility matrix is

$$\begin{Bmatrix} \dot{u}_4 \\ \dot{u}_5 \end{Bmatrix} = \begin{bmatrix} Y_{44} & Y_{45} \\ Y_{54} & Y_{55} \end{bmatrix} \begin{Bmatrix} F_4 \\ F_5 \end{Bmatrix} \quad \text{or, in vector form} \quad \dot{\mathbf{u}}_{\mathrm{B}} = \mathbf{Y}_{\mathrm{B}}\mathbf{F}_{\mathrm{B}} \tag{37}$$

However, as discussed before $\mathbf{Z}_{\mathrm{B}} = \mathbf{Y}_{\mathrm{B}}^{-1}$, so $\mathbf{F}_{\mathrm{B}} = \mathbf{Z}_{\mathrm{B}}\dot{\mathbf{u}}_{\mathrm{B}}$. To couple both subsystems it is necessary that the compatibility and force equilibrium equations are applied, then the forces and velocities in the connection points are given by

$$\begin{Bmatrix} F_4 \\ F_5 \end{Bmatrix} = -\begin{Bmatrix} F_2 \\ F_3 \end{Bmatrix} \text{ and} \tag{38a}$$

$$\begin{Bmatrix} \dot{u}_4 \\ \dot{u}_5 \end{Bmatrix} = \begin{Bmatrix} \dot{u}_2 \\ \dot{u}_3 \end{Bmatrix} \tag{38b}$$

Considering Equations (37) and (38), the new matrix that represents the subsystem B is

$$\begin{Bmatrix} 0 \\ F_2 \\ F_3 \end{Bmatrix} = -\begin{bmatrix} 0 & 0 & 0 \\ 0 & Z_{44} & Z_{45} \\ 0 & Z_{54} & Z_{55} \end{bmatrix} \begin{Bmatrix} \dot{u}_1 \\ \dot{u}_2 \\ \dot{u}_3 \end{Bmatrix} \tag{39a}$$

$$\mathbf{F} = -\mathbf{Z}\dot{\mathbf{u}} \tag{39b}$$

Substituting Equation (39) into Equation (36), it is possible to calculate the velocities for the coupled system, which results in

$$\dot{\mathbf{u}} = \left[\mathbf{I} + \mathbf{YZ}\right]^{-1} \mathbf{YF}_1 \tag{40}$$

This is the basic methodology to couple systems using the mobility and impedance approach. However, because of its simplicity there are some problems depending on the connections, and this is discussed in Section 2.3.

2.2.3.3 Transfer path analysis

Transfer path analysis (TPA) is a procedure based on experimental measurements, but could include finite element data, resulting in a hybrid model. This model can be used to identify the dominant paths of vibration transmission from a source to the coupled subsystems that may have different structural and acoustic transfer characteristics. Transfer path analysis has been widely applied to investigate noise problem in the automotive area, some examples, of which are given by Padilha (2006), Ibáñes (2008) and Auweraer et al. (2007).

With this methodology, it is possible to identify or predict the path that contributes more to the vibration transmission. Thus, the necessary changes can be made to either the source or the receiving structures to reduce the total vibration of the structure (VAN DER SEIJS et al, 2015). From classical TPA developed by Verheij (1986), a complex vibratory system can be divided into various simple subsystems that have three components, the source, the interface and the receiver. The source is the active component that causes the operational excitation, even if it is unmeasurable in practice. Gardonio and Brennan (2004) show that the source can either be represented as a blocked force that is a Thévenin equivalent source, or a free velocity, that is a Norton equivalent source. The choice of source representation depends upon personal preference and/or available data. Moreover, if the source is part of a larger, component that cannot be subdivided it could be represented by its vibration transmission at the interface. The interface is the connection points between the active component, or source and the passive component, or receiver. The receiver is represented by their responses at the

connection points of interest at the receiver structure. These responses could include acoustic pressure, mobility, impedance and other physical quantities.

Van der Seijs et al. (2015), give a complete description of transfer path analysis development, its history, theory and classification of techniques. However, the focus here is the transfer path from the assembled admittance methodology coupling. The term admittance is an electrical representation, in structural dynamics it is called receptance or mobility. To exemplify this method, consider the dynamic system AB shown in Figure 13. It is possible to indentify two subsystems, which are the active subsystem A, or source, and the passive subsystem B, or receiver structure. The two subsystems are rigidly connected at the interface at node 2, and the objective is to determine the vibration transmitted to node 3 generated by the source at node 1.

Figure 13 – Coupling of two subsystems using the transfer path from admittance assembly.

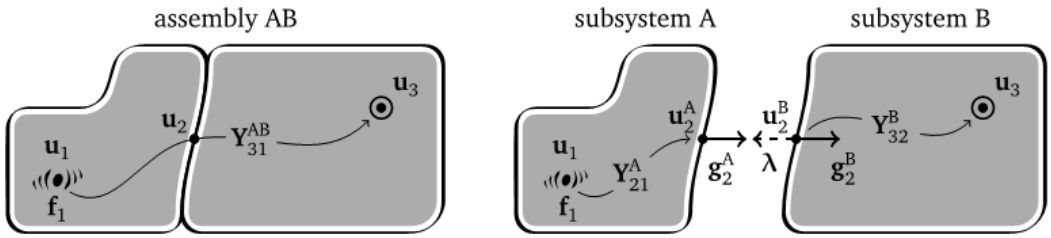

(a) Assembled system (b) Subsystems A and B

Source: Van der Seijs et al. (2015).

Considering Figure 13(a), for the assembled system, to determine the response spectra at the receiving structure, the solution is obtained from a superposition of the individual contributions. This means that the excitation force is multiplied by its respective transfer functions, contained in the columns of the admittance transfer function matrix $\mathbf{Y}^{AB}$, resulting in (Van der Seijs, 2015)

$$\mathbf{u}_3 = \mathbf{Y}_{31}^{AB}\mathbf{f}_1 \tag{41}$$

where $\mathbf{f}_1$ is the excitation force applied to the subsystem A. Note that the response $\mathbf{u}_3$ could include displacements, velocities or accelerations, so the rows of the transfer function matrix need to be obtained accordingly. In this work velocities are used and the transfer functions are mobilities.

Now, examining Figure 13(b), it is possible to generate the mobility matrix from both subsystems $\mathbf{Y}^{\mathrm{A}}$ and $\mathbf{Y}^{\mathrm{B}}$. As the operational excitation of the source, node 1, is unmeasurable in practice, the responses are generated by measurements from the source to the interface, nodes 1 and 2, and transfer functions that relate these vibrations to the receiving responses, nodes 2 and 3. The matrices can be written in block-diagonal format as

$$\begin{Bmatrix} \dot{u}_1 \\ \dot{u}_2^{\mathrm{A}} \\ \dot{u}_2^{\mathrm{B}} \\ \dot{u}_3 \end{Bmatrix} = \begin{bmatrix} Y_{11}^{\mathrm{A}} & Y_{12}^{\mathrm{A}} & 0 & 0 \\ Y_{21}^{\mathrm{A}} & Y_{22}^{\mathrm{A}} & 0 & 0 \\ 0 & 0 & Y_{22}^{\mathrm{B}} & Y_{23}^{\mathrm{B}} \\ 0 & 0 & Y_{32}^{\mathrm{B}} & Y_{33}^{\mathrm{B}} \end{bmatrix} \left\{ \begin{Bmatrix} f_1 \\ 0 \\ 0 \\ 0 \end{Bmatrix} + \begin{Bmatrix} 0 \\ g_2^{\mathrm{A}} \\ g_2^{\mathrm{B}} \\ 0 \end{Bmatrix} \right\} \quad \text{or} \tag{42a}$$

$$\dot{\mathbf{u}} = \mathbf{Y}(\mathbf{f} + \mathbf{g}) \tag{42b}$$

where the force vector has the excitation force and the forces at the interface. Consider the compatibility condition

$$\begin{aligned} g_2^{\mathrm{A}} &= -g_2^{\mathrm{B}} \quad \text{and} \\ \dot{u}_2^{\mathrm{A}} &= \dot{u}_2^{\mathrm{B}} \end{aligned} \tag{43}$$

So, the interface forces can be calculated by matching the second and third line of Equation (42a), that is

$$Y_{21}^{\mathrm{A}} f_1 + Y_{22}^{\mathrm{A}} g_2^{\mathrm{A}} = Y_{22}^{B} g_2^{B} \tag{44}$$

which can be written as

$$\left(Y_{22}^{\mathrm{A}} + Y_{22}^{\mathrm{B}}\right) g_2^{\mathrm{A}} = -Y_{21}^{\mathrm{A}} f_1 \tag{45}$$

Then

$$g_2^{\mathrm{A}} = -\left(Y_{22}^{\mathrm{A}} + Y_{22}^{\mathrm{B}}\right)^{-1} Y_{21}^{\mathrm{A}} f_1 \tag{46}$$

or

$$g_2^{\mathrm{B}} = \left(Y_{22}^{\mathrm{A}} + Y_{22}^{\mathrm{B}}\right)^{-1} Y_{21}^{\mathrm{A}} f_1 \tag{47}$$

The velocity response at the receiving structure, node 3, is found by substituting Equation (47) into the last line of Equation (42.a) to give.

$$\dot{u}_3 = \left[Y_{32}^{\mathrm{B}} \left(Y_{22}^{\mathrm{A}} + Y_{22}^{\mathrm{B}}\right)^{-1} Y_{21}^{\mathrm{A}} \right] f_1 \tag{48}$$

Comparing Equation (48) with Equation (41) it is possible to see that the terms in the brackets represent the mobility of the assembly $\mathbf{Y}_{31}^{AB}$ by coupling the mobilities of the subsystems.

To carry out the investigations in this thesis, coupling in the frequency domain is used. More specifically, mobility and/or impedance matrices are used. In the following sections the mobility and impedance methodologies presented are applied to two simple systems in order to identify possible errors.

2.3 MOBILITY OR IMPEDANCE METHOD

The objective of this section is to show some basic applications of the mobility method, and to determine if there is any case where the results for the coupled system do not give accurate solutions when compared to the values calculated with the complete system.

2.3.1 Mass-spring system

The system shown in Figure 14 is one of the simplest systems to apply the substructuring methodology. Considering that the values of the masses are $m_1 = 0.14\text{kg}$, $m_2 = 0.85\text{kg}$ and the stiffness of the spring is $k = 1000\,N/m$. The force applied to the mass m_1 is a harmonic force with amplitude $F_1 = 1\text{N}$.

Figure 14 – Mass-spring system.

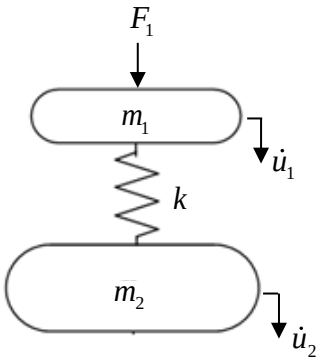

Source: Elaborated by the author.

As this system is formed only by components represented with lumped parameters the coupling between them can be carried out by analyzing the mobility or impedance diagram to determine if the components are connected in series or parallel.

Figure 15 – Mobility or impedance diagram.

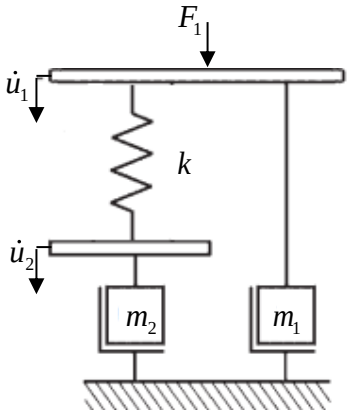

Source: Elaborated by the author.

Figure 15 shows the mobility or impedance diagram of the system. As the applied force is known, the velocity at the mass m_2 for the coupled system can be determined from the impedance equation given by

$$Z_c = Z_{m_1} + \frac{1}{\frac{1}{Z_{m_2}} + \frac{1}{Z_k}} \tag{49}$$

where

$$Z_m = i\omega m \quad \text{and} \quad Z_k = \frac{-ik}{\omega}$$

The mobility function is given by

$$Y_c = \frac{1}{Z_c} \tag{50}$$

Another way to calculate the coupled velocities of the system, as presented in the section 2.2.3.2, is to divide the system into subsystems and to calculate the driving point and transfer

mobilities of the subsystems. Figure 16 shows the subsystems and the respective connection points considered.

Figure 16 – Subsystems from the decoupled system.

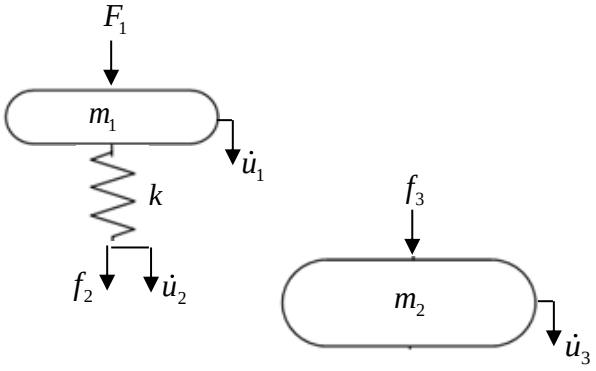

Source: Elaborated by the author.

The system containing mass m_1 and k can be described by

$$\begin{Bmatrix} \dot{u}_1 \\ \dot{u}_2 \end{Bmatrix} = \begin{bmatrix} Y_{11} & Y_{12} \\ Y_{21} & Y_{22} \end{bmatrix} \begin{Bmatrix} F_1 \\ 0 \end{Bmatrix} + \begin{bmatrix} Y_{11} & Y_{12} \\ Y_{21} & Y_{22} \end{bmatrix} \begin{Bmatrix} 0 \\ f_2 \end{Bmatrix} \tag{51a}$$

$$\dot{\mathbf{u}} = \mathbf{Y}\mathbf{f}_1 + \mathbf{Y}\mathbf{f}_2 \tag{51b}$$

where

$$Y_{11} = Y_{m1} = \frac{-i}{\omega m_1}$$
$$Y_{12} = Y_{21} = Y_{m1}$$
$$Y_{22} = Y_{m1} + Y_k$$

The system containing mass m_2 is described by

$$\dot{u}_3 = Y_{33} f_3 \tag{52}$$

where

$$Y_{33} = Y_{m2} = \frac{-i}{\omega m_2}$$

Considering the compatibility conditions at the interface

$$f_2 = -f_3$$
$$\dot{u}_2 = \dot{u}_3$$

Then, $f_2 = -Z_{33}\dot{u}_2$. In matrix form, the subsystem may be represented by

$$\begin{Bmatrix} 0 \\ f_2 \end{Bmatrix} = -\begin{bmatrix} 0 & 0 \\ 0 & Z_{33} \end{bmatrix} \begin{Bmatrix} \dot{u}_1 \\ \dot{u}_2 \end{Bmatrix} \tag{53a}$$

$$\mathbf{f}_2 = -\mathbf{Z}\dot{\mathbf{u}} \tag{53b}$$

Substituting equation (53) in to Equation (51), the coupled velocities are given by

$$\dot{\mathbf{u}} = \left[\mathbf{I} + \mathbf{YZ}\right]^{-1} \mathbf{YF}_1 \tag{54}$$

Figure 17 shows the driving point and transfer mobilities of the subsystems and Figure 18 shows a comparison between the calculated coupled velocities for the two methods presented.

Figure 17 – Mobilities from the subsystems.

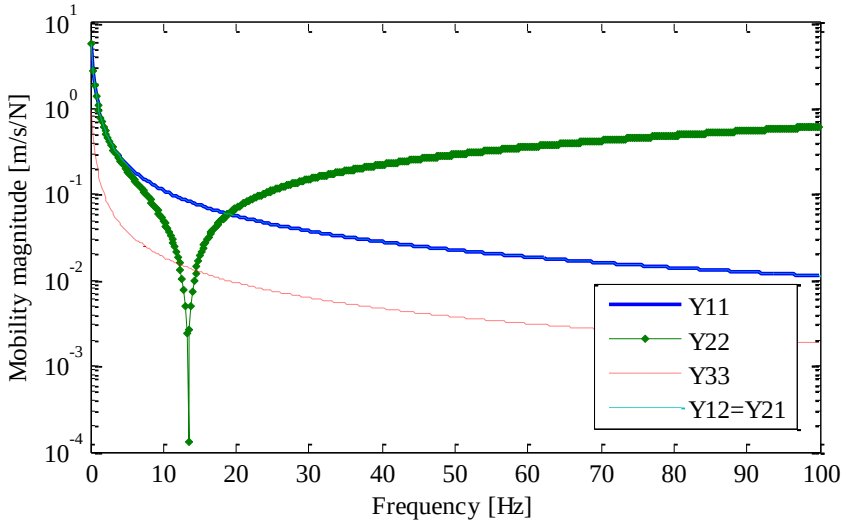

Source: Elaborated by the author.

Figure 18 – Velocities of the masses for the coupled system.

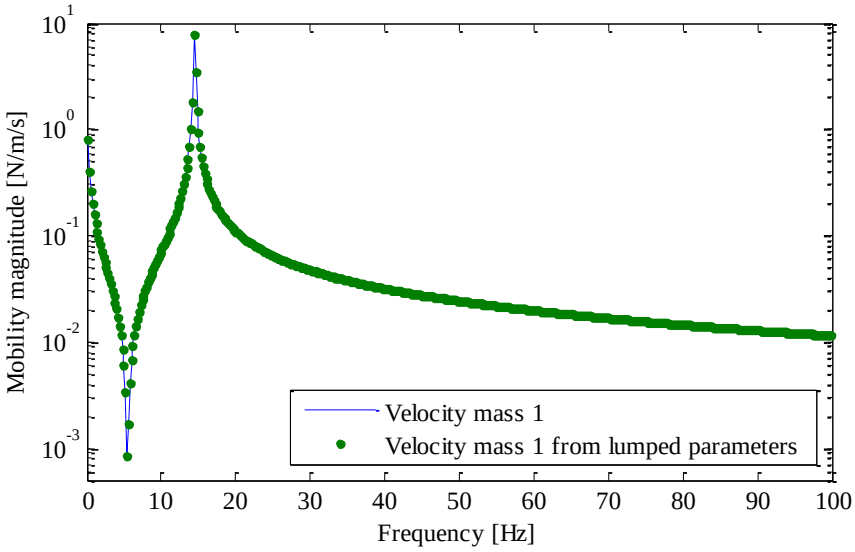

Source: Elaborated by the author.

Analyzing the results it is possible to see that for this simplest model both mobility method presented are valid. In the next section, a model including a beam and a change of excitation force position will be analyzed.

2.3.2 Mass-spring-beam system

Now consider the system presented in the Figure 19, where the mass is $m_1 = 0.006\text{kg}$, the stiffness of the spring is $k = 1000\,\text{N/m}$ and the dimensions of the beam are l = 0.5m, b = 0.03m and h = 0.005m. The beam has a Young modulus of $E = 200\text{GPa}$, a density of $\rho = 7850\,\text{kg/m}^3$ and loss factor $\eta = 0.001$.

Figure 19 – Mass-spring-beam system.

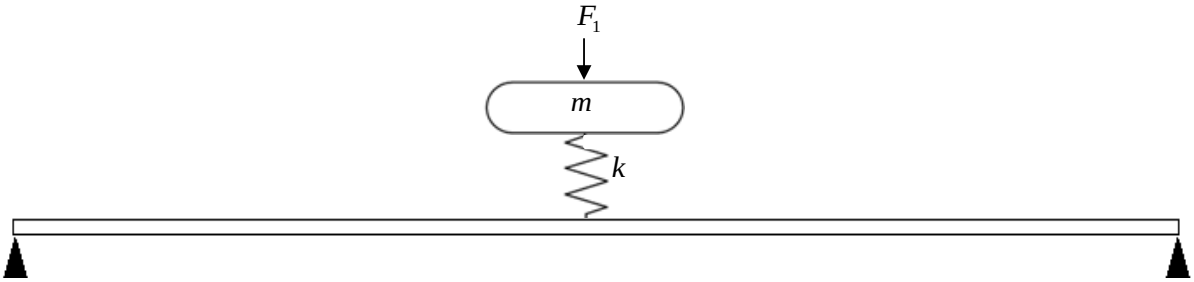

Source: Elaborated by the author.

In this case, to calculate the velocities of the mass and the beam for the coupled system it is not possible to use only lumped parameters because there is a beam in the system. The mobility of a finite beam with length l could be calculated using the modal summation or modal approach, in which the natural frequencies, ω_r, and mode shapes, ϕ_r, of the r^{th} mode are considered to calculate the driving point and transfer mobilities (Fahy and Gardonio, 2007). The mobility of the beam, considering flexural behavior is given by

$$Y_{v_b F_a}(\omega) = i\omega \sum_{r=1}^{\infty} \frac{\phi_r(b)\phi_r(a)}{M_r\left(\omega_r^{\,2}(1+i\eta) - \omega^2\right)} \tag{55}$$

where

$$\omega_r = \sqrt{\frac{K_r}{M_r}} \quad \text{in which} \quad M_r = ml\,, \quad K_r = EIk_{br}^4 l\,, \quad k_{br} = \frac{r\pi}{l}$$

so that

$$\omega_r = \frac{r^2\pi^2}{l^2}\sqrt{\frac{EI}{m}} \tag{56}$$

where

$$I = \frac{bh^3}{12}$$

Note that the velocity is measured at point (b) and the force is applied at point (a). For a simply supported uniform beam, the flexural mode shapes are given by

$$\phi_r = \sqrt{2}\sin\left(\frac{r\pi x}{l}\right) \tag{57}$$

In Equation (55) an infinite number of terms is needed to calculate the mobilities however, for real applications only a finite number of modes is taken into account.

Another method shown by Fahy and Gardonio, (2007), which reduces the error in the calculated mobilities, is to use an equation that considers a residue due to the truncation of the modes. Equation (55) is modified to

$$Y_{v_a F_b}(\omega) = i\omega\sum_{r=1}^{R}\frac{\phi_r(b)\phi_r(a)}{M_r\left(\omega_r^{\,2}(1+i\eta)-\omega^2\right)} + i\omega\sum_{r=R+1}^{\infty}\frac{\phi_r(b)\phi_r(a)}{M_r\omega_r^{\,2}} \tag{58}$$

where the additional term takes into account the response of the high frequency modes. With Equation (58) it is now possible to calculate the coupled velocities, considering the two subsystems. In the subsystem formed by the mass and spring, the mobilities are calculated using the lumped parameters, and for the beam subsystem, the mobilities are calculated using a modal summation.

To investigate the mobility method when the position of the force is changed, the coupled results are calculated for each case.

2.3.2.1 Force in the middle of the beam

First consider the force applied on the mass in the middle of the beam as show in the Figure 20.

Figure 20 – Subsystems from the mass-spring-beam system with the force applied to the mass.

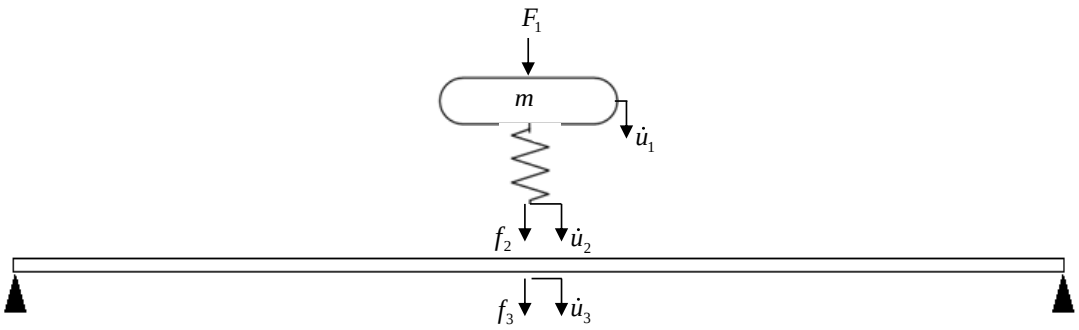

Source: Elaborated by the author.

The mobility matrices are generated and the coupling calculations are made as the same as shown in the Equations (51) to (54). The only difference is that the mobility Y_{33} is now calculated using the Equation (58), and as this is a point mobility. The points (a) and (b) in the equation are the same, i.e. (a) = (b). The analysis was made up to a frequency of 400 Hz, and Figure 21 show the mobilities from the subsystems mass-spring and beam.

Figure 21 – Mobilities from subsystem mass-spring, Y_{11}, Y_{12}, Y_{21} and Y_{22}, and beam, Y_{33}.

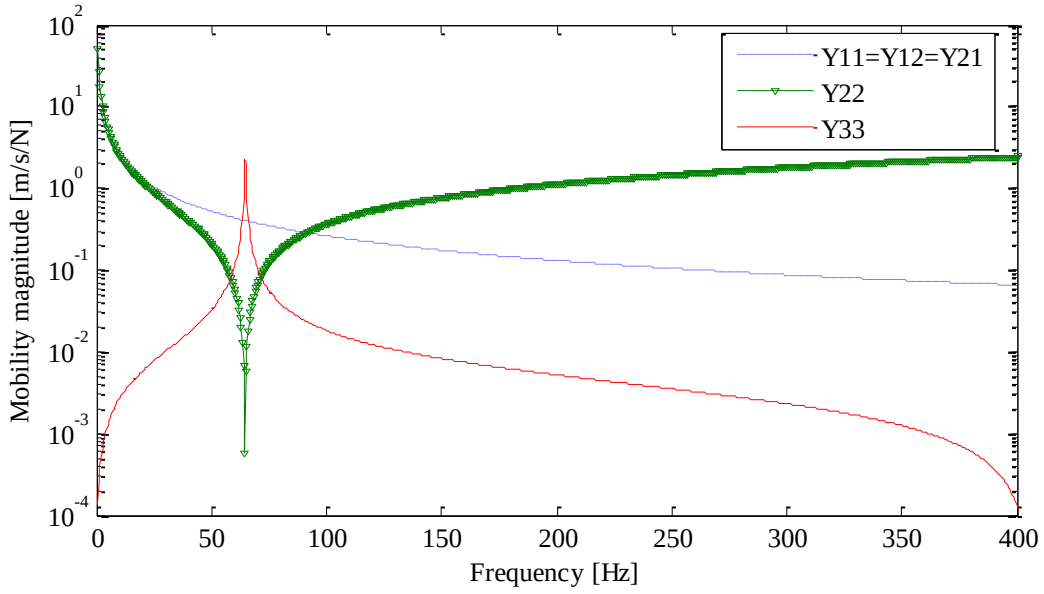

Source: Elaborated by the author.

As shown in Figure 21 the properties of the mass and spring were chosen so that mass-spring system has the same natural frequency as the first mode of the beam. In this case, when the beam is excited, the mass-spring subsystem acts like a dynamic vibration absorber. Solving Equation (54) gives the response of the coupled system. Figure 22 shows the resulting velocities of the mass and the beam for the coupled system.

Figure 22 – Coupled velocoty at the mass and at the point 3 in the beam.

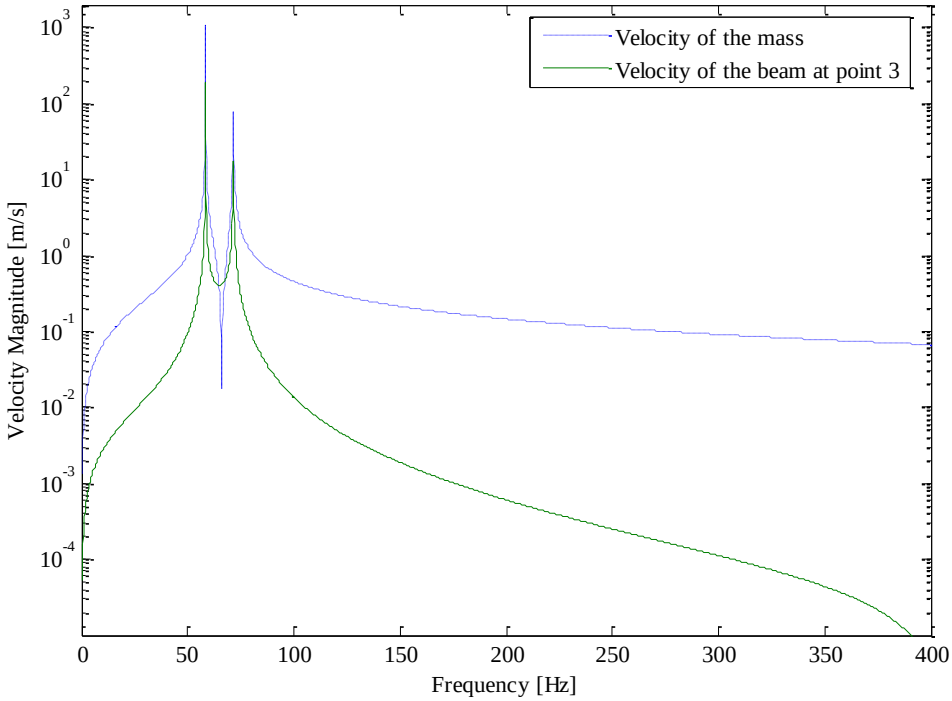

Source: Elaborated by the author.

2.3.2.2 Force applied to the beam

The methodology discussed above is applied to the same system as in Figure 20, but with excitation force being close to the end of the beam rather than on the mass. This is shown in Figure 23.

Figure 23 – Subsystems from the mass-spring-beam system with the force in the beam.

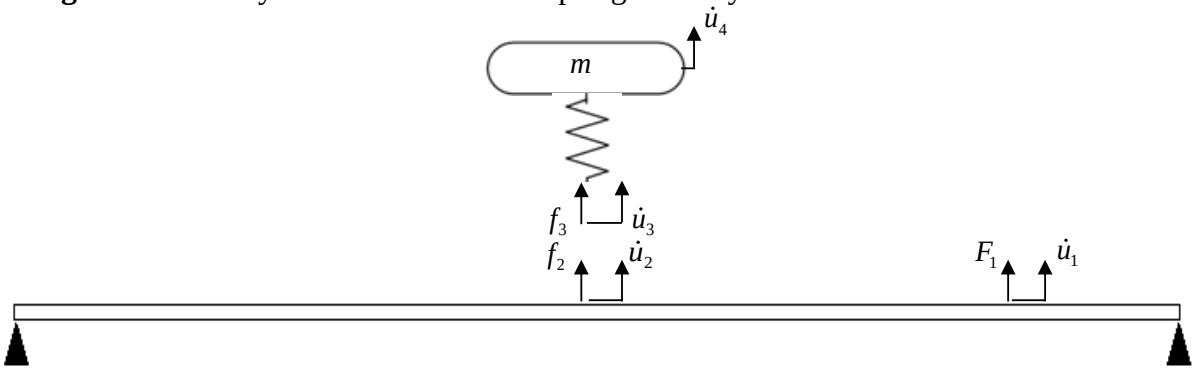

Source: Elaborated by the author.

The mobility matrices change a little because the force is applied to the beam, so the matrices for each subsystem are

Beam or source structure.

$$\begin{Bmatrix} \dot{u}_1 \\ \dot{u}_2 \end{Bmatrix} = \begin{bmatrix} Y_{11} & Y_{12} \\ Y_{21} & Y_{22} \end{bmatrix} \begin{Bmatrix} F_1 \\ 0 \end{Bmatrix} + \begin{bmatrix} Y_{11} & Y_{12} \\ Y_{21} & Y_{22} \end{bmatrix} \begin{Bmatrix} 0 \\ f_2 \end{Bmatrix} \tag{59a}$$

$$\dot{\mathbf{u}}_b = \mathbf{Y}_b \mathbf{f}_1 + \mathbf{Y}_b \mathbf{f}_2 \tag{59b}$$

Mass-spring or receiver structure.

$$\begin{Bmatrix} \dot{u}_3 \\ \dot{u}_4 \end{Bmatrix} = \begin{bmatrix} Y_{33} & Y_{34} \\ Y_{43} & Y_{44} \end{bmatrix} \begin{Bmatrix} f_3 \\ 0 \end{Bmatrix} \tag{60a}$$

$$\dot{\mathbf{u}}_{m-s} = \mathbf{Y}_{m-s} \mathbf{f}_3 \tag{60b}$$

In this case $f_4 = 0$ and considering the compatibility conditions

$$f_2 = -f_3$$
$$\dot{u}_2 = \dot{u}_3$$

Then, for the subsystem mass spring $\mathbf{f}_2 = -\mathbf{Z}_{m-s} \dot{\mathbf{u}}_{m-s}$, or in a matrix form, the subsystem is represented as.

$$\begin{Bmatrix} f_2 \\ 0 \end{Bmatrix} = -\begin{bmatrix} Z_{33} & Z_{34} \\ Z_{43} & Z_{44} \end{bmatrix} \begin{Bmatrix} \dot{u}_2 \\ \dot{u}_4 \end{Bmatrix} \tag{61}$$

However, it is necessary to write the matrices as a function of the complete velocity vector, so Equation (59) is rewritten as.

$$\begin{Bmatrix} \dot{u}_1 \\ \dot{u}_2 \\ \dot{u}_4 \end{Bmatrix} = \begin{bmatrix} Y_{11} & Y_{12} & 0 \\ Y_{21} & Y_{22} & 0 \\ 0 & 0 & 0 \end{bmatrix} \begin{Bmatrix} F_1 \\ 0 \\ 0 \end{Bmatrix} + \begin{bmatrix} Y_{11} & Y_{12} & 0 \\ Y_{21} & Y_{22} & 0 \\ 0 & 0 & 0 \end{bmatrix} \begin{Bmatrix} 0 \\ f_2 \\ 0 \end{Bmatrix} \tag{62}$$

$$\dot{\mathbf{u}} = \mathbf{Y}_b \mathbf{F}_1 + \mathbf{Y}_b \mathbf{f}_2$$

and for the mass-spring, the Equation (58) is rewritten as:

$$\begin{Bmatrix} 0 \\ f_2 \\ 0 \end{Bmatrix} = -\begin{bmatrix} 0 & 0 & 0 \\ 0 & Z_{33} & Z_{34} \\ 0 & Z_{43} & Z_{44} \end{bmatrix} \begin{Bmatrix} \dot{u}_1 \\ \dot{u}_2 \\ \dot{u}_4 \end{Bmatrix} \tag{63}$$

$$\mathbf{f}_2 = -\mathbf{Z}_{m-s} \dot{\mathbf{u}}$$

Substituting Equation (63) into Equation (62), the coupled velocities are given by

$$\dot{\mathbf{u}} = \left[\mathbf{I} + \mathbf{Y}_b \mathbf{Z}_{m-s} \right]^{-1} \mathbf{Y}_b \mathbf{F}_1 \tag{64}$$

Figure 24 shows the mobilities of the beam subsystem and the impedances from the mass-spring subsystem. Figure 25 shows the calculated coupled velocities.

Figure 24 – Mobilities and impedances from subsystems (a) beam and (b) mass-spring.

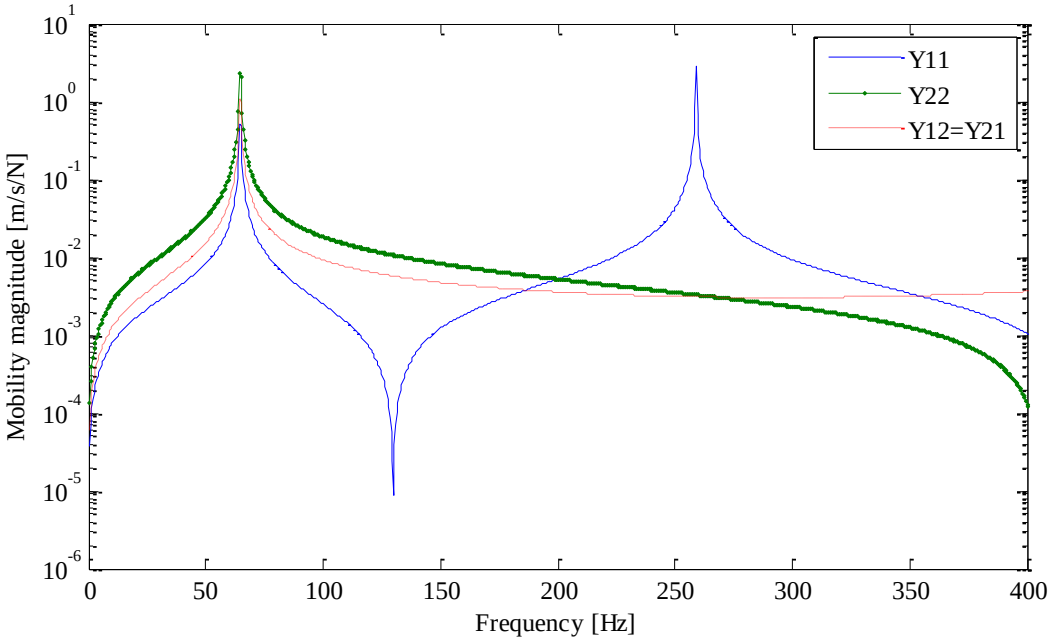

(a)

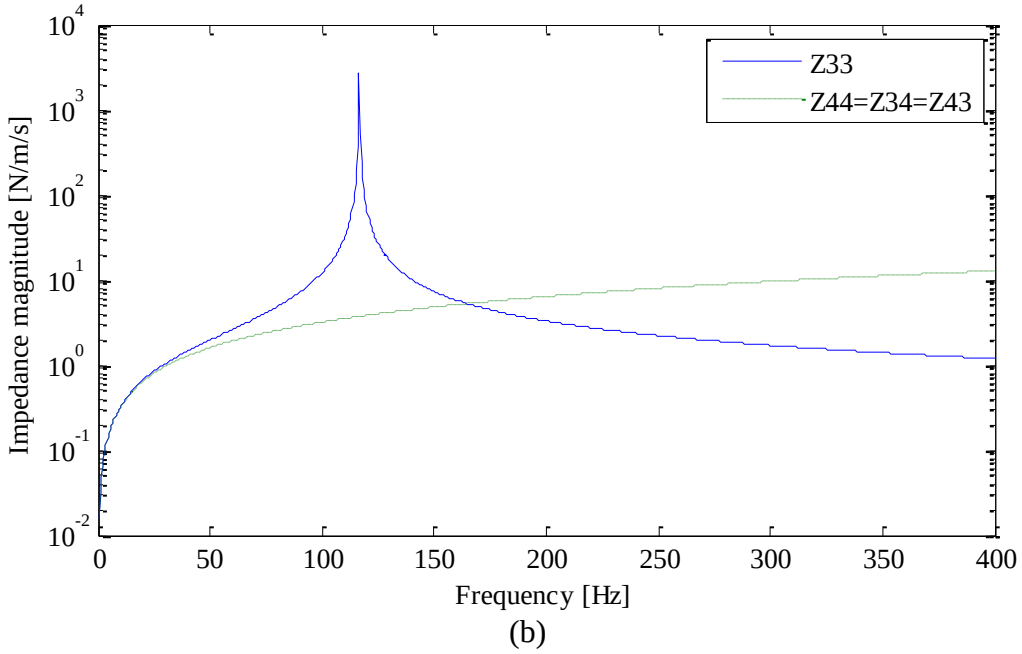

(b)

Source: Elaborated by the author.

Figure 25 – Calculated velocities for the coupled system.

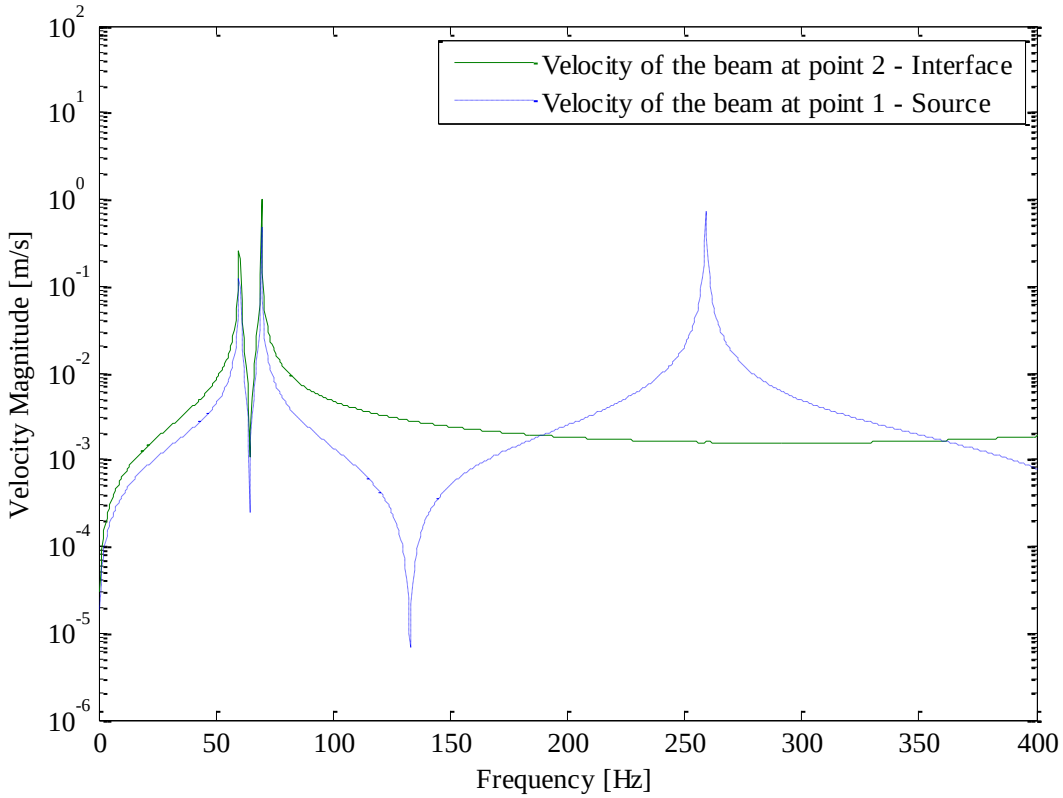

Source: Elaborated by the author.

As seen in Figure 25 the velocity of the mass at point 4 is missing, and analyzing the last row of Equation (62), it can be seen that this is not calculated using this approach. It

shows a weakness in this method. Every time it is desired to calculate the coupled velocity in a subsystem without an action-reaction force pair, it is not possible to calculate the velocity at this point. It is only possible to calculate the responses at the connection points and at the excitation point.

For cases when it is necessary to calculate the response at a remote point in the receiver structure it is necessary to use a different methodology. The transfer path analysis approach is a method that shows good results for this purpose, and the next section shows its application to the mass-spring-beam system.

2.4 TPA FROM THE SUBSYSTEM ADMITTANCE METHOD

As described in section 2.2.3.3, the TPA method allows the calculation of the response at a remote point of the receiver structure due to a source in the excitation structure.

2.4.1 Mass-spring-beam system with the force in the end of the beam

The system analyzed is the same as presented in Figure 23. Figure 26 shows this system with the nomenclature for the TPA method.

Figure 26 – Subsystems from the mass-spring-beam system for the TPA method.

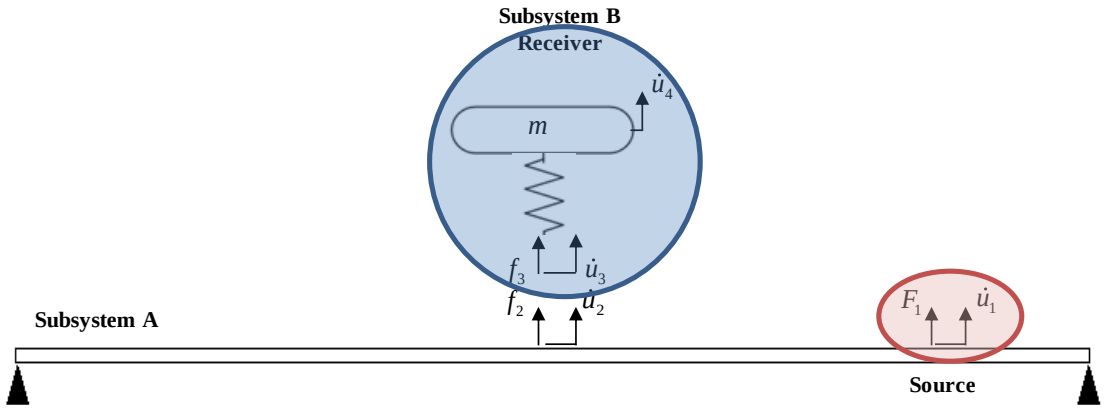

Source: Elaborated by the author.

Using the same mobilities calculated previously, and rewriting Equation (48) for this system, the response at the receiver structure in point 4 can be calculated as

$$u_4 = \left[Y_{43}^B \left(Y_{22}^A + Y_{33}^B \right)^{-1} Y_{21}^A \right] F_1 \tag{65}$$

Figure 27 shows the velocity at point 4, receiver structure, for the complete system, considering the coupling using the admittance subsystem assembly.

Figure 27 – Velocity at point 4 for the complete system.

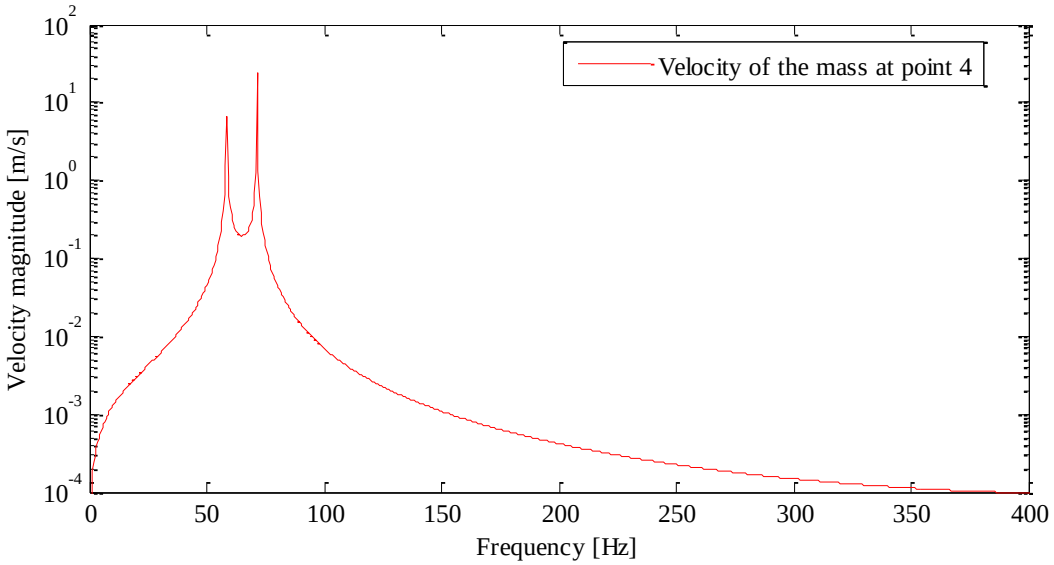

Source: Elaborated by the author.

The only disadvantage of this method is that it is not possible to predict the velocity at the excitation point, for the coupled system, but the velocities at the receiver structure and at the interface could be calculated just changing the mobilities using the TPA coupling method.

To verify if the methods show correct results for the coupled system a simulation using a finite element method was made with the complete system. Figure 28 shows the velocities of the beam at points 1, 2 and at the mass, receiver structure. In this case as can be seen the methods works well.

Figure 28 – Coupled velocities using finite element model.

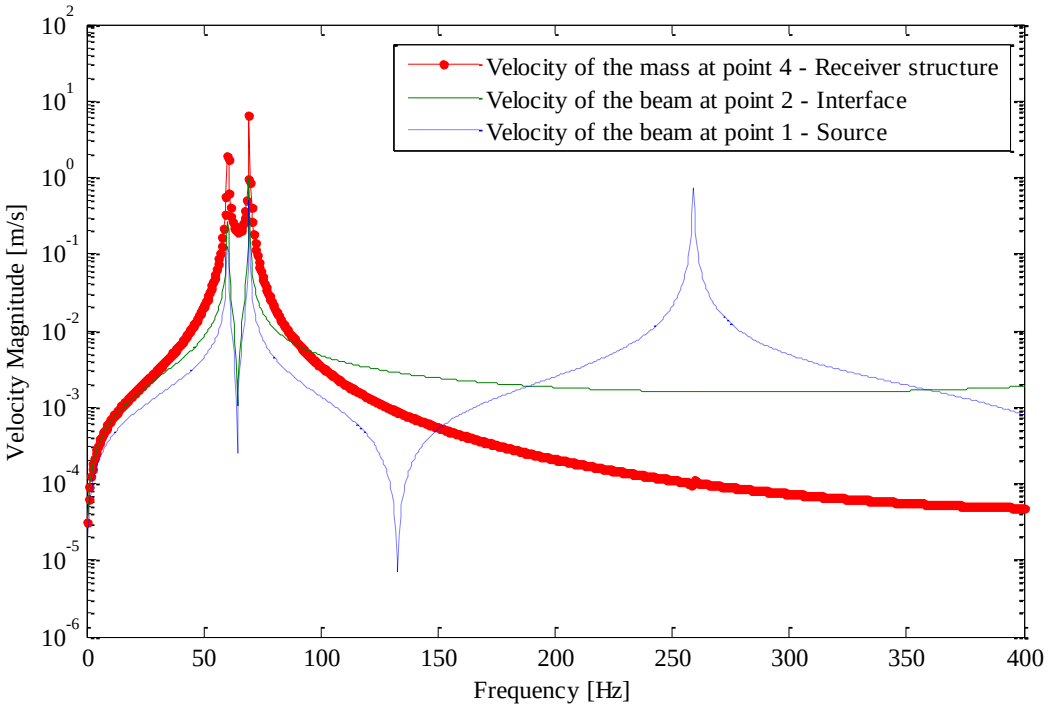

Source: Elaborated by the author.

2.5 CONCLUSIONS

In this chapter, the main ways to substructure and couple a structural system, considering the physical, modal and frequency domains has been described. A general mobility or impedance coupling was presented in section 2.3 and the transfer path analysis method from subsystem admittance method has been described in section 2.4, and then applied to a mass-spring-beam vibrational system to determine its behavior. The advantages and disadvantages have been discussed depending on the objective of the analysis. For example, when the general mobility method studied in this chapter is used, it is only possible to predict the responses at the connection points and at the excitation point. For cases when it is necessary to measure the response at a remote point in the receiver structure it is necessary to use the transfer path method, using this method is possible to calculate the velocities at the interface but it is not possible predict the velocities at the source, for the coupled system.

Until now only a point connection between the subsystems has been considered. The objective of the thesis is to substructure systems with isolators at the coupling points which have a distributed connection. Chapter 3 will show the application of the methods for a distributed connection.

3 SUBSTRUCTURING APPROACH APPLIED TO A DISTRIBUTED CONNECTION

In many engineering applications, where it is desirable to reduce the transmission of vibration, a rubber isolator is often used to connect the source to the receiver structure. This type of component has a distributed instead of a point connection. This chapter analyzes a distributed connection due to a rubber isolator, for a translational force applied to a system formed by a mass, isolator and a beam. The position of the subsystem mass-isolator on the beam is varied to determine the effect of position. To accomplish this work the material properties of the rubber isolator and the beam, are first determined experimentally.

3.1 DETERMINATION OF THE ISOLATOR MATERIAL PROPERTIES

To apply the coupling methodologies to a system with a distributed connection, it is first necessary to determine the properties of the rubber isolator and the beam. The experimental results are compared with the FE model and then the model is adjusted accordingly.

3.1.1 Rubber isolator

The rubber isolator used in this work is the same as that used in a refrigeration system to connect the compressor to the fridge. This type of isolator is made from vulcanized natural rubber. Figure 29 show this isolator which was donated by the company Whirlpool S. A.

Figure 29 – Rubber isolator used in the system.

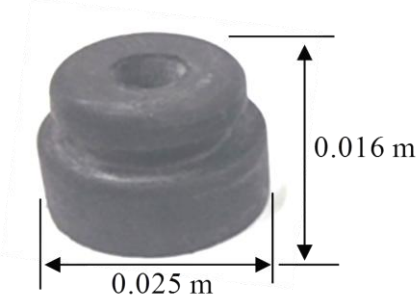

Source: Elaborated by the author.

First, it is necessary to determine the static properties and to calculate the static stiffness. An experiment was conducted using a compression testing machine as shown in the Figure 30, this is a universal testing machine for compression and traction model EMIC and has a 600kN loading capacity. A static force was applied to compress the elastomeric element, and the measurement was made five times each for three rubber isolators.

Figure 30 – Measurement scheme to determine the static properties.

Source: Elaborated by the author.

To better represent the rubber isolator, considering its application, the upper part of the isolator was removed and the measurements were carried out. Figure 31 shows the test from 1 mm to 3mm of compression.

Figure 31 – Measurements realized without the upper part of the isolator.

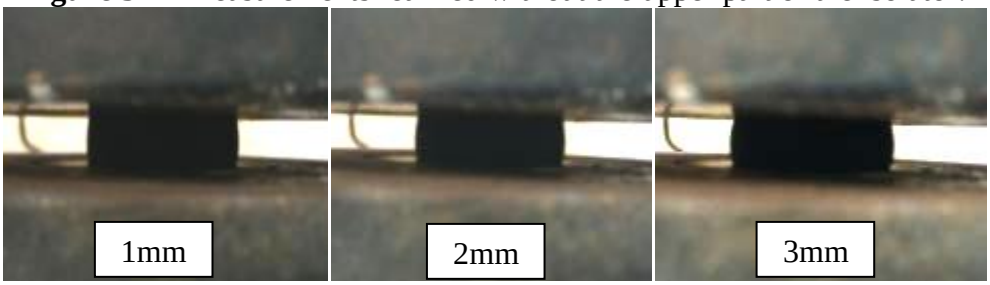

Source: Elaborated by the author.

The analytical model to complement this experiment is shown in Figure 32, where the function $A(u)$ could be non-linear. After the measurements were made, the polynomial order is determined using a polynomial regression methodology to best fit the measured data. In this method the sum of squares between measure data and model is minimized (Richards e Singh, 2001). This process is represented by

$$A(u) = \sum_{j=a}^{b} k_j u^j \tag{66}$$

where k_j are the coefficients of the polynomial determined for the force-deflection data measured and A is the empirical model.

Figure 32 – Analytic model for the static experiment.

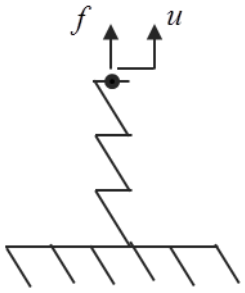

Source: Adapted from Richards e Singh, (2001).

Another important coefficient to determine the accuracy of the polynomial fit to the curve is the determination coefficient, R^2, that indicates the correlation with the measurement data and the curve fitted.

Figure 33 shows the experimental data with first and third order polynomial regression to determine if the isolator has non-linear geometrical behavior due to large deformations. To determine the accuracy of the curve fit the determination coefficient, which indicates the correlation between the experimental data and the polynomial was calculated.

Figure 33 – First measurements realized with the complete isolator.

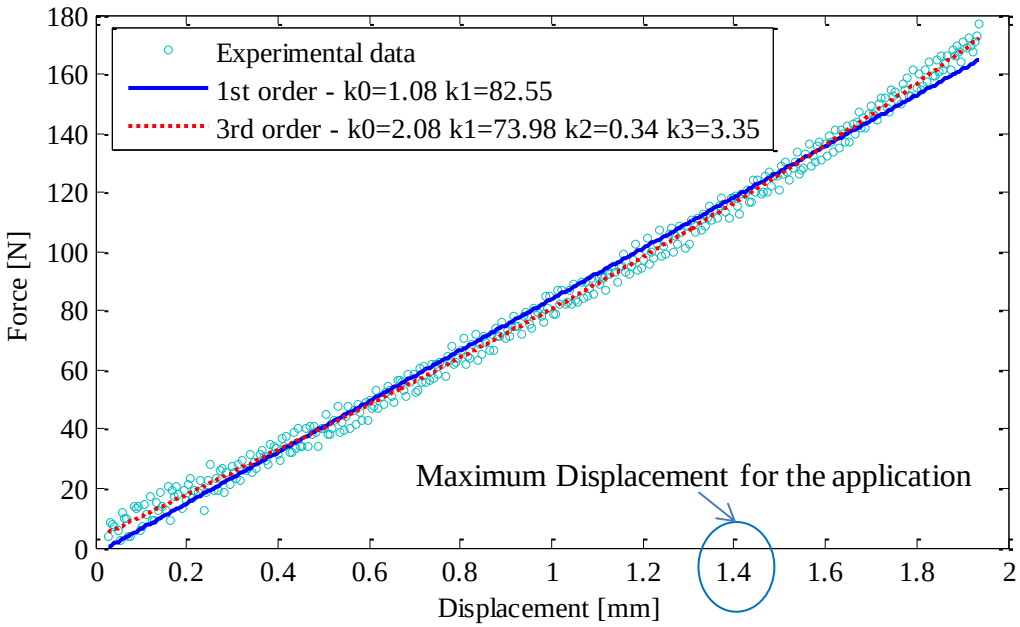

Source: Elaborated by the author.

For 2mm of deformation the determination coefficient is $R^2 = 0.9965$ to the first order and $R^2 = 0.9982$ for the third order polynomial regression. When only up to 1.4mm deformation is considered, that is the maximum displacement for the refrigeration system applications presented in the motivation, the determination coefficient is $R^2 = 0.9961$ and $R^2 = 0.9968$ for the first and third order respectively. This means that for small displacements the isolator could be represented as a linear system with the coefficients of the polynomial $k_0 = 1.08$, $k_1 = 82.55$, and so the static stiffness coefficient is estimated to be $k = 82550\,\mathrm{N/m}$.

To determine the Young's modulus of the rubber isolator, a static analysis was conducted in Ansys (2013) using a model of the isolator generated by solid elements, with ten nodes having three degrees of freedom at each node, translations in the nodal x, y, and z

directions as shown in the Figure 34, in the software this element is called as SOLID 187 and has a quadratic displacement behavior that is well suited to modeling irregular meshes.

Figure 34 – Ansys SOLID187 element type.

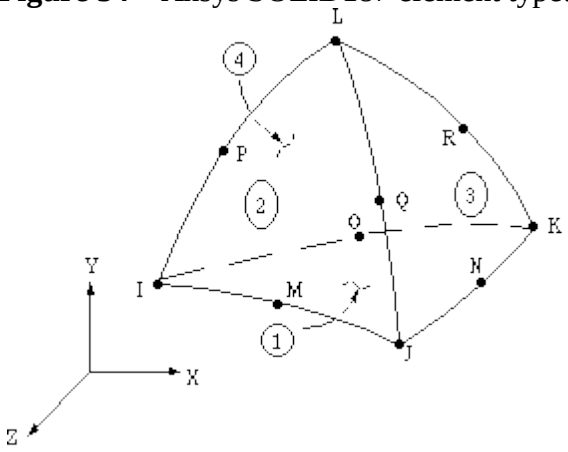

Source: Ansys (2013).

The mesh convergence curve was made to determine the largest element that represents the model with a small error. Figure 35 shows the relationship between the normalized displacement and the element size. Based on this, the element size used in the model was chosen to be 2 mm, but as the automatic mesh is chosen this element size can be more refined where there are geometric imperfections.

Figure 35 – Mesh convergence curve to rubber isolator.

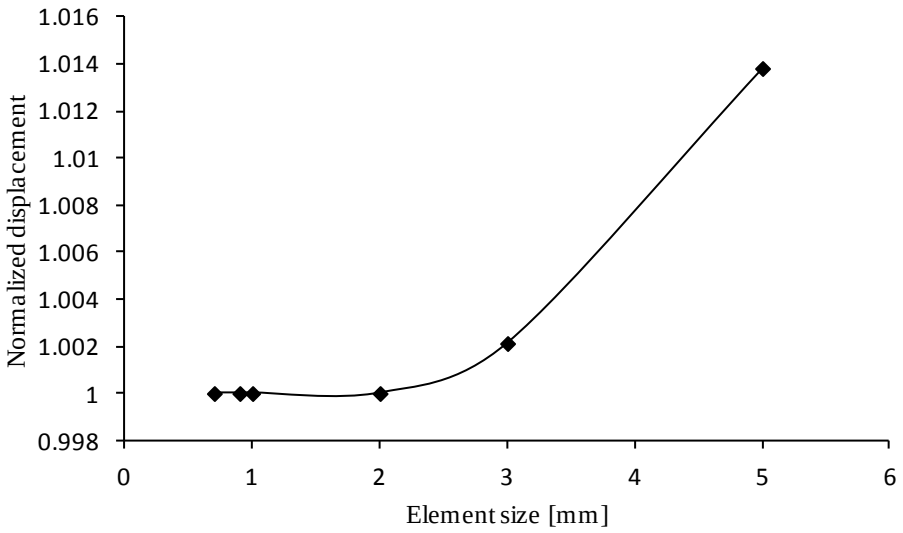

Source: Elaborated by the author.

The Young's modulus value of the rubber isolator was adjusted until the deformation of the simulated isolator was as close as possible to the experimental measurements, considering a constant temperature. Figure 36 shows the compressed rubber isolator in the simulation. Figure 37 show the displacement curve for the experimental and numerical results considering the first order polynomial regression. The Young's modulus is determined is $E = 1.3\text{x}10^{6}\ \text{N/m}^2$.

Figure 36 – Finite Elements mesh used in the static analysis.

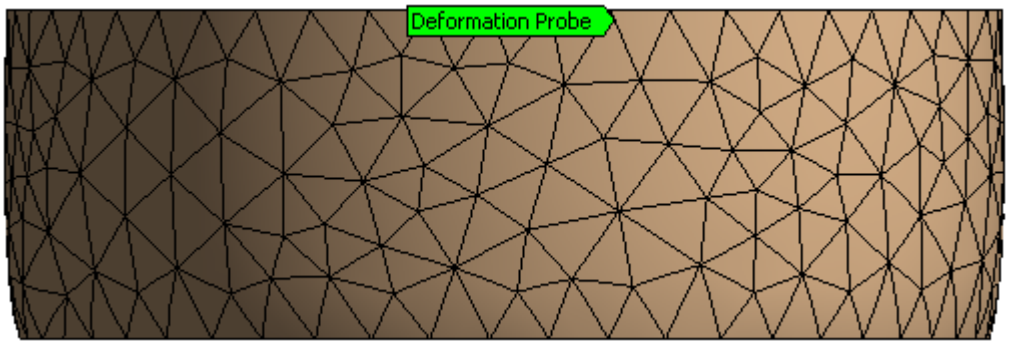

Source: Elaborated by the author.

Figure 37 – Displacement curve for the experimental and numerical results considering the first order polynomial regression.

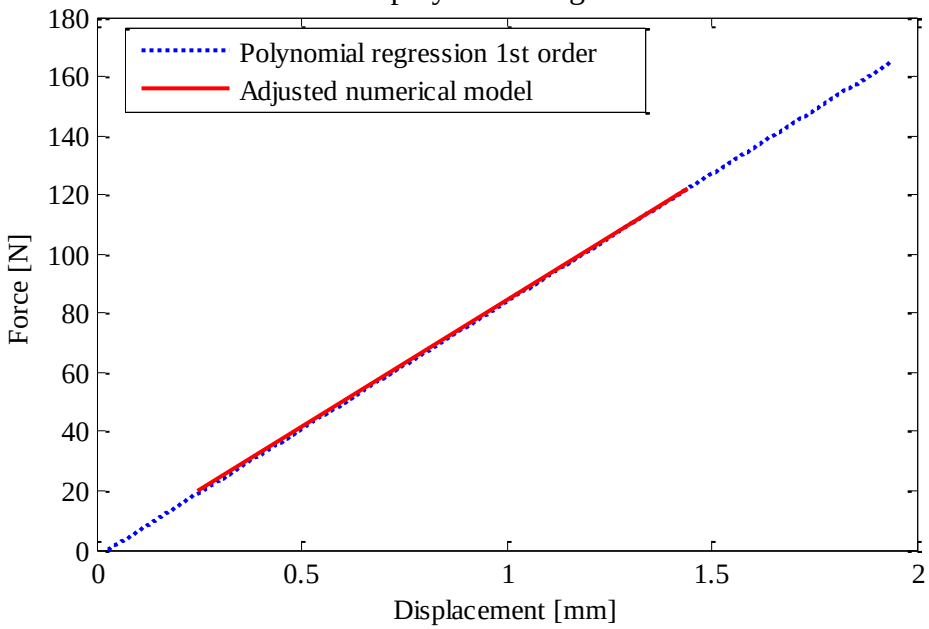

Source: Elaborated by the author.

According to Mott and Roland (2009), for rubber materials, Poisson's ratio is approximately $\nu = 0.499$ and this bibliographic value is used because of difficulties in measure experimentally due to the geometry of the rubber isolator. Therefore the shear modulus could be calculated as

$$G = \frac{E}{2(1+\nu)} = 4.34\text{x}10^5 \text{ N/m}^2 \tag{67}$$

The material density was determined, by measuring the mass and the volume of the isolator, resulting in $\rho = 1255 \text{kg/m}^3$.

Considering an experimental mount as showed in Figure 38, it is possible to determine dynamic stiffness and the loss factor of the model. To do this, the isolator was fixed to a rigid base and two different masses were placed on the isolator, 0.12kg and 0.76kg, to determine the dynamic stiffness. To realize the measurements, an accelerometer model PCB 352C03 and an impact hammer model PCB 086C02 were used. Figure 38 shows the experimental mount and measurements for the mass of 0.76kg.

Figure 38 – Experimental time results considering a mass of 0.76 kg.

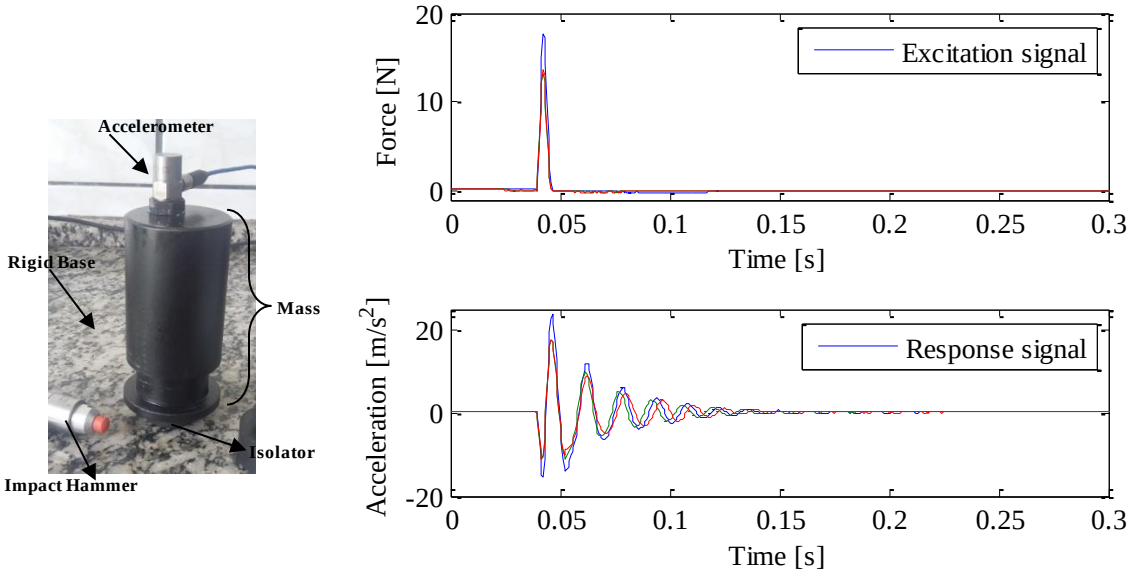

Source: Elaborated by the author.

Considering the experimental response time signal for the both masses, 0.12kg and 0.76kg, it is possible to determine the values of dynamic stiffness as given by.

$$k = \omega_n^2 m \tag{68}$$

Using the average time period measured in the experimental data, the natural frequency for the system is estimated to be approximately $\omega_n = 840\,\text{rad/s}$ for the mass of 0.12 kg, and $\omega_n = 333\,\text{rad/s}$ for the mass of 0.76 kg. With these measurements, the mean value of the dynamic stiffness is found to be approximately $k_{dynamic} = 84776\,\text{N/m}$.

The loss factor can be determined using the same time domain response signal. First, the damping ratio, ζ, is estimated through the logarithmic decrement method. According to Ewins (1994), the logarithmic decrement is a method used to measure damping in time domain. In this method, the free vibration displacement amplitude history of a system to an impulse is measured and recorded. A typical free decay curve is shown as in Figure 38. Logarithmic decrement is the natural logarithmic value of the ratio of two peak values of displacement in free decay vibration, X_i and X_{i+n}.

$$\delta_n = \ln\left|\frac{X_i}{X_{i+n}}\right| = \frac{2n\pi\zeta}{\sqrt{1-\zeta^2}} \tag{69}$$

where *n* is the number of periods considered between the peak values.
The mean value of the damping ratio found for the measurements is $\zeta = 0.062$. However, the objective is to determine the loss factor, η, where $\eta = 2\zeta$. So, the value determined for the loss factor is approximately $\eta = 0.1$.

Table 1 show a summary of all material properties for the rubber isolator. Note that for this work the effect of temperature changes, is not considered.

Table 1 – Summary of rubber isolator properties.

Material	E (N/m^2)	ν	G (N/m^2)	ρ (kg/m^3)	k_{static} (N/m)	$k_{dynamic}$ (N/m)	η
Rubber Isolator	$1.3\text{x}10^6$	0.499	$4.34\text{x}10^5$	1255	82550	84776	0.10

Source: Elaborated by the author.

Examining Table 1, it can be seen that there is a difference between the static and dynamic stiffness, $k_{dynamic} > k_{static}$. This could be explained because the static and the dynamic stiffness are calculated from experimental data in which could have some small errors, even from the experimental mounting as from the measurements.

3.1.2 Beam

The beam used in the vibratory system has the following dimensions 0.37 x 0.031 x 0.0017m. A finite element model of the beam was generated by shell elements, with four nodes having six degrees of freedom at each node, translations in the nodal x, y, and z directions, and rotations about the x, y, and z-axes as shown in the Figure 39, in the software this element is called SHELL181 and the same process of mesh convergence curve was made to determine the best element size for the beam models, resulting in elements with 3mm length. The FEM beam has the material properties adjusted so that the numerical response matches with experimental measurements. The density was calculated measuring its mass and volume, resulting in $\rho = 7900\,\mathrm{kg/m^3}$.

Figure 39 – Ansys SHELL181 element type.

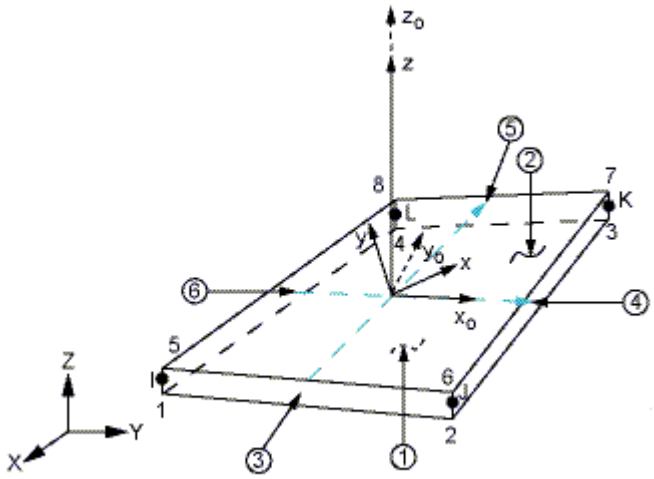

Source: Ansys (2013).

Figure 40 shows the experimental arrangement used to determine the Young's modulus and the loss factor of the beam. To measure the data, an accelerometer model PCB 352A25 and an impact hammer model PCB 086C02 were used, and for the acquisition of the signals a LMS SCADAS XS system was used. The loss factor was determined by performing an experimental frequency response function measurement as shown in Figure 40 and the half-power bandwidth method is used to estimate it from the frequency domain data as described by Rao (2009). In this method, for each natural frequency, ω_n, there is a peak in the FRF amplitude and three decibels less than the peak there are two points corresponding to half

power points, ω_1 and ω_2. If there is greater damping in the system, the frequency range between these two points is larger. The loss factor is defined as the ratio of the frequency range between the two half power points to the natural frequency of this mode (Maia and Silva, 1996), i.e.,

$$\eta = \frac{\omega_2 - \omega_1}{\omega_n} \tag{70}$$

The value calculated and used in the FE model is an average of the loss factor calculated for each natural frequency, resulting in $\eta = 0.001$.

Figure 40 – Experimental mount to determine beam material properties.

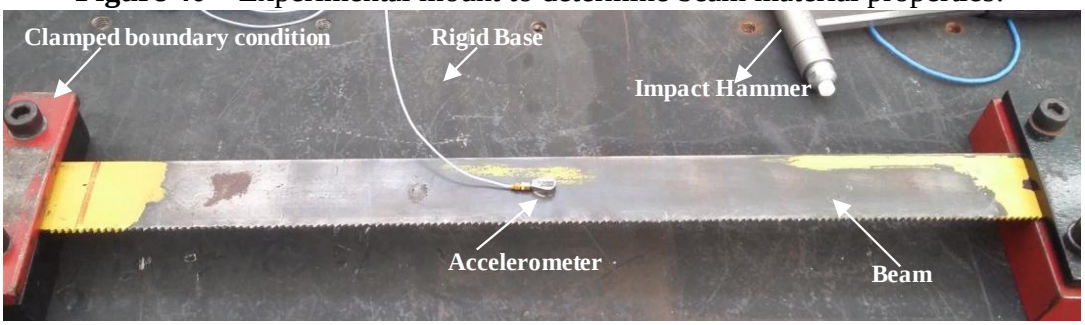

Source: Elaborated by the author.

The system shown in Figure 40 was expected to have boundary conditions as a clamped-clamped beam and the adjusted Young's modulus was found to be $E = 178 \times 10^9 \ \mathrm{N/m^2}$. To adjust the beam model, the value of the Young's modulus was varied between $170 \mathrm{x} 10^9 \ \mathrm{N/m^2}$ from $200 \mathrm{x} 10^9 \ \mathrm{N/m^2}$ until the optimal value that best represents the experimental data was found. Figure 40 shows a comparison between an experimental data that is an average of 5 measurements of the beam and numerical driving point accelerance close to the end of the beam. The frequency range considered for the next studies consider the first four flexural beam modes, which occur in the frequency up to 700Hz.

Figure 41 – Beam driving point function close to the end of the beam.

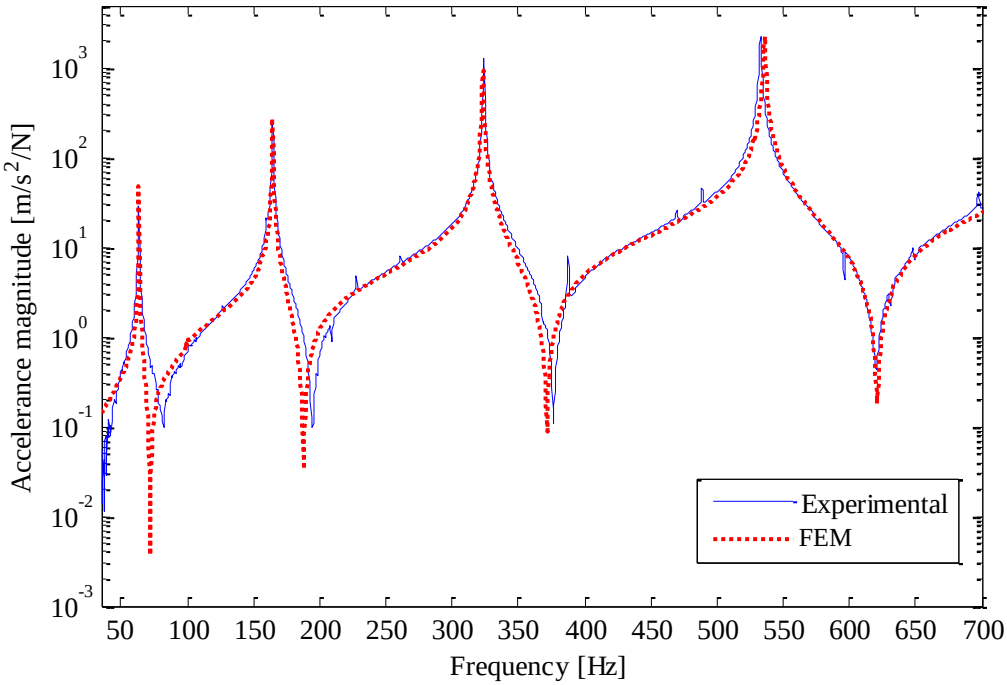

Source: Elaborated by the author.

With the finite element models of the rubber isolator and beam adjusted as described above, it is possible to use the finite element method to study the substructuring methodology applied to a distributed connection rubber isolator connected to the beam. The following sections discuss the variation of the isolator position over the beam, in the middle, ¼ of beam and ⅛ of beam, with a normal force applied to the beam.

3.2 MASS-ISOLATOR-BEAM SYSTEM WITH A NORMAL FORCE EXCITATION

The system studied is shown in Figure 42. It consists of the FE models of the isolator and the beam, with properties chosen as described previously. In this case a normal force is applied to the upper beam, over the isolator. This beam has the following dimensions 0.06 x 0.03 x 0.0015m with the same material properties determined for the lower beam, and the position of the isolator is changed from the middle of the beam to ¼ of the beam and close to the end of the beam as shown in Figure 43.

Figure 42 – Finite element structural model.

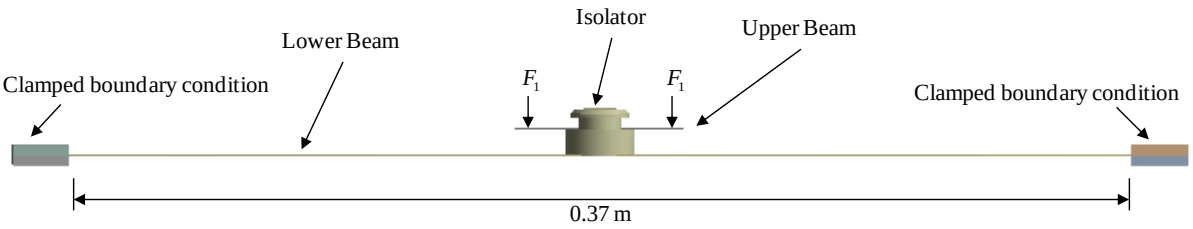

Source: Elaborated by the author.

The objective of the section is to analyze the coupling of the modes of the beam and the isolator when the position of the isolator on the beam was changed and to determine if the distributed connection of the isolator could be represented as a point connection or multi point connection.

3.2.1 Effect of isolator position

To identify if the position of isolator modifies the coupling between the beam and isolator modes, an analysis was made. The modes of beam and isolator, considered separately, are compared with the modes for the coupled system when a normal force is applied to the plate above the isolator. The isolator was placed on the beam, at positions of ½ , ¼ and ⅛ of the beam as shown in Figure 43.

Figure 43 – Position of isolator coupling, (a) in the middle of the beam, (b) at ¼ of the beam and (c) at ⅛ of beam.

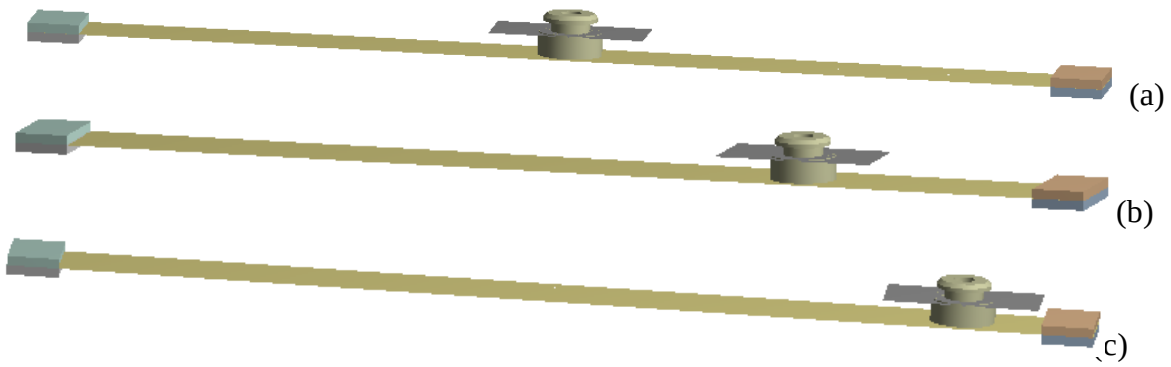

Source: Elaborated by the author.

With the aim of determining if the position of isolator on the beam changed the modal coupling, some analysis was made. First, a modal and a harmonic analysis for the isolator and beam isolated, from each other, was calculated, considering the boundary conditions of the beam as clamped-clamped and the isolator with its base as a fixed support. Then a modal and harmonic analysis was carried out for the complete system for the three cases, shown in Figure 43. For the harmonic analysis a harmonic normal force with an amplitude of 1N was applied to the upper beam over the isolator for frequencies up to 700Hz. Only the flexural modes of the beam were excited. Figure 44 shows an example of harmonic response of the beam alone, and for the complete system with the isolator in the middle of the beam. The same comparison was made for the other positions on the beam as shown in the Figures 45 and 46. More details about the studies made for the coupling of the modes is given in Appendix B.

Figure 44 – Velocity in the middle of the beam, with the isolator in the middle of the beam compared with the beam isolated.

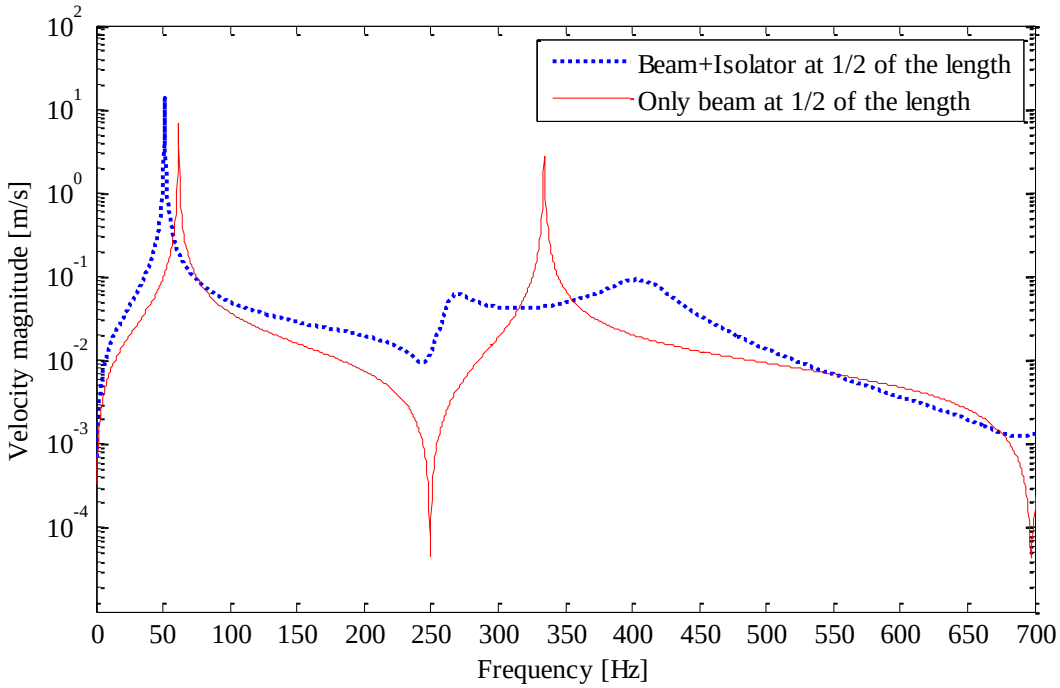

Source: Elaborated by the author.

Figure 45 – Velocty at ¼ of the beam, with the isolator at ¼ of the beam compared with the beam isolated.

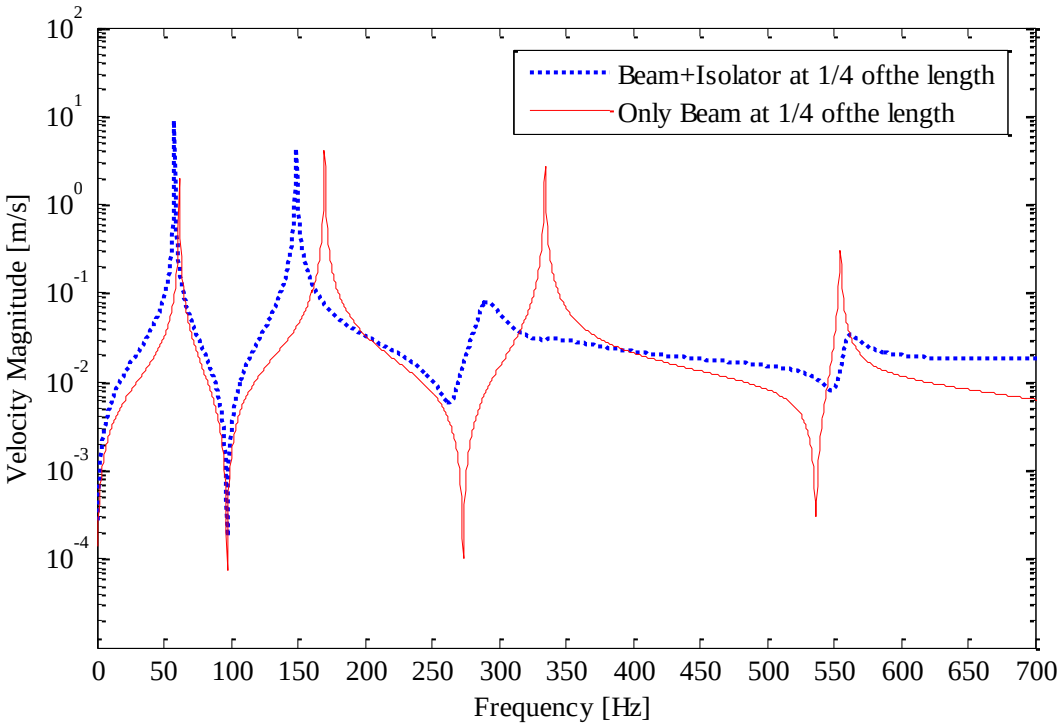

Source: Elaborated by the author.

Figure 46 – Velocty at ⅛ of the beam, with the isolator at ⅛ of the beam compared with the beam isolated.

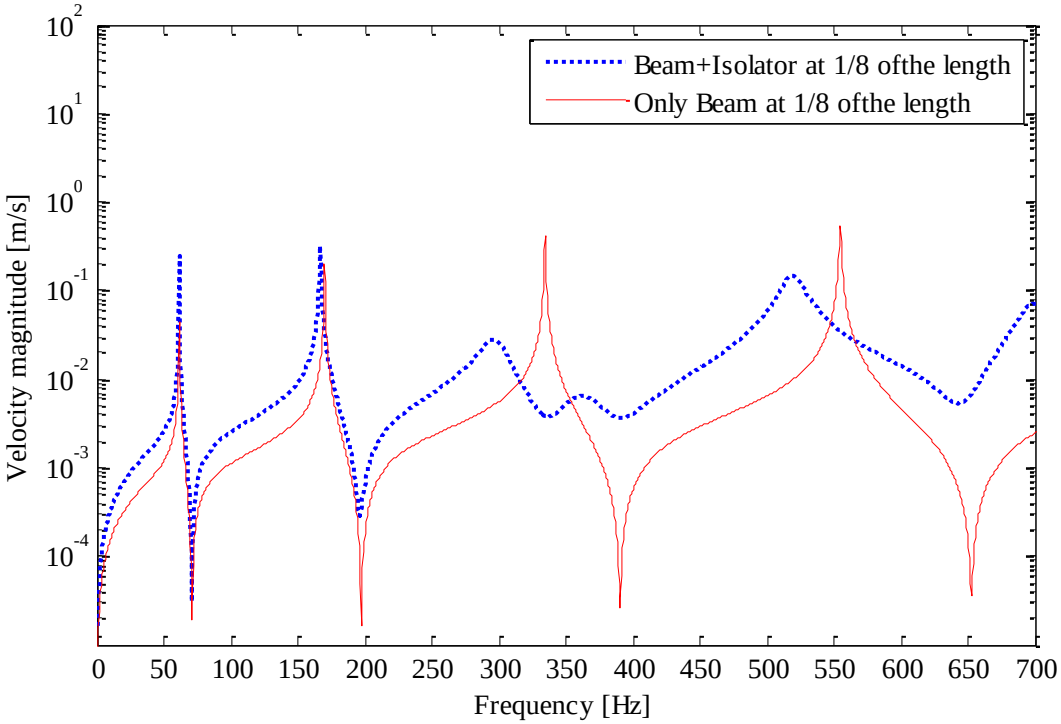

Source: Elaborated by the author.

Considering the results from Figure 44, table 2 shows the modes for beam alone and the isolator alone in the frequency range of interest, and which ones are connected to form new modes in the complete system.

Table 2 – Modes of beam, isolator and complete system for the excitation in the middle of the beam.

Bandwidth 0 – 200Hz	
Flexural modes of beam (Hz)	
61.7 Hz 	
Isolator Modes (Hz)	
There is no mode of isolator in this bandwidth	
Complete system modes (Hz)	
52.2 Hz 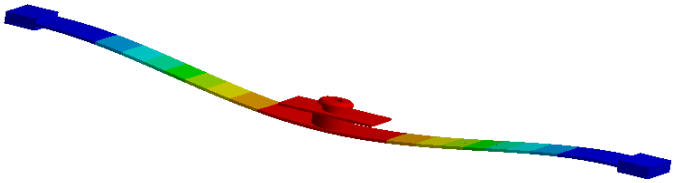	
Bandwidth 200 – 700Hz	
Flexural modes of beam (Hz)	
334.4 Hz 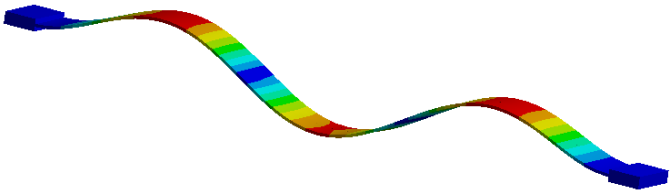	
Isolator Modes (Hz)	
346.1Hz 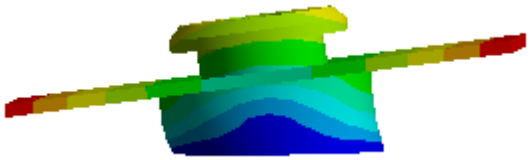	
Complete system modes (Hz)	
332.1 Hz 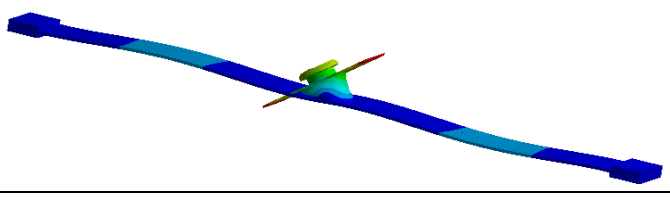	446.5 Hz 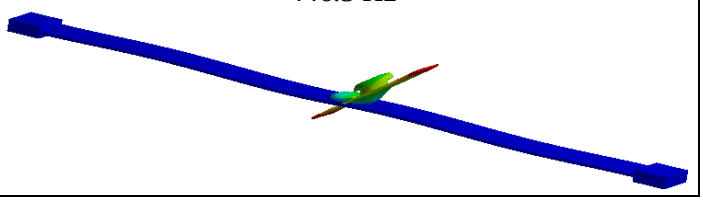

Source: Elaborated by the author.

In this system, there are basically three modes that couple, in the frequency range of interest. For example, for the first and second flexural modes of the beam, when the isolator is connected, regardless of the position, the natural frequencies for the complete system are decreased. It represents an addition of mass to the beam because the coupling occurs in a mass-like region of the isolator.

Considering the fourth flexural mode of the beam and rubber isolator coupled at ¼ of the beam, the situation is different. For this case, the coupled frequency is higher than the beam isolated frequency, as shown in the Appendix B.

The last situation that occurs for the third mode of the beam. In this case the isolator mode is close to the beam mode, so in the coupled system the isolator acts like a vibration absorber. The effectiveness of the dynamic vibration absorber depends on the position the isolator on the beam. When the rubber isolator is positioned at points with higher deflection, the effectiveness of the Dynamic Vibration Absorber is great, as discussed in Appendix B.

In this section, it has been observed that the modes of the beam and rubber isolator couple, independently of the position of isolator connection on the beam. With this knowledge, the next section studies, the distributed connection of the isolator and the beam when frequency domain coupling is used, only for the isolator in the middle of the beam.

3.2.2 Distributed connection represented as a multi-point coupling

Considering the isolator in the middle of the beam, as shown in Figure 42, and the force applied in the upper beam, over the isolator, represented in Figure 47. In this section, the distributed connection between the rubber isolator and the lower beam is analysed considering multi-point coupling instead of a single point of connection between the subsystems.

Using the TPA substructuring approach, that allows the responses at different points in the receiver structure to be calculated, the system shown in the Figure 41 was substructured. This was done by first considering the rubber isolator to be coupled to the beam at two points and then the number of coupling points are increased to four and eight points of connection.

Initially, the connection between the subsystems mass-isolator (source or subsystem A), and beam (receiver structure or subsystem B), is considered to have only two points of

connection, points 2 and 3 in the isolator and points 4 and 5 in the beam, as shown in Figure 46. The velocity response for the coupled system is calculated in the points 6, middle of the beam, point 7, ¼ of the beam and point 8, ⅛ of the beam.

Figure 47 – System substructuring.

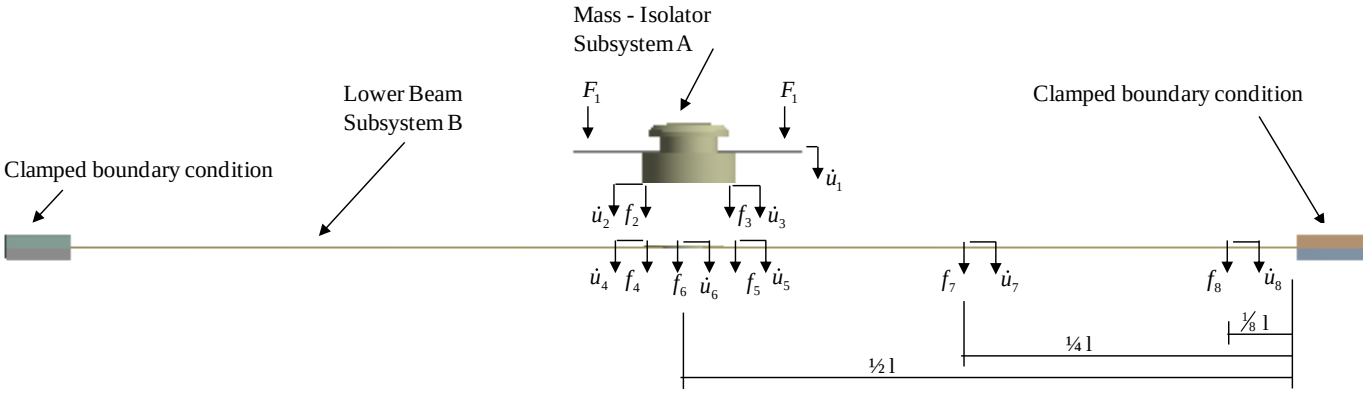

Source: Elaborated by the author.

Considering the transfer path analysis method, the velocities at the points 6, 7 and 8 in the receiver structure (beam), can be calculated using Equation (42) which is rewritten as

$$\begin{Bmatrix} \dot{u}_1^A \\ \dot{u}_2^A \\ \dot{u}_3^A \\ \dot{u}_4^B \\ \dot{u}_5^B \\ \dot{u}_6^B \\ \dot{u}_7^B \\ \dot{u}_8^B \end{Bmatrix} = \begin{bmatrix} Y_{11}^A & Y_{12}^A & Y_{13}^A & 0 & 0 & 0 & 0 & 0 \\ Y_{21}^A & Y_{22}^A & Y_{23}^A & 0 & 0 & 0 & 0 & 0 \\ Y_{31}^A & Y_{32}^A & Y_{33}^A & 0 & 0 & 0 & 0 & 0 \\ 0 & 0 & 0 & Y_{44}^B & Y_{45}^B & Y_{46}^B & Y_{47}^B & Y_{48}^B \\ 0 & 0 & 0 & Y_{54}^B & Y_{55}^B & Y_{56}^B & Y_{57}^B & Y_{58}^B \\ 0 & 0 & 0 & Y_{64}^B & Y_{65}^B & Y_{66}^B & Y_{67}^B & Y_{68}^B \\ 0 & 0 & 0 & Y_{74}^B & Y_{75}^B & Y_{76}^B & Y_{77}^B & Y_{78}^B \\ 0 & 0 & 0 & Y_{84}^B & Y_{85}^B & Y_{86}^B & Y_{87}^B & Y_{88}^B \end{bmatrix} \left(\begin{Bmatrix} F_1 \\ 0 \\ 0 \\ 0 \\ 0 \\ 0 \\ 0 \\ 0 \end{Bmatrix} + \begin{Bmatrix} 0 \\ f_2^A \\ f_3^A \\ f_4^B \\ f_5^B \\ 0 \\ 0 \\ 0 \end{Bmatrix} \right) \tag{71}$$

or $\dot{\mathbf{u}} = \mathbf{Y}(\mathbf{f} + \mathbf{g})$

As described in section 2.2.3.3, the velocity of the receiver structure (beam), can be calculated by

$$\dot{\mathbf{u}}_3 = \left[\mathbf{Y}_{32}^{\mathbf{B}} \left(\mathbf{Y}_{22}^{\mathbf{A}} + \mathbf{Y}_{22}^{\mathbf{B}} \right)^{-1} \mathbf{Y}_{21}^{\mathbf{A}} \right] \mathbf{F}_1 \tag{72}$$

where, for this case

$$\dot{\mathbf{u}}_{\mathbf{3}} = \begin{Bmatrix} \dot{u}_6^A \\ \dot{u}_7^A \\ \dot{u}_8^A \end{Bmatrix}, \quad \mathbf{Y}_{\mathbf{32}}^{\mathbf{B}} = \begin{bmatrix} Y_{64}^B & Y_{65}^B \\ Y_{74}^B & Y_{75}^B \\ Y_{84}^B & Y_{85}^B \end{bmatrix}, \quad \mathbf{Y}_{\mathbf{22}}^{\mathbf{A}} = \begin{bmatrix} Y_{22}^A & Y_{23}^A \\ Y_{32}^A & Y_{33}^A \end{bmatrix}, \quad \mathbf{Y}_{\mathbf{22}}^{\mathbf{B}} = \begin{bmatrix} Y_{44}^B & Y_{45}^B \\ Y_{54}^B & Y_{55}^B \end{bmatrix} \text{ and } \quad \mathbf{Y}_{\mathbf{21}}^{\mathbf{A}} = \begin{Bmatrix} Y_{21}^A \\ Y_{31}^A \end{Bmatrix}$$

Using the parameters given in Table 1, for the rubber isolator and in section 3.1.2, for the beam, the mobilites are calculated using finite element software Ansys. Figure 47 show the calculated mobilities for the source, subsystem A, and Figure 48 shows three transfer mobilities calculated for the subsystem B, receiver structure of the vibratory system.

The range of frequency analyzed is from 0 Hz up to 700Hz, within which there are the first four flexural natural frequencies of the beam.

Figure 48 – Source mobilities, subsystem A – mass-isolator.

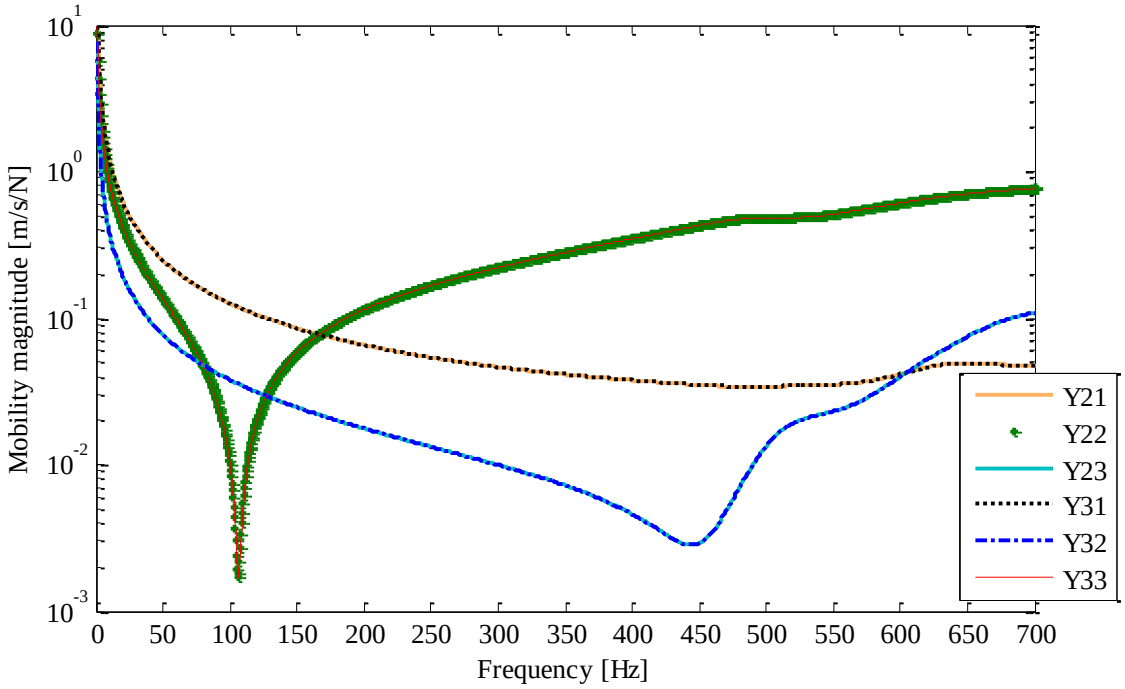

Source: Elaborated by the author.

Figure 49 – Receiver structure transfer mobilities, subsystem B, beam.

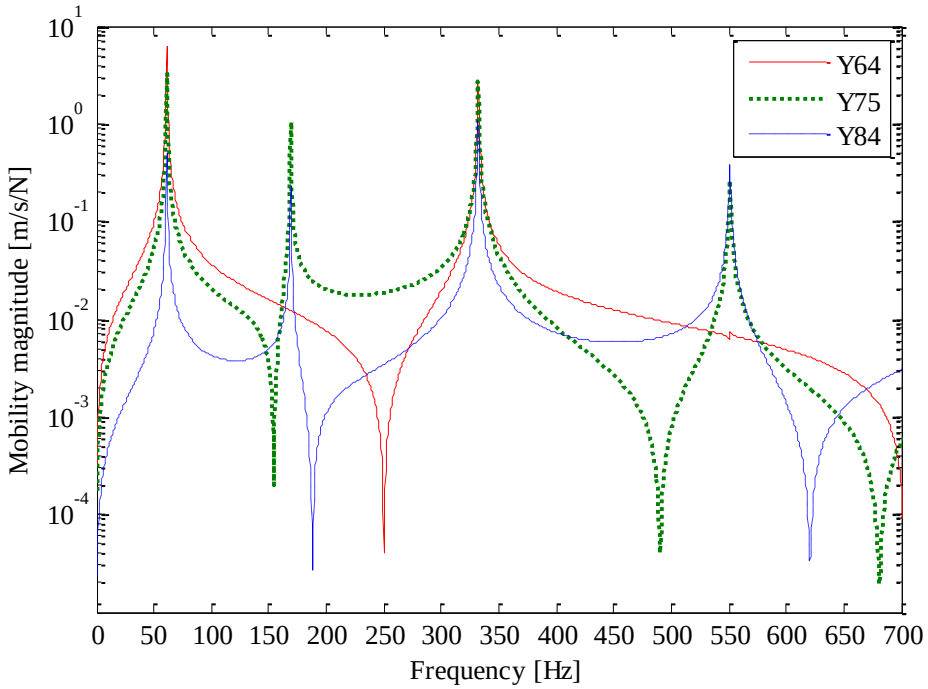

Source: Elaborated by the author.

Considering the calculated mobilities and Equation (72), the coupled velocities in the points 6, 7 and 8 at the lower beam could be compared with the velocities estimated for the complete system calculated using Ansys. A comparison for point 6, in the middle of the beam, is shown in the Figure 49 and, as observed in the figure the results do not match for frequencies higher than the first mode of the system. Thus, it can be concluded that the substructuring methods, which works well for point connection subsystems does not work as well for the distributed connection depending on the frequency of interest.

Figure 50 – Comparison of the TPA and Ansys complete system velocities in the point 6.

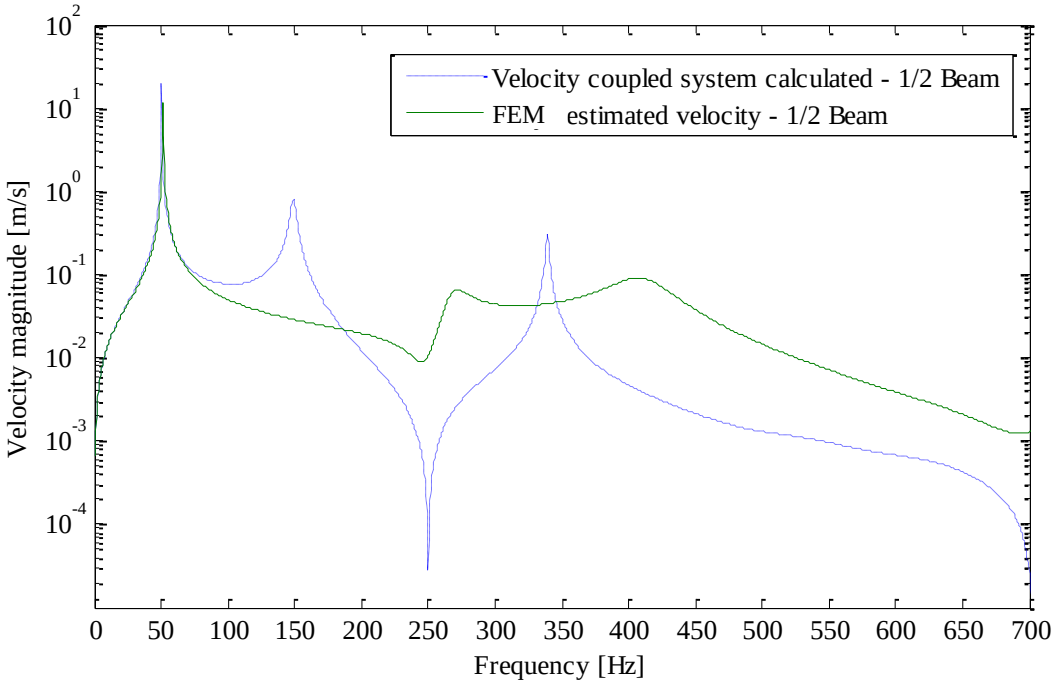

Source: Elaborated by the author.

To determine why there are differences some tests were made, first the number of connection points were increased, and then the Young's modulus of the isolator was increased, to determine the influence of the soft rubber isolator in the distributed coupling.

The Figure 50 show the division in the isolator base where the connection between the subsystems is considered, for four and eight points of connection. The matrices of Equation (72) are rewritten to cover all connection points for each case.

Figure 51 – Considered connection points in the isolator and beam with four points and eight points.

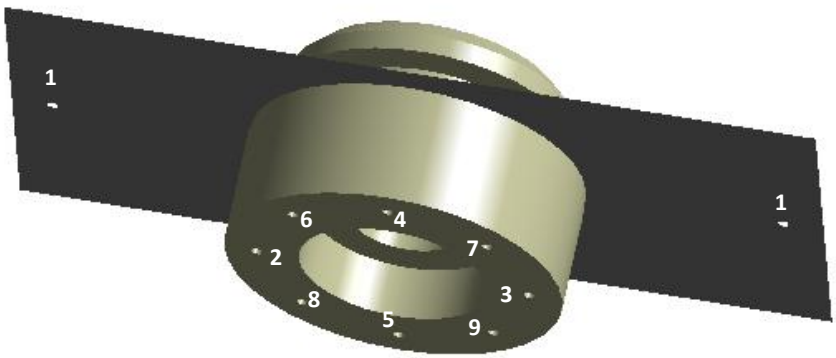

Source: Elaborated by the author.

Considering the calculated mobilities for all connection points and solving Equation (72) for these two new subsystems, the results for the coupled system considering the TPA substructuring methodology are shown in the Figure 51. The complete system and the TPA coupled system response are compared considering two, four and eight connection points.

Figure 52 Comparison of the TPA and FEM complete system velocities considering two, four and eight connection points.

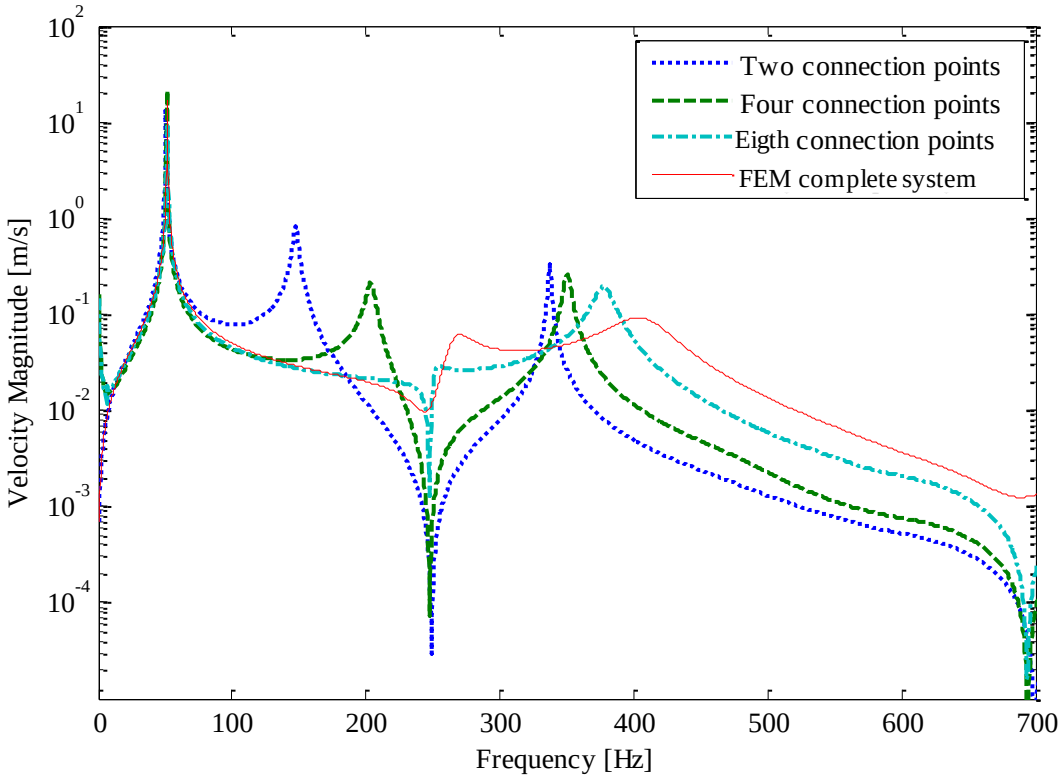

Source: Elaborated by the author.

Examining the results, it is possible to see that even increasing the number of connection or coupling points the results from the TPA substructuring methodology calculations and the complete system just agree up to the frequency of about 100 Hz considering four and eight connection points.

These results could explain why the calculations for the transfer path analysis in the refrigeration system, presented in Chapter 1. In that work point connections were considered. To further investigate the effect of the soft distributed connection of the rubber isolator on the substructuring method, in the next section the Young's modulus of the isolator is increased and the results are recalculated.

3.2.3 Increasing the stiffness of the rubber isolator distributed connection

In the previous section it was shown that, even increasing the connection points, the agreement between the results for complete system and the solution from TPA are poor. Figure 52 show the results for point 7, on the beam, considering two points of connection. Only the first natural frequency is predicted in an accurate way. This can be explained because one of the components has a soft contact area with a harder structure. In this case this is the contact between the rubber isolator and the beam.

Figure 53 – Comparison of the TPA and FEM complete system velocities in the point 7.

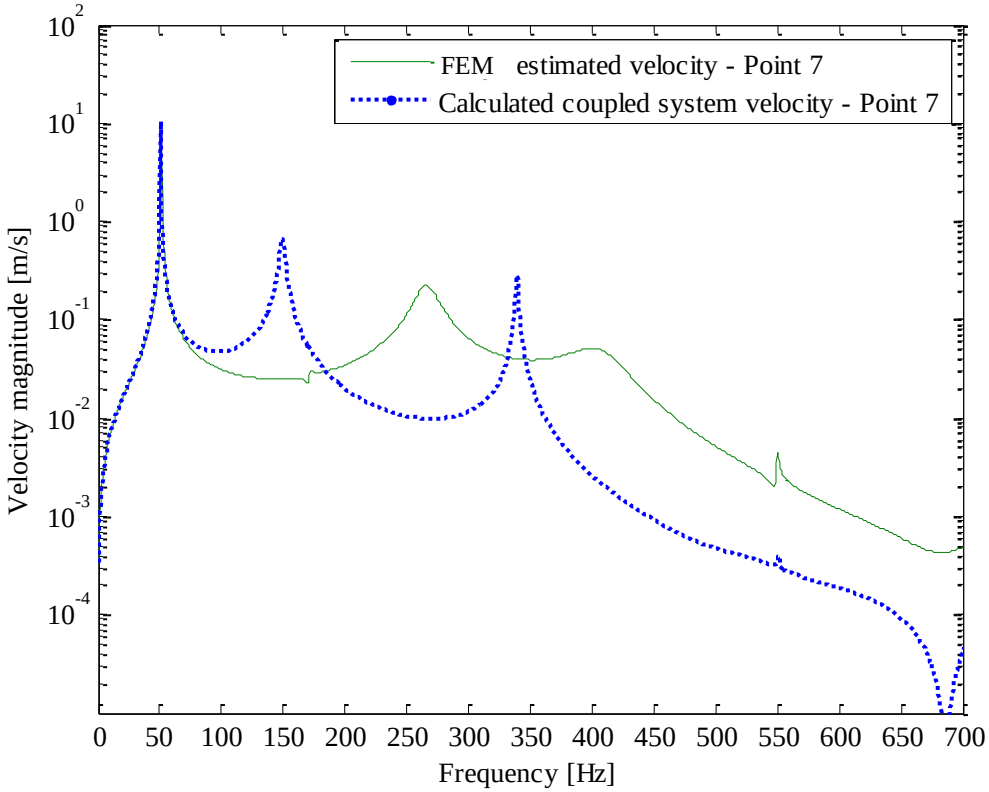

Source: Elaborated by the author.

To investigate the influence of the flexible distributed connection on the results of the substructuring methodology, it is necessary to observe that the flexural wavelength in each material has a different value because it depends on the material properties and geometry of each structure and can be calculated as

$$\lambda = \frac{2\pi}{k} \tag{73}$$

where *k* is the wavenumber and is described as

$$k = \left(\frac{\rho A}{EI} \right)^{1/4} \omega^{1/2} \quad \text{in which} \quad I = \frac{bh^3}{12} \tag{74}$$

Now considering the same system as shown in the Figure 46, with two connection points distant in d = 0.02m. The wavelengths for the first four flexural modes of the beam are shown in Table 3, noting that the Young's modulus of the beam is $E_{beam} = 178\text{x}10^9 \, \text{N}/\text{m}^2$.

Table 3 – Wavelength for the first four flexural modes of the beam.

Mode	1st – 61.7Hz	2nd – 170.2Hz	3rd – 334.4Hz	4rd – 554.8Hz
λ (m)	0.49	0.29	0.21	0.16

Source: Elaborated by the author.

The wavelength in the rubber isolator is calculated assuming a rectangular section with dimensions of 0.024 x 0.013m and the Young's modulus $E_1 = 1.3\text{x}10^6 \, \text{N}/\text{m}^2$. The wavelength in the isolator, considering the four flexural frequencies of the beam are calculated and shown in the Table 4.

Table 4 – Wavelength in the rubber isolator for the same four frequencies.

Frequency	61.7Hz	170.2Hz	334.4Hz	554.8Hz
λ (m)	0.11	0.068	0.048	0.037

Source: Elaborated by the author.

The results show that, in the rubber isolator, the wavelength is smaller than in the beam for the same frequency. This means that the rubber isolator has a different flexural movement when compared with the beam, which could cause the problem in the mobility coupling results considering just a few connection points.

The idea is to increase the rubber isolator Young's modulus to test this thesis. So, the Young's modulus of the isolator is changed to be $E_2 = 13\text{x}10^6 \, \text{N}/\text{m}^2$, $E_3 = 130\text{x}10^6 \, \text{N}/\text{m}^2$ and

$E_4 = 1300\text{x}10^6\ \text{N/m}^2$, to give differences in the wavelength. Table 5 shows the new wavelengths for the more rigid isolators created just in a finite element models.

Table 5 – Wavelength for the first four flexural frequencies of the beam in each material.

	Frequency	61.7Hz	170.2Hz	334.4Hz	554.8Hz
λ (m)	Isolator $E_2 = 13\text{x}10^6\ \text{N/m}^2$	0.20	0.12	0.085	0.066
	Isolator $E_3 = 130\text{x}10^6\ \text{N/m}^2$	0.35	0.21	0.15	0.12
	Isolator $E_4 = 1300\text{x}10^6\ \text{N/m}^2$	0.62	0.38	0.27	0.21

Source: Elaborated by the author.

As it is possible to see in the Table 5, the wavelengths in the new isolators are higher, being closer to the values for the beam flexural wavelengths. A non-dimensional ratio is calculated to compare the results and try to determine a value where the mobility coupling methodology works even for a flexible contact area, this value is the ratio between the distance of the connection points in the isolator, which is 0.02 m, and the wavelength in the isolator for this four different Young's modulus, Table 6 shows these values.

Table 6 – Ratio d/λ in each material.

	Frequency	61.7Hz	170.2Hz	334.4Hz	554.8Hz
d/λ	Isolator $E_1 = 1.3\text{x}10^6\ \text{N/m}^2$	0.18	0.29	0.42	0.54
	Isolator $E_2 = 13\text{x}10^6\ \text{N/m}^2$	0.10	0.17	0.24	0.30
	Isolator $E_3 = 130\text{x}10^6\ \text{N/m}^2$	0.057	0.095	0.13	0.17
	Isolator $E_4 = 1300\text{x}10^6\ \text{N/m}^2$	0.032	0.053	0.074	0.095

Source: Elaborated by the author.

The TPA methodology coupling is used to calculate the resulting velocities in the beam considering Equation 72 for the new systems with the more rigid rubber isolators.

Figures 53 to 56 show the comparison between the TPA substructuring calculated velocity in the beam and the velocity when the complete system is simulated in the Ansys.

In each figure, the frequency is shown when the calculated and simulated response start to deviate. The ratio d/λ was calculated for each one of this points and the results are shown in Table 7, considering only two points of connection with distance d = 0.02m.

Figure 54 – Comparison of TPA calculated velocity and the velocity of the complete FEM for isolator $E_1 = 1.3\text{x}10^6\ \text{N/m}^2$ in the middle of the beam.

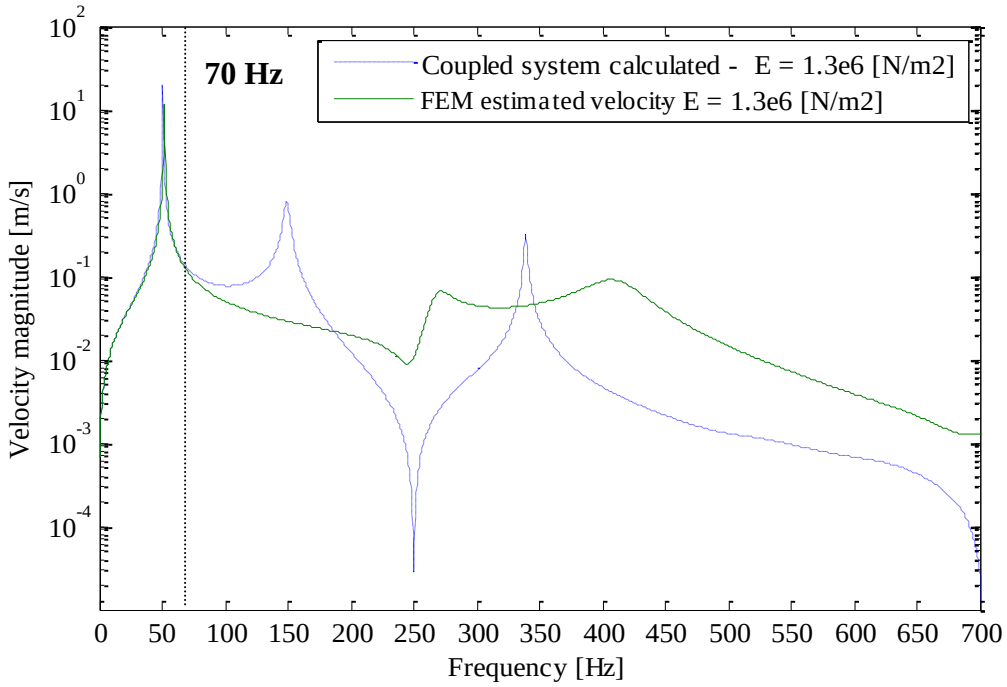

Source: Elaborated by the author.

Figure 55 – Comparison of TPA calculated velocity and the velocity of the complete FEM for isolator $E_2 = 13\text{x}10^6\ \text{N/m}^2$ in the middle of the beam.

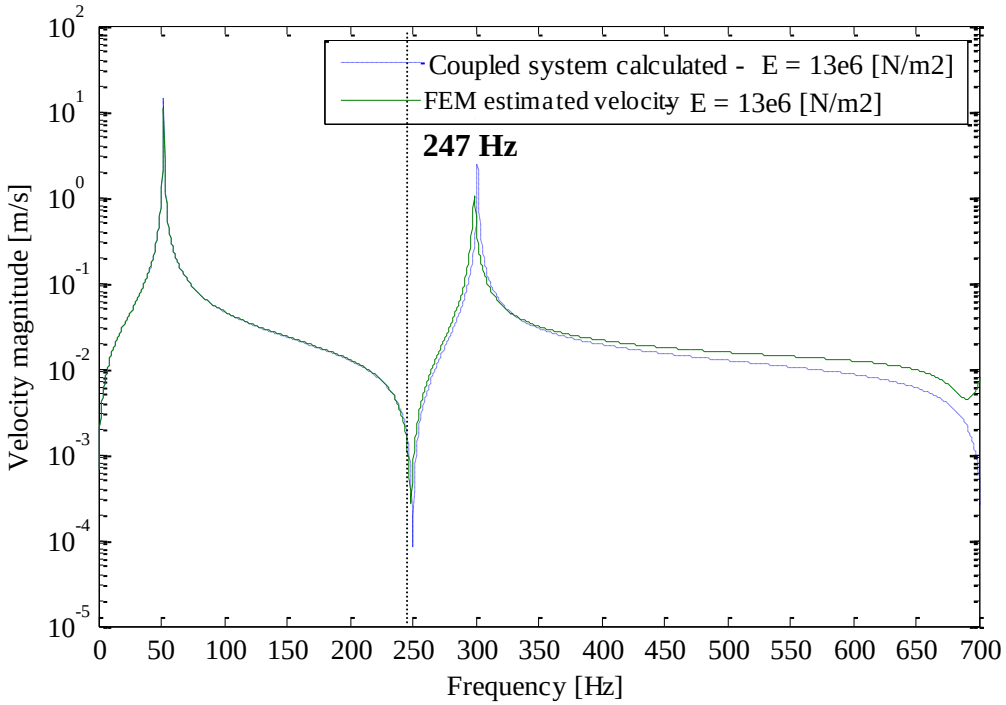

Source: Elaborated by the author.

Figure 56 – Comparison of TPA calculated velocity and the velocity of the complete FEM for isolator $E_3 = 130\text{x}10^6\ \text{N/m}^2$ in the middle of the beam.

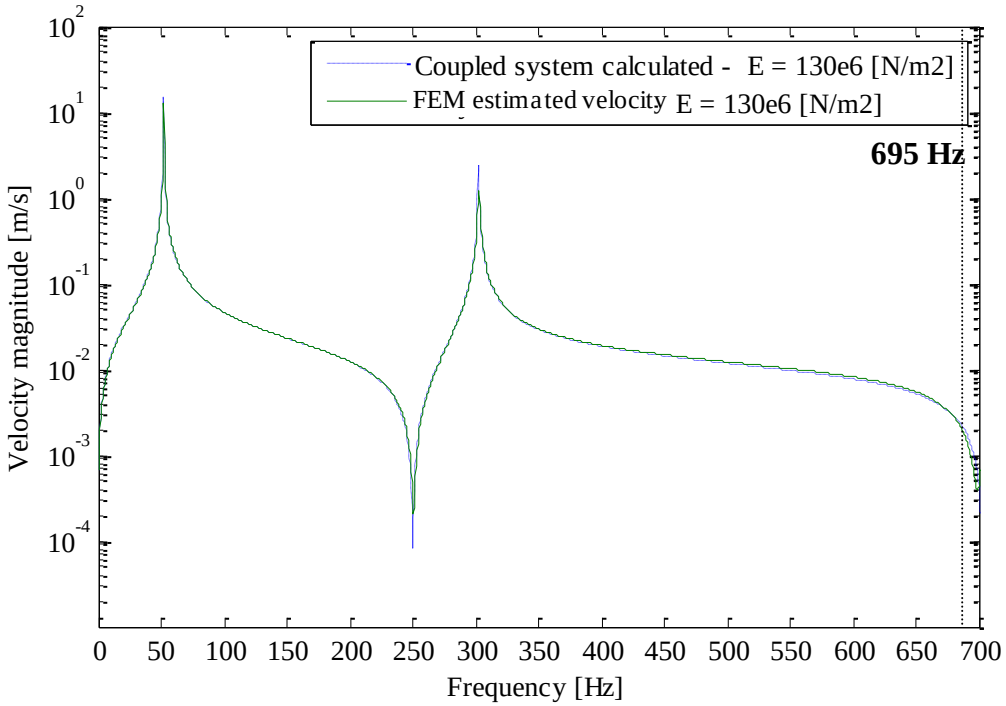

Source: Elaborated by the author.

Figure 57 – Comparison of TPA calculated velocity and the velocity of the complete FEM for isolator $E_4 = 1300\text{x}10^6\ \text{N/m}^2$ in the middle of the beam.

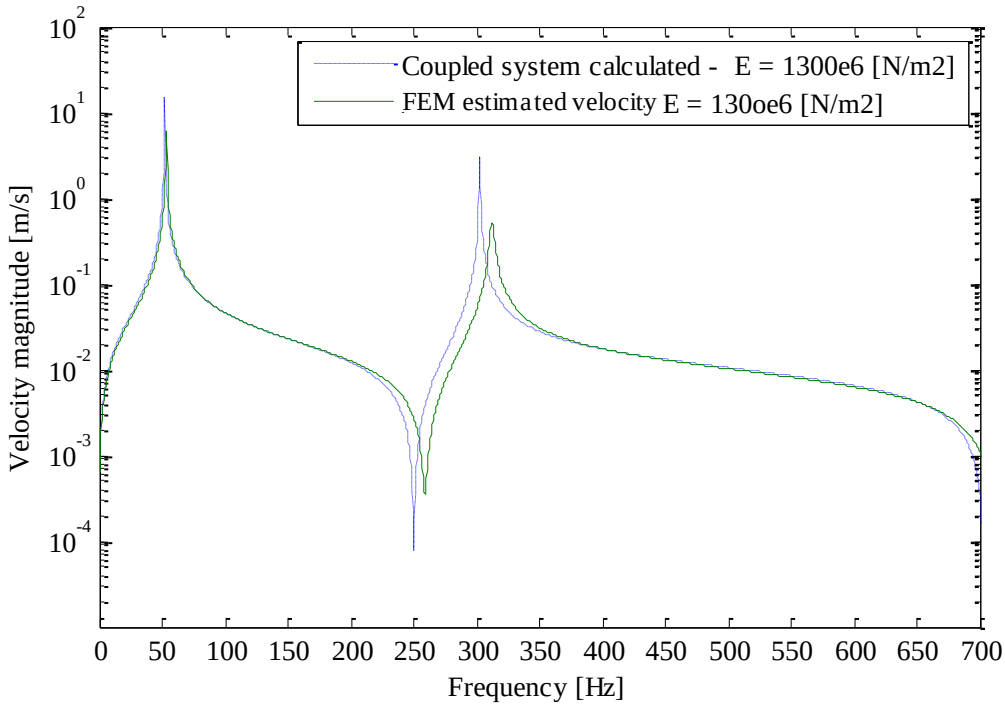

Source: Elaborated by the author.

The objective is to find the value of the ratio d/λ, in that the TPA coupling methodology using a few points in the connection could be used to have good results for the coupled system. Table 7, show the ratio d/λ for each one of the points marked in Figures 53 to 55. For the Young's modulus of $E_4 = 1300\text{x}10^6\ \text{N/m}^2$ the results do not match. This occurs in this case because the isolator is more rigid than the beam, which means that the isolator adds some stiffness in the beam, changing the connection way in the opposite way to when the isolator is soft.

Table 7 – Ratio d/λ until that the calculated velocity is the same as FEM.

Isolator	$E_1 = 1.3\text{x}10^6\ \text{N/m}^2$	$E_2 = 13\text{x}10^6\ \text{N/m}^2$	$E_3 = 130\text{x}10^6\ \text{N/m}^2$
Frequency	70Hz	247Hz	695Hz
d/λ	0.202	0.210	0.201

Source: Elaborated by the author.

So, it is possible to assume that, for soft materials, the mobility coupling method could be used considering just a small number of connection points in the contact region only if the relation d/λ is less than approximately 0.2.

3.3 CONCLUSIONS

The objective of this chapter was to analyse the distributed connection between the rubber isolator and a beam and its effects on the substructuring technique. To achieve this, the material properties of the rubber isolator and the beam were first experimentally determined, then a finite element model for each of the components was developed. Using the static results from the rubber isolator, and considering that the displacements of the vibratory system are less than 1.5 mm, the isolator could be considered as a linear subsystem.

The analysis with both finite element models of the vibratory system involves the mass-isolator subsystem in three different positions of the beam, ½, ¼ and $\frac{1}{8}$ of beam length. First a mode coupling study shows that, independent of the position of mass-isolator subsystem over the beam, the same modes are coupled and generally present the same coupling phenomena.

To study the distributed connection of the rubber isolator, the TPA substructuring approach was used, because this method allows the prediction of responses at different points in the receiver structure. First it was considered that the rubber isolator was coupled to the beam at two points and then the number of coupling points were increased to four and eight points. Even with the connection points increased, the results for the coupled system did not had significant improvement. This meant that the vibratory system could not be substructured in this way.

To show that the flexible distributed connection of the rubber isolator had a high influence in the results of the substructuring, a study considering the flexural wavelength in each material was carried out. Then, the Young's modulus of the isolator was increased and the results for TPA substructuring recalculated. After the analysis, it was possible to show that, for soft materials, the mobility coupling method could be used by considering just a few number of connection points in the contact region only if the ratio between the distance between connection points and a wavelength in the isolator, was less than about 0.2.

To show that the way of substructuring influences the results of the coupled vibratory system with a distributed rubber isolator connection, in Chapter 4 one more component will be add to the vibratory system, This system will then be analysed using the substructuring approach.

4 AN ALTERNATIVE WAY OF SUBSTRUCTURING VIBRATORY SYSTEMS WITH A DISTRIBUTED CONNECTION

Substructuring methods have been widely used to solve engineering problems since 1960 when Hurty developed the first ideas of dynamic substructuring as reduction techniques. Subsequently the method became known as component-mode synthesis, Klerk et al. (2008).

This thesis has shown that although the substructuring method can solve engineering problems, the way of substructuring can cause errors in the solution for a complete vibratory system. In this chapter, an alternative way of substructuring is investigated for a system in which there is a flexible distributed interface. The system, similar to that discussed in previous chapters, is analysed to determine the differences when the system is substructured in different ways.

4.1 VIBRATORY SYSTEM

The vibratory system under consideration is shown schematically in Figure 57. Besides the mass, the isolator and the beam described previously, an additional beam is included with the same material properties, $E = 180\text{x}10^9\ \text{N/m}^2$, $\rho = 7900\,\text{Kg/m}^3$, $\eta = 0.001$ It has a thickness, 0.0017m, a width, 0.031m, and a length of 0.41m. The connection between the beams consists of two simple supports and the lower beam has clamped-clamped boundary conditions to ground.

Figure 58 – Schematic of the new vibratory system.

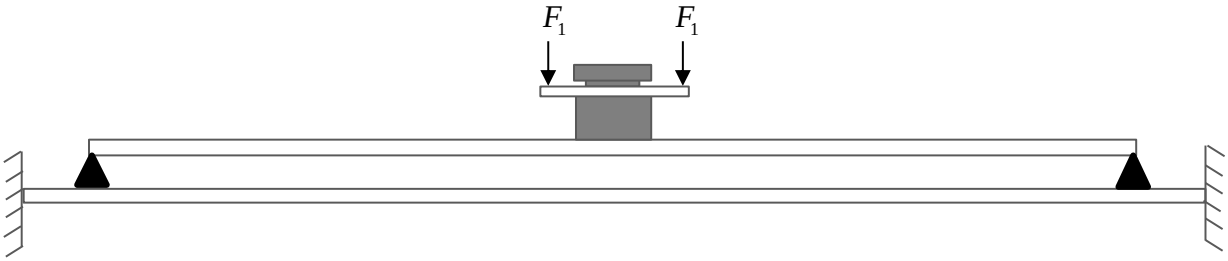

Source: Elaborated by the author.

To simulate the new vibratory system in Ansys, a spring with large stiffness is used to represent each pinned connection, so that only the translational forces are transmitted. Figure 58 shows the Ansys model of the system. The new beam is modeled using the same SHELL181 element and the process of mesh convergence curve was made to determine the element size for this beam, resulting in elements with 3 mm length as in the other beam models.

Figure 59 – New finite element model of the vibratory system.

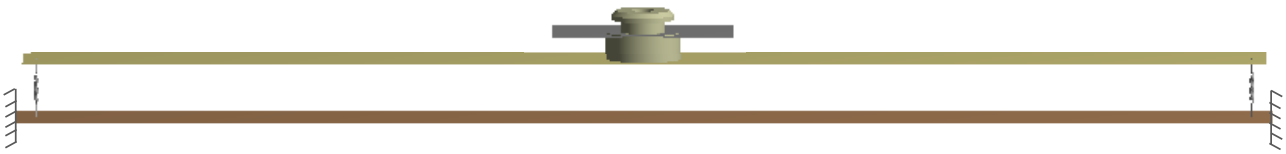

Source: Elaborated by the author.

Harmonic response analysis is used to calculate the mobilities in the frequency range from 0 to 700Hz as in the previous chapters, and a translational harmonic force of 1N applied at the isolator, as shown in the Figure 58, excites the structure over the whole frequency range.

4.2 ALTERNATIVE SUBSTRUCTURING APPROACH

In the alternative substructuring approach the vibratory system is substructured at the junction between the two beams, as shown in Figure 59, instead of at the rubber isolator. This is because at this junction there are point connections, which is easier to manage in the coupling methodology.

Referring to the refrigeration system problem discussed in the Introduction, the structure would be split at the base plate connection to the fridge and not at the rubber isolators as carried out previously, as shown in Figure 2.

Figure 60 – Alternative substructuring model of vibratory system.

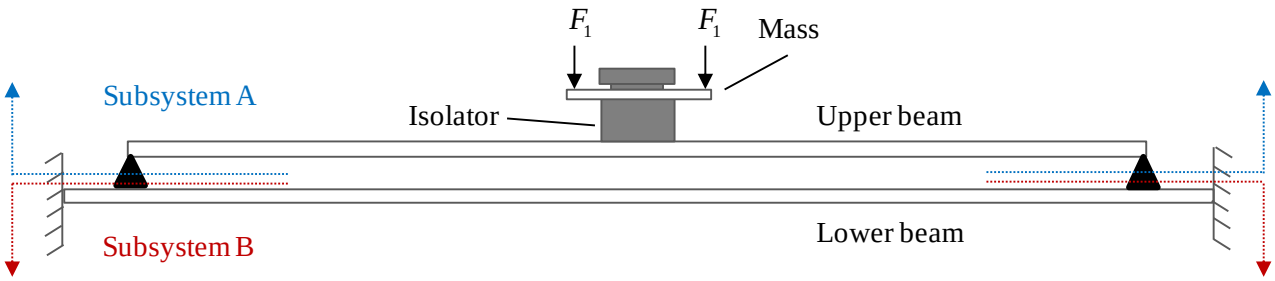

Source: Elaborated by the author.

Using this substructuring approach, subsystem A, or the source is composed of the mass, isolator and the upper beam, and subsystem B, or the receiver structure, is composed of the lower beam. The points where the mobilities are calculated in the FE model are shown in Figure 60, and the solution for the complete system is calculated for point 6 in the middle of the lower beam and points 7 and 8, at $1/4$ and $1/8$ of the length of the lower beam respectively.

Figure 61 – Mobility calculation points in the vibratory system.

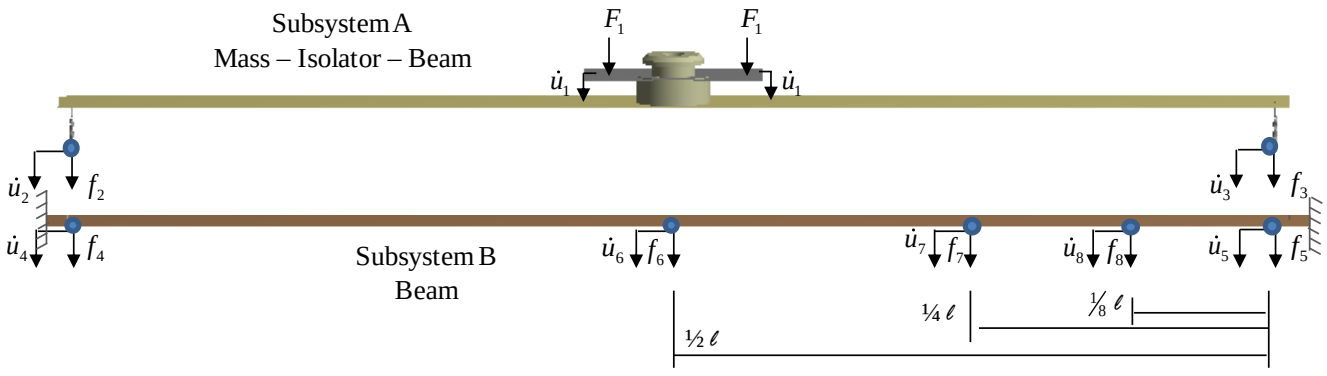

Source: Elaborated by the author.

Considering the transfer path analysis method described in the Chapter 2, the velocities at points 6, 7 and 8 in the receiver structure, lower beam, can be calculated. The matrix equation describing the system is given by

$$\begin{Bmatrix} \dot{u}_1^A \\ \dot{u}_2^A \\ \dot{u}_3^A \\ \dot{u}_4^B \\ \dot{u}_5^B \\ \dot{u}_6^B \\ \dot{u}_7^B \\ \dot{u}_8^B \end{Bmatrix} = \begin{bmatrix} Y_{11}^A & Y_{12}^A & Y_{13}^A & 0 & 0 & 0 & 0 & 0 \\ Y_{21}^A & Y_{22}^A & Y_{23}^A & 0 & 0 & 0 & 0 & 0 \\ Y_{31}^A & Y_{32}^A & Y_{33}^A & 0 & 0 & 0 & 0 & 0 \\ 0 & 0 & 0 & Y_{44}^B & Y_{45}^B & Y_{46}^B & Y_{47}^B & Y_{48}^B \\ 0 & 0 & 0 & Y_{54}^B & Y_{55}^B & Y_{56}^B & Y_{57}^B & Y_{58}^B \\ 0 & 0 & 0 & Y_{64}^B & Y_{65}^B & Y_{66}^B & Y_{67}^B & Y_{68}^B \\ 0 & 0 & 0 & Y_{74}^B & Y_{75}^B & Y_{76}^B & Y_{77}^B & Y_{78}^B \\ 0 & 0 & 0 & Y_{84}^B & Y_{85}^B & Y_{86}^B & Y_{87}^B & Y_{88}^B \end{bmatrix} \left(\begin{Bmatrix} F_1 \\ 0 \\ 0 \\ 0 \\ 0 \\ 0 \\ 0 \\ 0 \end{Bmatrix} + \begin{Bmatrix} 0 \\ f_2^A \\ f_3^A \\ f_4^B \\ f_5^B \\ 0 \\ 0 \\ 0 \end{Bmatrix} \right) \tag{75}$$

$$\text{or } \dot{\mathbf{u}} = \mathbf{Y}(\mathbf{f} + \mathbf{g})$$

where $\dot{u}_i$ are the velocities, Y_{ij} are the mobilities, F_1 is the excitation force and f_2 to f_5 are the interface forces. The subscripts A and B correspond to the subsystems A and B respectively.

As described in section 2.2.3.3, the velocities of at the receiver structure can be calculated using Equation (48) which is written again here for convenience.

$$\dot{\mathbf{u}}_\mathbf{3} = \left[\mathbf{Y}_{\mathbf{32}}^{\mathbf{B}} \left(\mathbf{Y}_{\mathbf{22}}^{\mathbf{A}} + \mathbf{Y}_{\mathbf{22}}^{\mathbf{B}} \right)^{-1} \mathbf{Y}_{\mathbf{21}}^{\mathbf{A}} \right] \mathbf{F}_\mathbf{1} \tag{76}$$

where, for this case

$$\dot{\mathbf{u}}_\mathbf{3} = \begin{Bmatrix} \dot{u}_6^B \\ \dot{u}_7^B \\ \dot{u}_8^B \end{Bmatrix}, \quad \mathbf{Y}_{\mathbf{32}}^{\mathbf{B}} = \begin{bmatrix} Y_{64}^B & Y_{65}^B \\ Y_{74}^B & Y_{75}^B \\ Y_{84}^B & Y_{85}^B \end{bmatrix}, \quad \mathbf{Y}_{\mathbf{22}}^{\mathbf{A}} = \begin{bmatrix} Y_{22}^A & Y_{23}^A \\ Y_{32}^A & Y_{33}^A \end{bmatrix}, \quad \mathbf{Y}_{\mathbf{22}}^{\mathbf{B}} = \begin{bmatrix} Y_{44}^B & Y_{45}^B \\ Y_{54}^B & Y_{55}^B \end{bmatrix} \text{ and } \quad \mathbf{Y}_{\mathbf{21}}^{\mathbf{A}} = \begin{Bmatrix} Y_{21}^A \\ Y_{31}^A \end{Bmatrix}$$

As already described in the previous chapters it is necessary calculate the mobilities for each subsystem. Here, they are calculated using the finite element model. The driving point mobilities for subsystem A are shown in Figure 61. They are calculated considering points 1, 2 and 3 shown in Figure 60. In this case the rubber isolator is not disconnected and is

considered as part of the whole subsystem A. Besides the driving point mobilities shown in the figure, the transfer mobilities are calculated considering the same connection points.

Figure 62 – Driving point mobilities for the subsystem A.

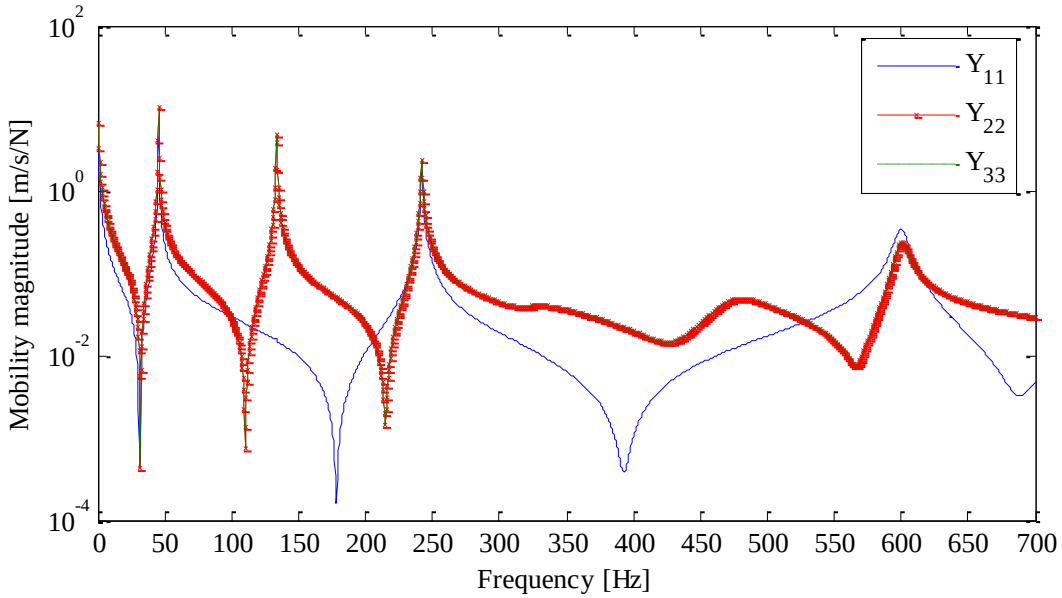

Source: Elaborated by the author.

The driving point mobilities at the connection points for subsystem B, at points 4 and 5 are shown in Figure 62. The transfer point mobilities between the points 4, 5, 6, 7 and 8 as shown in the Equation (78) are also calculated using the finite element model.

Figure 63 – Driving point mobilities for the subsystem B.

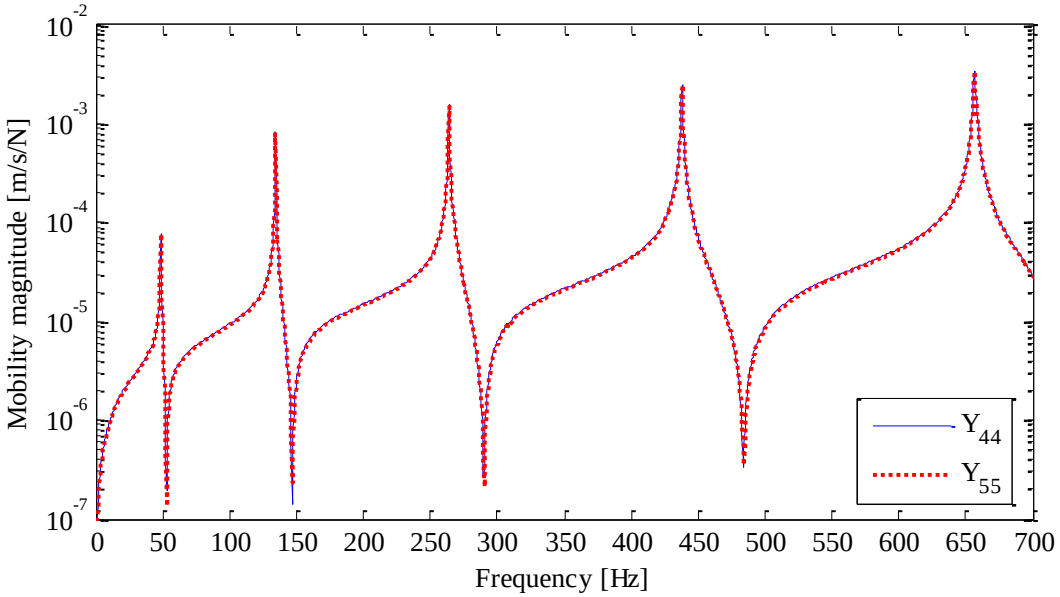

Source: Elaborated by the author.

Once all the mobilities have been calculated the velocities for the coupled system at points 6, 7 and 8 in the lower beam, can be calculated. To determine if the alternative substructuring method shows better results than the previous method, the results are compared for the coupled system velocities.

A comparison between the results from the transfer path method and for the complete system are shown in Figures 63, 64 and 65 for points 6, 7 and 8 on the receiver structure respectively.

Figure 64 – Velocity results for the alternative substructuring at point 6.

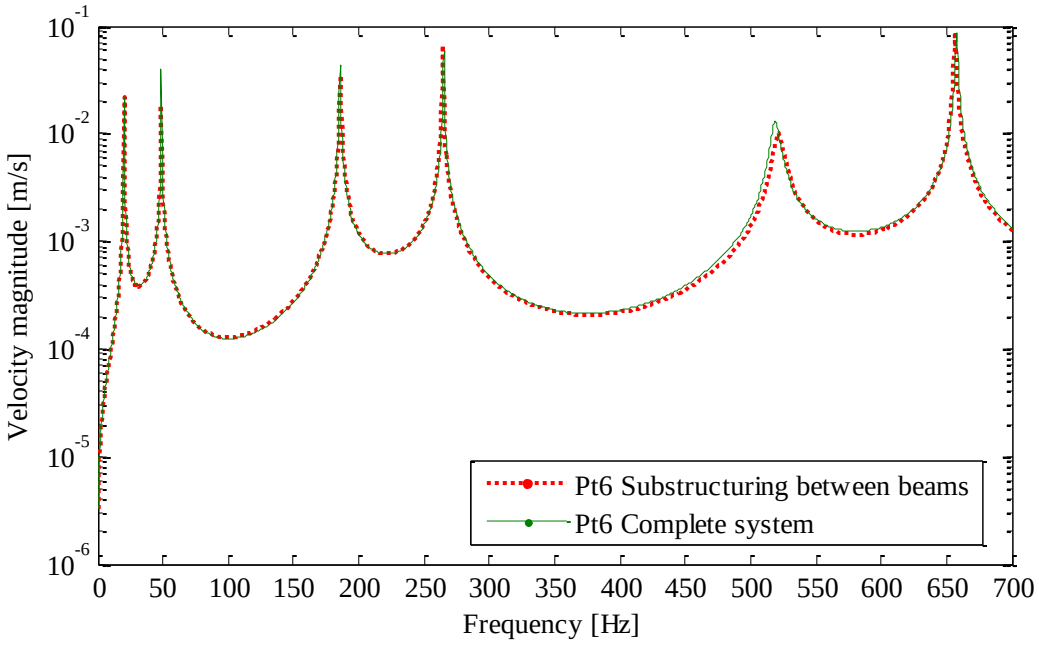

Source: Elaborated by the author.

Figure 65 – Velocity results for the alternative substructuring at point 7.

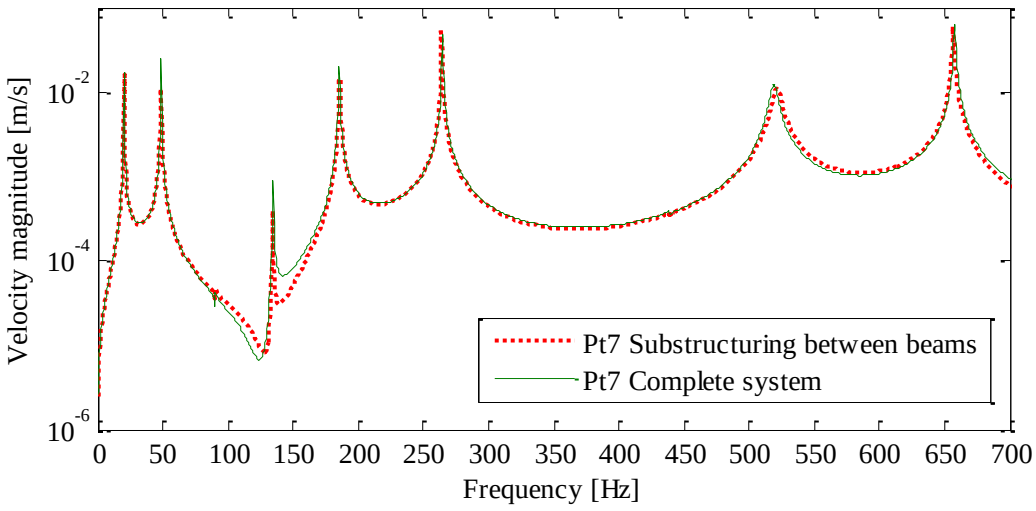

Source: Elaborated by the author.

Figure 66 – Velocity results for the alternative substructuring at point 8.

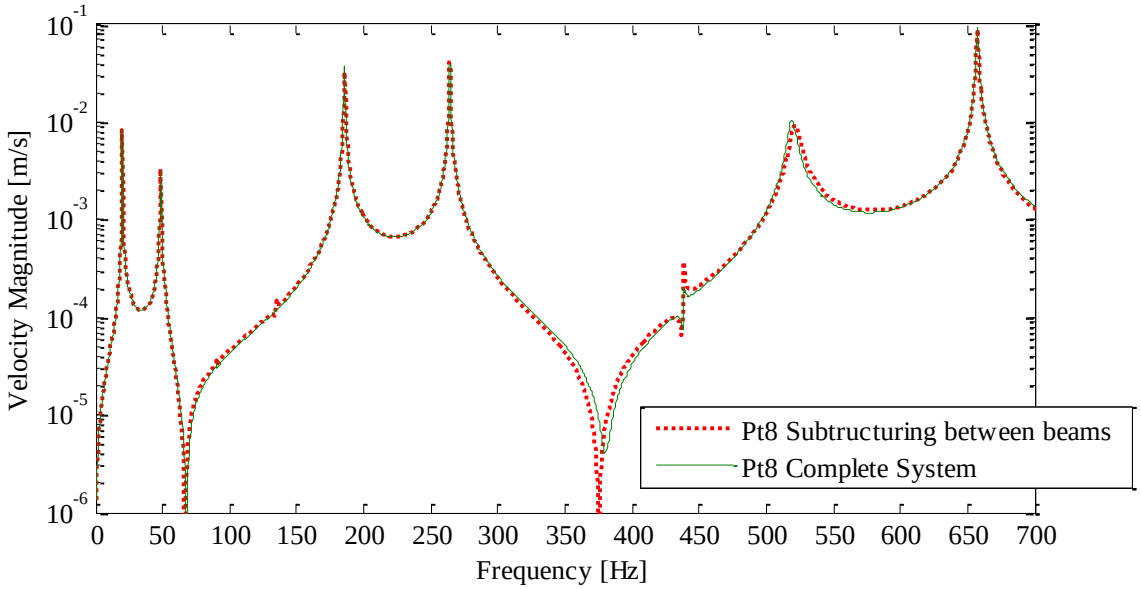

Source: Elaborated by the author.

Analyzing Figures 64 and 65, there is some differences in the results around the frequency of 130 Hz and 370 Hz respectively that could be explained because of the small differences in the connection points 2 and 3 when the mobilities are calculated for use in the transfer path methodology, compared to when the system is modelled as a complete structure. The accuracy of this alternative methodology to substructure the vibratory system, however, shows a great improvement in the velocity results for coupled system. To determine that it is the alternative substructuring approach and not the new vibratory system that improves the accuracy of the solution, the same vibratory system presented in the Figure 57 is considered and the system is substructured as described in Chapter 3, at the rubber isolator distributed interface.

Figure 67 – New system substructuring, considering the connection in the rubber isolator.

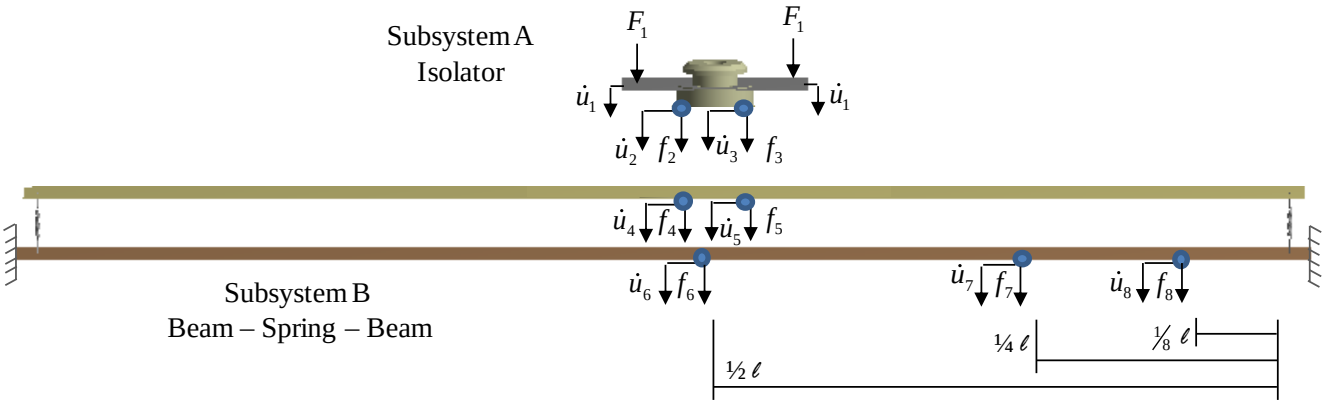

Source: Elaborated by the author.

The results for the coupled system considering the system to be substructured as shown in Figure 66 for points 6, 7 and 8 in the lower beam are compared with the velocity calculated directly in the complete system finite element model for the same points in the receiver structure. These comparisons are shown in the Figures 67, 68 and 69.

Figure 68 – Velocity results for the substructuring at rubber isolator at point 6.

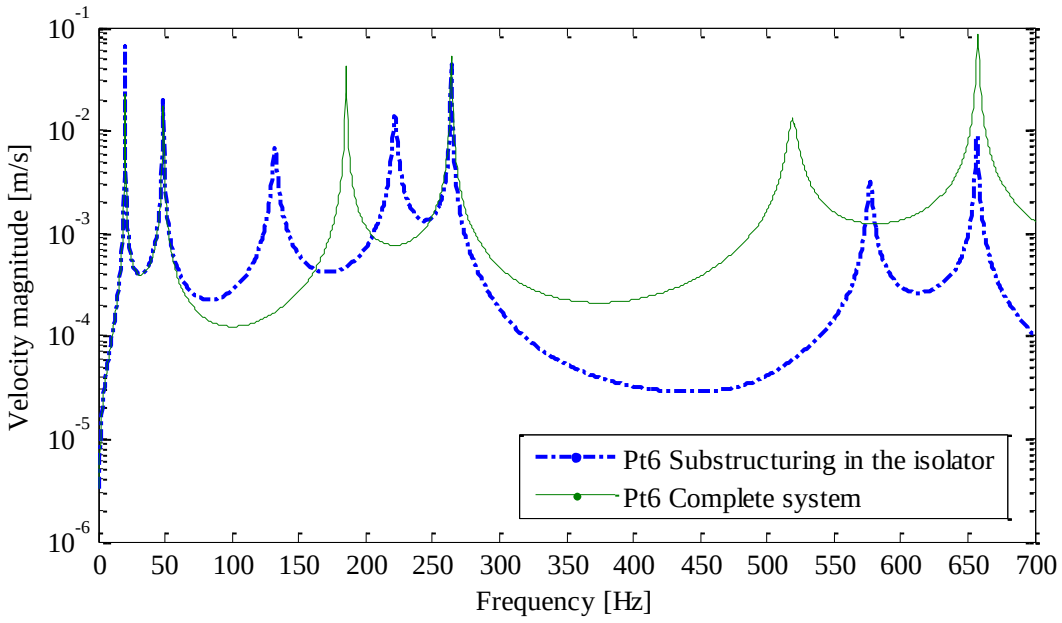

Source: Elaborated by the author.

Figure 69 – Velocity results for the substructuring at rubber isolator at point 7.

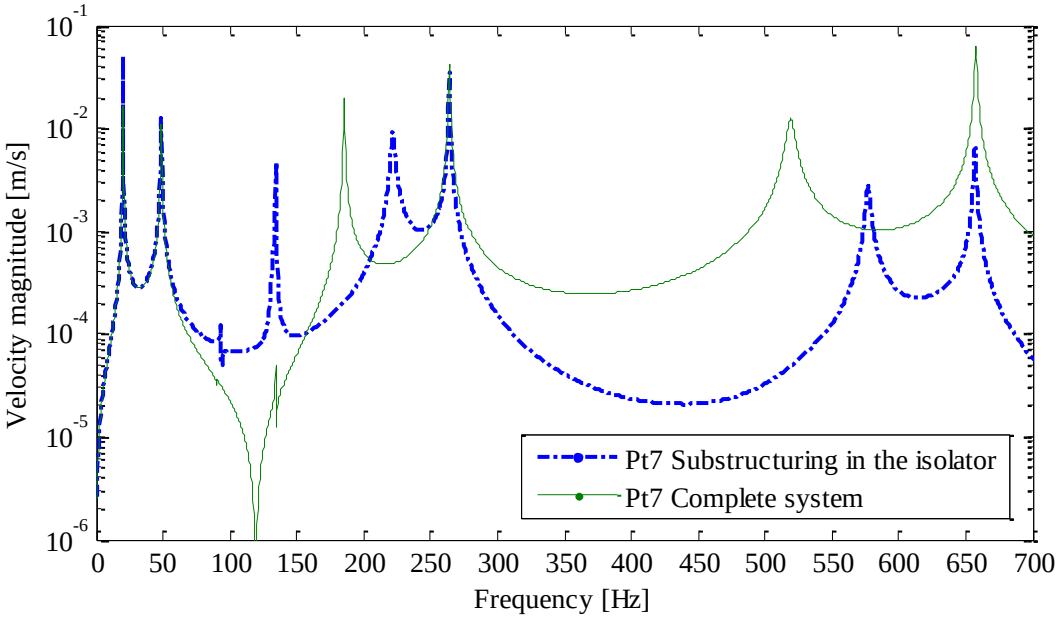

Source: Elaborated by the author.

Figure 70 – Velocity results for the substructuring at rubber isolator at point 8.

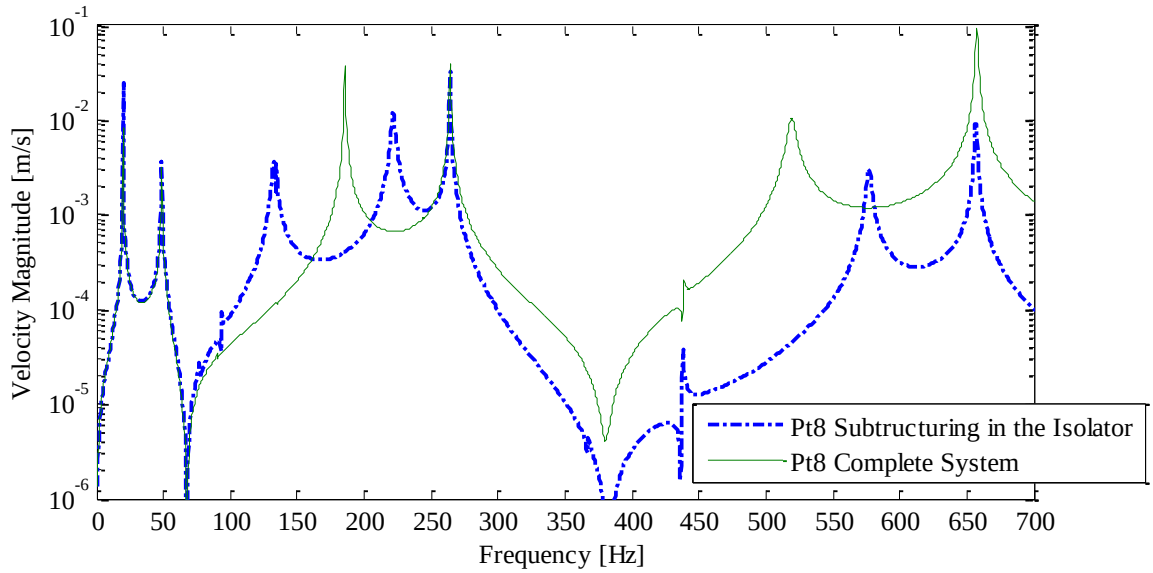

Source: Elaborated by the author.

As expected, the results for the coupled system considering the system to be substructured at the rubber isolator, are accurate only up to the frequency of about 70 Hz, because the distance between the connections points in the rubber isolator are the same as in Chapter 3. The results for the coupled system considering the system to be substructured at the connection between the beams is much better than when the system is substructured at the

isolators, when compared with the complete system calculated directly using a finite element model.

4.3 CONCLUSIONS

In this chapter, a new vibratory system was used to determine if a way of substructuring could change the solution for the coupled system, when a rubber isolator is part of the global structure. The results were analysed for this alternative substructuring approach and showed that there was a significant improvement.

To determine that the improvement was due to the alternative substructring approach, the vibratory system was substructured as shown in Chapter 3, at the rubber isolator. The results for both substructuring approaches were compared. It was shown that if the system is substructured at the distributed connection, the results are only accurate up to a frequency of about 70 Hz, which corresponds to the results in chapter 3.

With the alternative substructuring method, the solution for the coupled vibratory system has been greatly improved. Referring to the refrigeration system problem discussed in Chapter 1, it means that the structure should be split at the base plate connection to the fridge instead of at the rubber isolators to give a more accurate solution.

5 CONCLUSIONS

Dynamic substructuring is an efficient way to reduce the size of dynamic problems and to analyse the dynamical behaviour of large models. For example, assembling reduced models of subparts of a structure enables the designers in the industry to share models between design groups, and if a single component of a system is changed, only that component needs to be reanalyzed and the system as a whole can be analysed at low additional cost. Thus, dynamic substructuring offers a flexible and efficient approach to dynamic analysis, even when a rubber isolator distributed connection is a component of the large structure, considering a linear behaviour.

The motivation for this thesis was a problem that was encountered by the author in her master degree dissertation. The principal idea was to analyse a dynamic structure that contains rubber isolators with flexible distributed connections between the component parts and to determine if the way of substructuring can change and improve the results. The frequency domain transfer path methodology was chosen to carry out the analysis because of the facility to calculate the mobilities mainly in the finite element models and to manage the calculations. A more complete explanation about the dynamic substructuring was given in Chapter 2.

In Chapter 3, a simple model with a mass, isolator and beam were generated and the transfer path methodology was used to substructure the system in the rubber isolator, with poor results even when the number of connection points was increased. Using the same model, some analysis was conducted to determine the reasons why the results for the coupled system are not accurate, relating the flexural wavelength in the two different materials of the system - rubber and steel. The maximum frequency, for which the coupled velocities were accurate, could be related to the ratio between the distance between the connection points in a distributed connection, and a wavelength. It was found that if this ratio is less than about 0.2 then the transfer path methodology of substructuring provides good results, even for a flexible distributed connection. These results could provide a reason why the calculations for the transfer path analysis in the refrigeration system shown in Chapter 1, had some large differences in the transfer path with an isolator, when only one point of connection between the substructures was modelled.

With the objective to analyse the way in which substructuring could influence the results of the coupled velocity of vibratory system with a flexural distributed interface, in

Chapter 4 a new vibratory system, considering more one beam was modeled. This vibratory system was a crude representation of a compressor – isolator – fridge dynamic system, and an alternative substructuring way was used to analyse the results. For this case, the system was substructured at a point connection between the beams and not at the rubber isolator. The results for this substructuring approach show greatly improved results, when compared with the system substructured at the isolator.

It was possible to determine that this alternative methodology of substructuring for dynamic systems with a rubber isolator distributed interface, improve the accuracy for the coupled vibratory system when compared with the complete system. Referring to the refrigeration system problem, it could mean that a split in the structure at the base plate connection to the fridge instead of at the rubber isolators, could result in a more accurate solution in the transfer path that contains the rubber isolators.

5.1 RECOMMENDATIONS FOR FURTHER WORK

A direct continuation of this research could be to apply this new methodology of substructuring to the refrigeration system. It will be necessary measure the mobilities of the base plate and carcass of the fridge at the connection points of this two structures, instead of at the isolators. Using this new solution and the old results for the other transfer path analysis it will be possible to analyse if it improves the solution for the complete system.

BIBLIOGRAPHY

ANDERSEN, K. S. Analyzing muffler performance using the transfer matrix method. In: COMSOL CONFERENCE, 2008, Hannover, 2008. p. 1-7.

ANSYS Product launcher Release 15: Ansys Multiphysics. **SAS IP Ansys Inc.**, 2013.

AZEVEDO, A. F. M. **Método dos elementos finitos.** Porto: Faculdade de Engenharia da Universidade do Porto, 2003.

AUWERAER, V., MAS, H., DOM. P., VECCHIO, S., JANSSENS, A. **Transfer path analysis in the critical path of vehicle refinement: the role of fast, hybrid and operational Path Analysis**. Bruxelas: LMS International, 2007.

BAARS, E. **Fluxo de potência vibratória em componentes estruturais tipo barra e vigas**. Florianópolis: Universidade Federal de Santa Catarina, 1996.

BALACHANDRAN, B., MAGRAB, E. B. **Vibrações mecânicas**. São Paulo: Editora Cengage Learning, 2011.

BARBIERI, R., BARBIERI, N., LIMA, K. F. Application of the Galerkin-FEM and the improved four-pole parameter method to predict acoustic performance of expansion chambers. **Journal of Sound and Vibration**, London, v. 276, p. 1101-1107, 2004.

BITTENCOURT, M. L. **Análise computacional de estruturas: com aplicação do método de elementos finitos.** Campinas: Editora Unicamp, 2010.

CARRELLA, A.; BRENNAN, M. J.; WATERS, T. P. Static analysis of a passive vibration isolator with quasi-zero-stiffness characteristic. **Journal of Sound and Vibration**, London, v. 301, p. 678 – 689, 2007.

CARRELLA, A.; BRENNAN, M. J., KOVACIC, I.; WATERS, T. P. On the Force Transmissibility of a Vibration Isolator With Quasi-zero-stiffness. **Journal of Sound and Vibration**, London, v. 322, p. 707 – 717, 2009.

CLOUGH, R. W. Original formulation of the finite element method. **Finite Elements in Analysis and Design**, Amsterdam, v. 7, p. 89-101, 1990.

CRAIG, R. R.; KURDILA, A. J. **Fundamentals of structural dynamics,** 2nd. ed. New York: Wiley, 2006. ISBN: 0-471-43044-7.

CRAIG, R. R. A brief tutorial on substructure analysis and testing. In: CONFERENCE SOCIETY FOR EXPERIMENTAL MECHANICS SERIES, 18., 2000, [S. l.]. **Proceedings.** Bethe: SEM, 2000. p. 899–908.

DICKENS, J. D., NORWOOD, C. J. Universal Method to Measure Dynamic Performance of Vibration Isolators Under Static Load. **Journal of Sound and Vibration**, London, v. 244, n. 4, p. 685-696, 2000.

DICKENS, J. D. Review of methods to dinamically represent vibration isolators. **The Shock and Vibration Digest**, Thousand Oaks, v. 34, n. 6, p. 447-453, 2002.

DIEZ-IBARBIA, A., BATTARRAB, M., PALENZUELAC, J., CERVANTESC, G., WALSHE, S., DE-LA-CRUZD, M., THEODOSSIADESD, S., GAGLIARDINIF, L. Comparison between transfer path analysis methods on an electric vehicle. **Applied Acoustics**, v. 118, p. 83–101, 2017.

EWINS, D. J. **Modal testing:** theory and practice. 2.ed. Taunton: Research Studies, 1994.

FAHY, F.; GARDONIO, P., **Sound and structural vibration:** radiation, transmission and response. 2. ed. Reino Unido: Elsevier, 2007.

GARDONIO, P.; BRENNAN, M. J.; **Advanced applications in acoustics, noise and vibration**. Ingleterra: Spon, 2004.

GRUBER, F. M.; RUTZMOSER, J. B.; RIXEN, D. J. Comparison between primal and dual craig-bampton substructure reduction techniques. In: INTERNATIONAL CONFERENCE ON ENGINEERING VIBRATION, 11., Ljubljana. **Proceedings.** 2015.

HARRIS, C. M.; CREDE, C. E. **Shock and vibration handbook.** New York: McGraw-Hill, 1976.

HUEBNER, K.; THORNTON, E. The finite element method for engineers. 2. ed. New York: John Wiley & Sons, 1982.

HURTY, W. C.; COLLINS, J. D.; HARTZ, G. C. Dynamic analysis of large structures by modal synthesis techniques. **Computers & Structures**, Kidlington, v. 1, p. 535-563, 1971.

HYNNA, P. **Vibrational power methods in control of sound and vibration**. Finlândia: VTT Technical Research Centre of Finland, 2002.

IBÁÑEZ, D. E. S. **TPA Hibrido: simulações e medições experimentais em laboratório**. Florianópolis: Universidade Federal de Santa Catarina, 2008.

IBRAHIM, R. A. Recent advances in nonlinear passive vibration isolators. **Journal of Sound and Vibration**, London, v. 314, p. 371 – 452, 2008.

ISTVAN, L.; BERANEK, L. **Noise and vibration control engineering:** principles and applications. New York: John Wiley & Sons, 2006.

INTERNATIONAL ORGANIZATION FOR STANDARDIZATION – ISO. **ISO 2041:** vibration and shock. Vernier, 1990.

JEROME, A. **Vibration analysis of connected structures.** London: Imperial College of Science and Technology, 1980.

JONES, D. I. G. **Handbook of viscoelastic vibration damping**. Chichester: John Wiley & Sons, 2001.

KEERSMAEKERS, L. **Decoupling of mechanical systems based on in-situ frequency response functions: the LPD method**. PhD thesis. Vrije Universiteit Brussel. Universiteit Antwepen, 2015.

KIM, S.; SINGH, R. Vibration Transmission Through an Isolator Modelled by Continuous System Theory. **Journal of Sound and Vibration**, London, v. 248, n. 5, p. 925 – 953, 2001.

KLERK, D.; RIXEN, D. J.; VOORMEEREN, S. N. General framework for dynamic substructuring: history, review and classification of techniques. **AIAA Journal,** v. 46, n. 5, p. 1169–1181, 2008. Doi: 10.2514/1.33274.

KLERK, D., OSSIPOV, A. Operational transfer path analysis: Theory, guidelines and tire noise application. **Mechanical Systems and Signal Processing**, v. 24, p. 1950-1962, 2010.

KOVACIC, I.; BRENNAN, M. J., WATERS, T. P. A Study of a nonlinear vibration isolator with a quasi-zero stiffness characteristic. **Journal of Sound and Vibration**, London, v. 315, p. 700 – 711, 2008.

LI, J., CUI, X., WANG, Z., MAK, C. M. Improved Method of the four-pole parameters for calculating transmission loss on acoustics silence. **Journal of Information and Coupling Science**, v. 2, n. 1, p. 61-65, 2007.

LU, Z.; BRENNAN, M. J., YANG, T., LI, X., LIU Z. An investigation of a two-stage nonlinear vibration isolation system. **Journal of Sound and Vibration**, London, v. 332, p. 1456 – 1464, 2013.

MAIA, N. M. M., SILVA, J. M. M. **Theoretical and experimental modal analysis**. Taunton, Inglaterra: Research Studies, 1997.

MALLIK, A. K.; KHER, V.; PURI, M.; HATWAL, H. On the Modelling of Non-linear Elastomeric Vibration Isolators. **Journal of Sound and Vibration**, London, v. 219, n. 2, p. 239 – 252, 1999.

MANZATO, S.; RISALITI, E.; NAPOLI, C.; TAMAROZZI, T.; PEETERS, B. **A review of frequency-based substructuring methods and their applicability to engineering structures.** Proceedings of the International Conference on Structural Engineering Dynamics, 2015.

MARQUES, V. C. **Auralização de um sistema vibroacústico considerando a influência dos graus de liberdade dos acoplamentos**. Florianópolis: Universidade Federal de Santa Catarina, 2010.

MATTHEW, S. A.; HARRISON M. G.; RANDALL L. M. Experimental modal substructuring to stimate fixed-base modes from tests on a flexible fixture. **Journal of Sound and Vibration,** London, v. 330, p. 4413–4428, 2011.

MOLLOY, C. T. Use of Four-pole Parameters in Vibration Calculations. **The Journal of Acoustical Society of America**, Melville, v. 29, n. 7, p. 842-853, 1957.

MONDOT, J. M., PETERSON B. A. T. Caracterization of Structure-borne Sound Sources: the Source Descriptor and the Coupling Function. **Journal of Sound and Vibration**, London, v. 114, n. 3, p. 507-518, 1987.

MOTT, P. H.; ROLAND, C. M. Limits to poisson's ratio in isotropic materials. **Physical Review B,** College Park, v. 80, p. 132 – 104, 2009.

PADILHA, P. E. F. **Comparação de técnicas de análise de caminhos de transferência vibroacústicos**. 2006. 63 f. Dissertação (Mestrado em Engenharia Mecânica) - Universidade Federal de Campinas, Campinas. 2006.

PETERSON, B. A. T., PLUNT, J.. On Effective Mobilities in the Prediction of Structure-borne Sound Transmission Between a Source and a Receiving Structure, Part II: Procedures for the Estimation of Mobilities. **Journal of Sound and Vibration**, London, v. 82, n. 4, p. 531-540, 1982

RAO, S. **Vibrações mecânicas**. 4. ed. São Paulo: Prentice-Hall, 2009.

RICHARDS, C. M.; SINGH, R. Comparison of two non-linear system identification approaches derived from "reverse path" spectral analysis. **Journal of Sound and Vibration**, London, v. 237, n. 2, p. 361 – 376, 2000.

RICHARDS, C.M.; SINGH, R. Characterization of rubber isolator nonlinearities in the context of single- and multi-degree-of-freedom experimental systems. **Journal of Sound and Vibration**, London, v. 247, n. 5, p. 807 – 834, 2001.

RIXEN, D. J. Experimental substructuring-easy test and analysis through component assembly. **Keynote In:** International Conference on Noise and Vibration Engineering, Leuven, International Conference on Noise and Vibration Engineering, 2016.

SNOWDON, J. C. Vibration isolation: use and characterization. **The Journal of Acoustical Society of America**, Melville, v. 66, n. 5, p. 1245- 1274, 1979.

STENTI, A.; MOENS, D.; SAS, P.; DESMET, W. A Three-level Non-deterministic Modeling Methodology for the NVH Behavior of Rubber Connections. **Journal of Sound and Vibration**, London, v. 329, p. 912 – 930, 2010.

SUN, S.;SONG, Y.;ZHENG, Q. Thermo-molded wheat gluten plastics plasticized with glycerol: effect of molding temperature. **Food Hydrocolloids,** Amsterdam, v. 22, p. 1006–1013, 2008.

TAO, J. S.; LIU, G.R.; LAM, K. Y. Design Optimization of Marine Engine–Mount System, **Journal of Sound and Vibration**, London, v. 235, n. 3, p. 477-494, 2000.

YANG, Y.B.; YAU, J.D. Vertical and Pitching Resonance of Train Cars Moving over a Series of Simple Beams, **Journal of Sound and Vibration**, London, v. 337, p. 135–149, 2015.

VERHEIJ, J. **Multi-path sound transfer from resiliently mounted shipboard machinery**. Dissertation (PHD) - Institute of Applied Physics TNO-TH, Holanda, 1986.

VAN DER SEIJS, M. V.; KLERK, D.; RIXEN, D. J. General framework for transfer path analysis: History, theory and classification of techniques. **Mechanical System Signal Processing,** London, v. 68-69, p. 217-244, 2005.

WAHYUNI, E.; JI, T. Relationship between static stiffness and modal stiffness of structures. **The Journal for Technology and Science**, Surabaya, v. 21, n. 2, p. 1-5, 2010.

WANG, L.R.; WANG, J. C.; HAGIWARA, I. Integrated Characteristic Simulation Method for Hydraulically Damped Rubber Mount of Vehicle Engine. **Journal of Sound and Vibration**, London, v. 286, p. 673 – 696, 2005.

WANG, J.; QIN, D.; LIM, T. C. Dynamic Analysis of Horizontal Axis Wind Turbine by Thin-Walled Beam Theory, **Journal of Sound and Vibration**, London, v. 329, n. 17, p. 3565–3586, 2010.

WANG, Y.; INMAN, D. J. Finite element analysis and experimental study on dynamic properties of a composite beam with viscoelastic damping. **Journal of Sound and Vibration**, London, v. 332, n. 23, p. 6177–6191, 2013.

APPENDIX A – Primal and Dual formulation

According to Gruber et al. (2015), dynamic substructuring techniques can be classified into two categories depending on the underlying modes which are used. That could be a primal or a dual formulation. The term mode can refer to all kind of structural shape vectors. The first class consists in using fixed-interface vibration modes and interface constraint modes to represent the substructure dynamics. The modes chosen are the interface displacements, in order to enforce the interface compatibility, for the primal formulation. The second class consists of free-interface vibration modes and attachment modes. This represents a dual formulation, which uses interface forces. As a consequence, this method enforces only weak interface compatibility between the substructures, thereby avoiding interface locking problems as sometimes experienced in the primal assembly approaches. An example is the assembly shown in the work by Manzato et al. (2015), in which a dual formulation is used to represent the substructuring of an airplane with comparisons between numerical and experimental results.

To discuss the two substructuring techniques, consider a finite element model of a global domain Ω. This domain Ω is divided into *N* non-overlaping substructures called Ω^a such that every node belongs to exactly one substructure except for the nodes on the interface boundaries (Gruber et al., 2015). The equation of motion of one substructure *a* is the same as shown in Equation (1) which is rewritten here for convenience.

$$\mathbf{M}^{(a)}\ddot{\mathbf{u}}^{(a)} + \mathbf{C}^{(a)}\dot{\mathbf{u}}^{(a)} + \mathbf{K}^{(a)}\mathbf{u}^{(a)} = \mathbf{f}^{(a)} + \mathbf{g}^{(a)} \tag{77}$$

where $\mathbf{M}^{(a)}$, $\mathbf{C}^{(a)}$ and $\mathbf{K}^{(a)}$ are the mass, damping and stiffness matrices of substructure *a*. $\mathbf{u}^{(a)}$ denotes its displacement vector of the substructure, $\mathbf{f}^{(a)}$ is the external force vector, and $\mathbf{g}^{(a)}$ is the vector of connecting forces with the other substructures. This means the reaction force on the substructure is due to its connection to adjacent substructures at its boundary. In a general way the local displacements of each substructure $\mathbf{u}^{(a)}$, that can have translational and rotational displacements, can be divided in local internal DOF $\mathbf{u}_i^{(a)}$ and boundary DOF $\mathbf{u}_b^{(a)}$.

$$\mathbf{u}^a = \begin{Bmatrix} \mathbf{u}_b^{(a)} \\ \mathbf{u}_i^{(a)} \end{Bmatrix} \tag{78}$$

The equation of motion of *n* substructures that are to be coupled can be rewritten in a block-diagonal matrix format as

$$\mathbf{M}\ddot{\mathbf{u}} + \mathbf{C}\dot{\mathbf{u}} + \mathbf{K}\mathbf{u} = \mathbf{f} + \mathbf{g} \tag{79}$$

with

$$\mathbf{M} \triangleq diag\left(\mathbf{M}^{(1)},\ldots,\mathbf{M}^{(n)}\right) = \begin{bmatrix} \mathbf{M}^{(1)} & \cdots & . \\ \vdots & \ddots & \vdots \\ . & \cdots & \mathbf{M}^{(n)} \end{bmatrix}$$

$$\mathbf{C} \triangleq diag\left(\mathbf{C}^{(1)},\ldots,\mathbf{C}^{(n)}\right)$$

$$\mathbf{K} \triangleq diag\left(\mathbf{K}^{(1)},\ldots,\mathbf{K}^{(n)}\right)$$

$$\mathbf{u}(t) \triangleq \begin{Bmatrix} \mathbf{u}^{(1)} \\ \vdots \\ \mathbf{u}^{(n)} \end{Bmatrix}, \qquad \mathbf{f}(t) \triangleq \begin{Bmatrix} \mathbf{f}^{(1)} \\ \vdots \\ \mathbf{f}^{(n)} \end{Bmatrix}, \qquad \mathbf{g}(t) \triangleq \begin{Bmatrix} \mathbf{g}^{(1)} \\ \vdots \\ \mathbf{g}^{(n)} \end{Bmatrix}$$

The compatibility condition can be expressed by

$$\mathbf{B}_b\mathbf{u}_b = 0 \tag{80}$$

The $\mathbf{B}_b$ matrix operates on the interface degrees-of-freedom, this is a signed Boolean matrix if the interface DOF are matching and, represents the compatibility condition state in that any pair of matching interface degrees of freedom $u_b^{(k)}$ and $u_b^{(l)}$ must have the same displacement. It means that $u_b^{(k)} - u_b^{(l)} = 0$.

The equilibrium condition is expressed by

$$\mathbf{L}_b^T\mathbf{g}_b = 0 \tag{81}$$

The matrix $\mathbf{L}$ is a Boolean matrix that localizes the interface DOF of the substructures in the global dual set of DOF, and $\mathbf{L}^T$ is the transposed matrix of $\mathbf{L}$. The expression states that when the dual connection forces are summed, their resultant must be equal to zero, it means that $g_b^{(k)} + g_b^{(l)} = 0$. Now the total system could be described as

$$\begin{cases} \mathbf{M}\ddot{\mathbf{u}} + \mathbf{C}\dot{\mathbf{u}} + \mathbf{K}\mathbf{u} = \mathbf{f} + \mathbf{g} & \text{(82a)} \\ \mathbf{B}_b\mathbf{u}_b = 0 & \text{(82b)} \\ \mathbf{L}_b^T\mathbf{g}_b = 0 & \text{(82c)} \end{cases}$$

Equation (82), shows a connection between any number of substructures with any number of arbitrary couplings. Using this set of equations, the coupled system can be obtained in either a primal or a dual way.

PRIMAL ASSEMBLY

In primal formulation, a unique set of interface degrees of freedom is defined, and the compatibility between the substructures is enforced using the same boundary displacements for adjacent substructures. According to Klerk et al. (2008), mathematically, this is obtained by

$$\mathbf{u}_b = \mathbf{L}_b \mathbf{q}_b \tag{83}$$

where $\mathbf{q}_b$ is the unique set of interface DOF for the system, so the compatibility condition, Equation (80) is satisfied for any set of $\mathbf{q}_b$

$$\mathbf{B}_b \mathbf{u}_b = \mathbf{B}_b \mathbf{L}_b \mathbf{q}_b = \mathbf{0} \text{ to any } \mathbf{q}_b \tag{84}$$

Because the compatibility condition in Equation (82) is satisfied by the choice of the $\mathbf{q}_b$, the system is now described as

$$\begin{cases} \mathbf{ML}\ddot{\mathbf{q}} + \mathbf{CL}\dot{\mathbf{q}} + \mathbf{KLq} = \mathbf{f} + \mathbf{g} & \text{(85a)} \\ \mathbf{L}_b^T \mathbf{g}_b = 0 & \text{(85b)} \end{cases}$$

Pre-multiplying the equilibrium equation by $\mathbf{L}^T$ and knowing that $\mathbf{L}^T \mathbf{g}(t) = 0$, so the primal assembled system is reduced to

$$\tilde{\mathbf{M}}\ddot{\mathbf{q}} + \tilde{\mathbf{C}}\dot{\mathbf{q}} + \tilde{\mathbf{K}}\mathbf{q} = \tilde{\mathbf{f}} \tag{86}$$

where:

$$\begin{cases} \tilde{\mathbf{M}} \triangleq \mathbf{L}^T \mathbf{ML} \\ \tilde{\mathbf{C}} \triangleq \mathbf{L}^T \mathbf{CL} \\ \tilde{\mathbf{K}} \triangleq \mathbf{L}^T \mathbf{KL} \\ \tilde{\mathbf{f}} \triangleq \mathbf{L}^T \mathbf{f} \end{cases}$$

DUAL ASSEMBLY

Another way to enforce the interface compatibility between the substructures is to consider the interface connecting forces as unknowns. These forces must be determined to satisfy the interface compatibility conditions, so the forces are determined as

$$\mathbf{g}_b = -\mathbf{B}_b^T \boldsymbol{\lambda} \tag{87}$$

where $\boldsymbol{\lambda}$ corresponds to the interface force, that act in opposite directions for any pair of dual interface degree-of-freedom. Due to the construction of $\mathbf{B}$ Boolean matrix, and the equilibrium condition is thus written as

$$\mathbf{L}_b^T \mathbf{g}_b = -\mathbf{L}_b^T \mathbf{B}_b^T \boldsymbol{\lambda} = 0 \tag{88}$$

Consequently, the system of Equation (80) is now described as.

$$\begin{cases} \mathbf{M}\ddot{\mathbf{u}} + \mathbf{C}\dot{\mathbf{u}} + \mathbf{K}\mathbf{u} + \mathbf{B}^T \boldsymbol{\lambda} = \mathbf{f} \\ \mathbf{B}_b \mathbf{u}_b = \mathbf{0} \end{cases} \tag{89}$$

In this hybrid formulation the Lagrange multiplier with the interface forces $\boldsymbol{\lambda}$ enforce the interface compatibility constrains and can be identified as interface forces. According to Klerk et al. (2008) the dual assembly became popular in the 1990s as a way of implement efficient solvers on parallel processing computers.

The dual assembled system, Equation (89), is equivalent to the primal assembled system, Equation (86), since both systems express the same local equilibrium for each substructure and enforce the same interface compatibility.

APPENDIX B – Mode Coupling for a Mass-Isolator-Beam System

The subsystems of a complex system are not isolated, they interact with each other. If, for example, two or more subsystems capable of oscillating have any type of interaction, or coupling, a wide variety of interesting phenomena may occur, (Balachandran and Magrab, 2011). The modes of each subsystem interact to generate new modes of the coupled system.

Considering the system presented in Chapter 3, Figure 41, and the subsystems as presented in Figure 70, the objective is to identify if the position of isolator modifies the coupling of the subsystems modes. The modes of beam and isolator, are calculated separately and compared with the modes for the coupled system when a normal force was applied. The subsystem A, mass and isolator, was positioned in the middle, at ¼ of beam and ⅛ of beam.

Figure 71 – System substructuring.

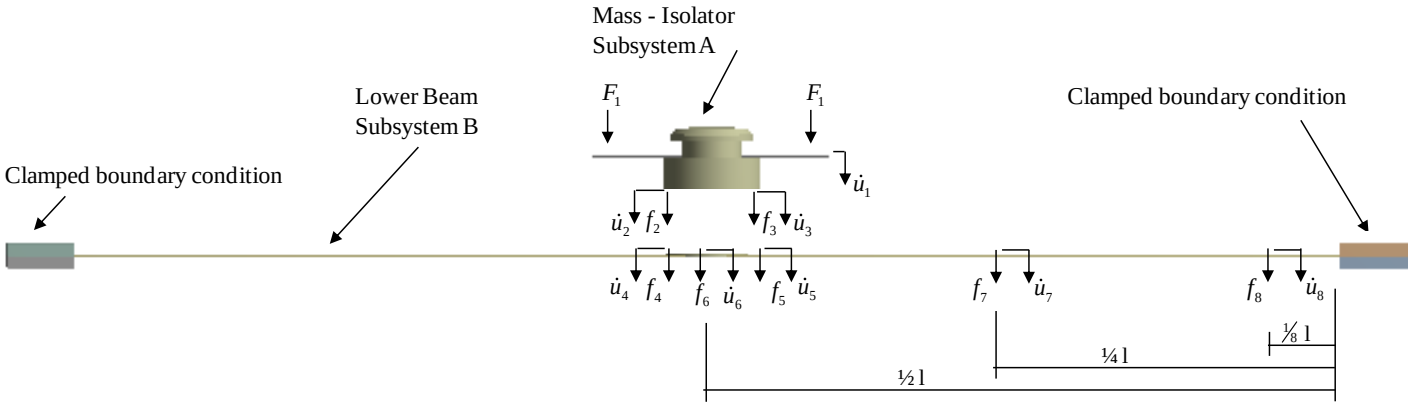

Source: Elaborated by the author.

First, a modal and a harmonic analysis for the isolator and beam isolated was carried out, considering the boundary conditions of the beam as clamped-clamped and the isolator with its base as a fixed support. Then a modal and harmonic analysis is carried out for the complete system for the three isolator positions.

Table 8 shows the isolated modes of the beam and isolator and the modes for the complete system excited with a normal force. The modes of isolator only occur above a frequency of 300Hz.

Table 8 – Modes of beam, isolator and complete system.

Mass-Isolator modes (Hz)	Beam flexural modes (Hz)	Mass-Isolator + Beam modes (Hz)		
		Isolator at ½ of the beam	Isolator at ¼ of the beam	Isolator at $\frac{1}{8}$ of the beam
-	61.7 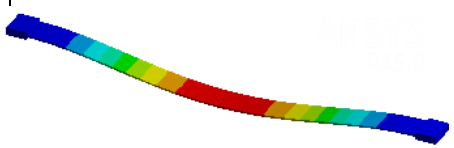	52.2 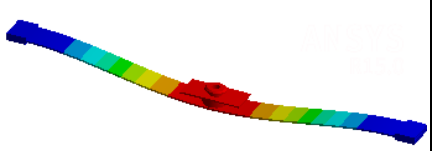	58.1 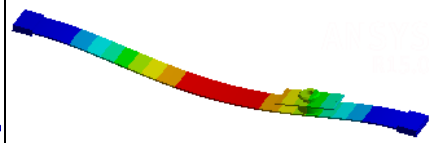	61.5 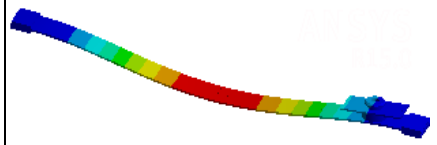
-	170.2 	164.9 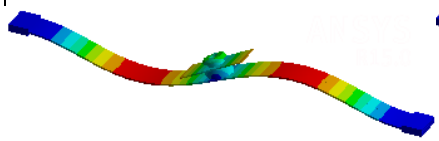	148.8 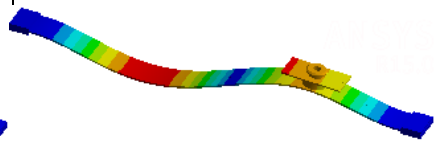	166.8 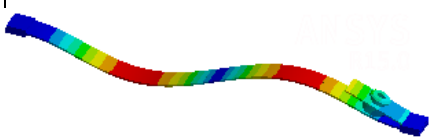
346.2 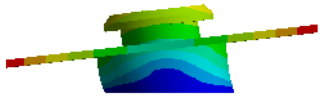	334.4 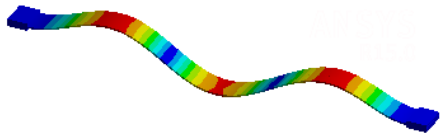	285.3 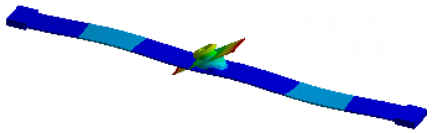	290.2 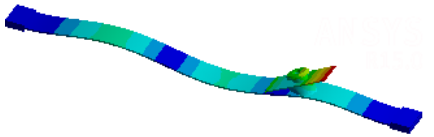	297.5 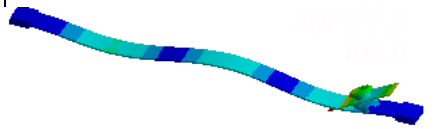
		446.6 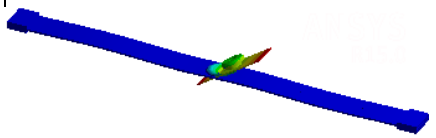	337.9 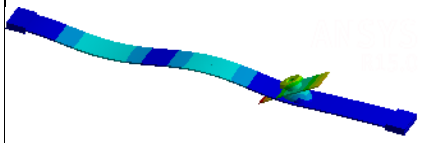	365.3 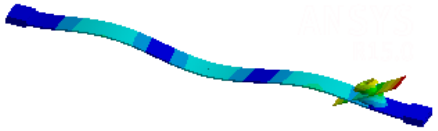
449.8 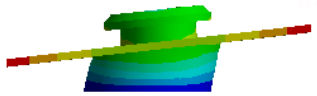	554.8 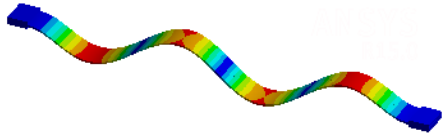	550.2 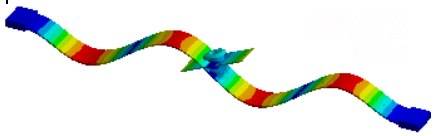	560.2 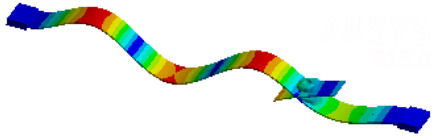	518.8 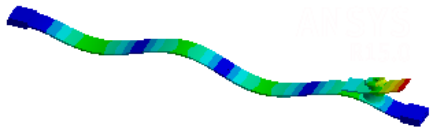

Source: Elaborated by the author.

In this system, there are basically three phenomena occurring. For example, for the first and second flexural modes of the beam, when the isolator is connected, regardless of the position, the natural frequencies for the complete system decrease. This is because the isolator adds mass to the beam because the coupling occurs in a mass-like region of the isolator, as shown in the Figure 71. Examining the figures in the Table 8 it is possible to see that the isolator only follows the movement of the beam, because there is no isolator natural frequency up to these two frequencies. Moreover, the decrease of the frequency is smaller, the closer to the fixed support the isolator is connected.

Figure 72 – Coupled modes for the first and second flexural modes of beam, with the isolator attached to the middle of the beam.

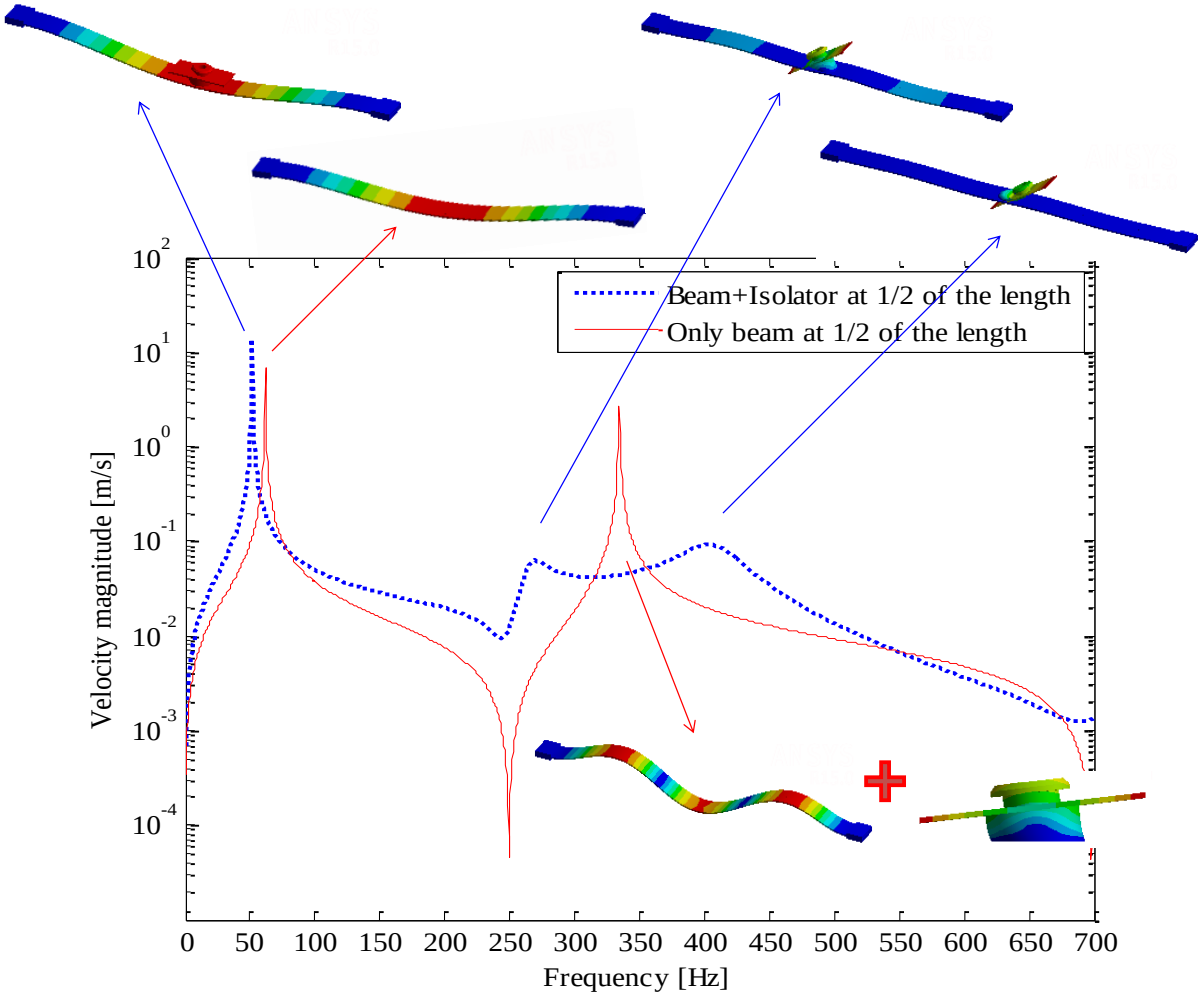

Source: Elaborated by the author.

The same phenomenon occurs for the fourth flexural mode of the beam, with the isolator applied in the ½ and ⅛ of the beam, with the difference that for these cases the

isolator has a vibration mode. As the mass is applied close to the peak amplitudes of vibration of the modes, the greater will be the reduction of the natural frequency of the coupled system.

Considering the same fourth flexural mode of the beam and rubber isolator but with coupling occurring at the ¼ of the beam there is a difference in the phenomena, for this case the coupled natural frequency is higher than that of the beam alone. This behavior is because the coupling occurs in a stiffness-like region of the isolator and not in a mass-like region as before.

Figure 72 shows schematically how this mode coupling behaves, using a Two DOF system. It is a semi-definite system where one of its natural frequencies is equal to zero and has a rigid body mode behavior, i e. the two masses move equally.

Figure 73 – Mode coupling schematically representation for a semi definite system.

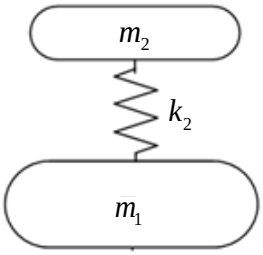

Source: Elaborated by the author.

According to Rao (2009), semi systems are also known as unrestricted systems or degenerate systems. Considering the arrangement of Figure 72, that represents two masses connected by a coupling spring, the natural frequencies are.

$$\omega_1 = 0$$
$$\omega_2 = \sqrt{\frac{k_2\left(m_1 + m_2\right)}{m_1 m_2}} \tag{90}$$

Analyzing the Equation (90) the second frequency of the 2 DOF system will be higher than the frequency of the basic 1 DOF system, composed by m_1 and k_2, due to the fact that the two masses are also considered in the numerator. As the mass, m_2, increases the frequency will also increase, this is what happens with the coupled system.

The last phenomenon that occurs is the shown in the third flexural mode of the beam, in this case the isolator mode are close to this beam mode, so in the coupled system the isolator act like a vibration absorber for these frequencies, considering the harmonic excitation above the upper beam in the isolator.

For a more general idea of what happens to the coupled system natural frequency when the natural frequencies of the one DOF systems vary, consider a simple system as shown in Figure 74. Where a base system is composed by a mass m_1 and a stiffness k_1, subject to a harmonic frequency excitation Ω. A secondary vibrating system is coupled to this base system with a mass m_2 and stiffness k_2.

Figure 74 – Coupling of subsystems with close natural frequencies.

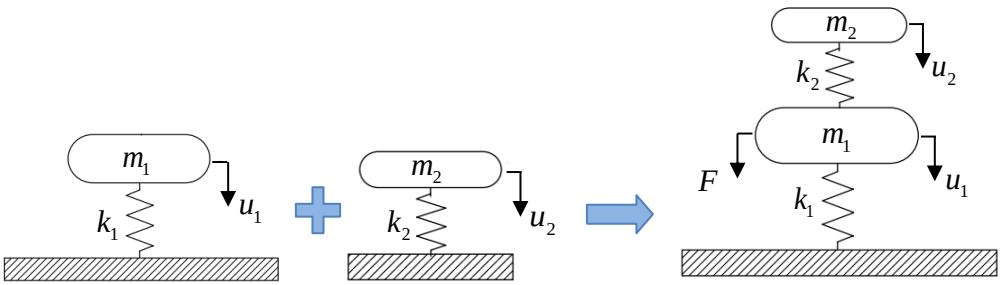

Source: Elaborated by the author.

According to Rao, (2009) the frequency response of the coupled system considering a non dimensional parameters is described as.

$$\left|\frac{x_1}{Fk_1^{-1}}(\Omega)\right| = \sqrt{\frac{\left(g^2 - f^2\right)^2}{\left[\mu g^2 f^2 - \left(g^2 - 1\right)\left(g^2 - f^2\right)\right]^2}} \tag{91}$$

$$\left|\frac{x_2}{Fk_1^{-1}}(\Omega)\right| = \sqrt{\frac{f^2}{\left[\mu g^2 f^2 - \left(g^2 - 1\right)\left(g^2 - f^2\right)\right]^2}} \tag{92}$$

Where

$\mu = \frac{m_2}{m_1}$ Mass ratio

$\omega_1^2 = \frac{k_1}{m_1}$ Natural frequency of the base system

$\omega_2^2 = \frac{k_2}{m_2}$ Natural frequency of the DVA

$g = \frac{\Omega}{\omega_1}$ Normalized excitation frequency

$f = \frac{\omega_2}{\omega_1}$ Ratio of natural frequencies

When a passive dynamic vibration absorber is designed, the objective is frequently to reduce the amplitude of vibration in the base system at a natural frequency, so it is necessary choose the parameters m_2 and k_2 of the DVA system to have the same frequency of the base, or primary system.

Figure 74 shows a comparison of the response from the primary system alone and the system with the DVA attached, considering $\mu = 0.1$ and $f = 1$. Now the system has two natural frequencies, which will vary depending of the parameters of mass ratio and natural frequency ratio.

Figure 75 – Coupling of subsystems with close natural frequencies.

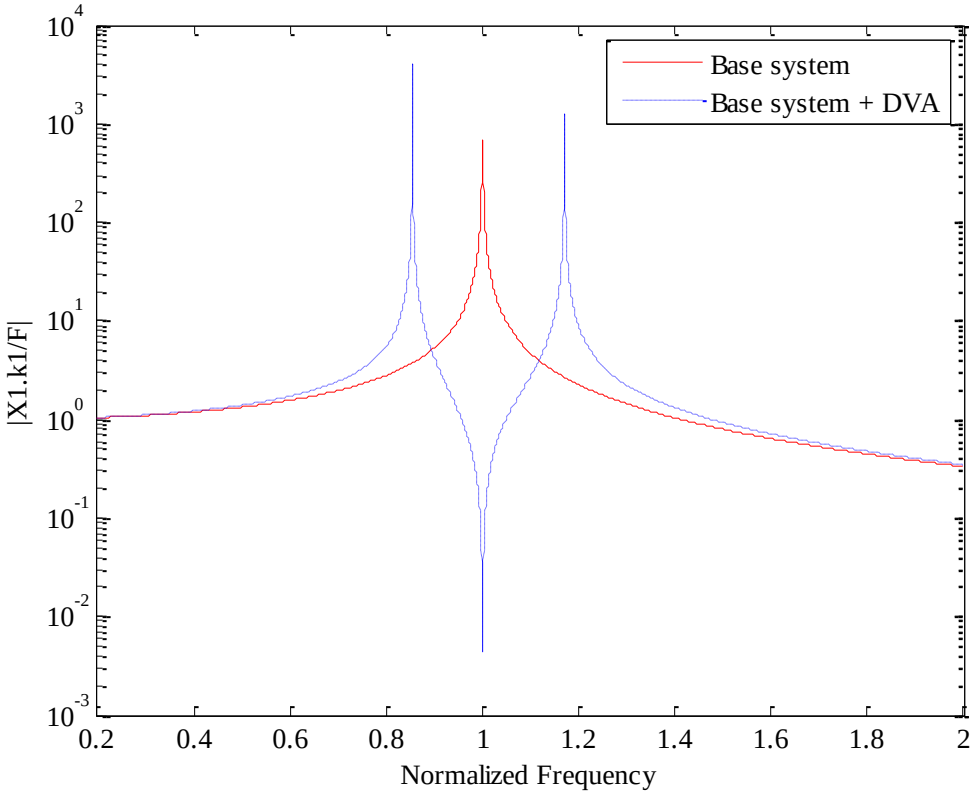

Source: Elaborated by the author.

To analyze the behave of the new frequencies in coupled system depending on the variation of the natural frequencies ratio, the value of f is varied from 0.2 to 2. This means that the frequency of the DVA, ω_2, is changed from being less than the primary system and increased until it is twice the primary system natural frequency.

Figure 75 shows the behaviour of the coupled system frequency to the variation of f.

Figure 76 – Coupled frequency variation depending on the value of f.

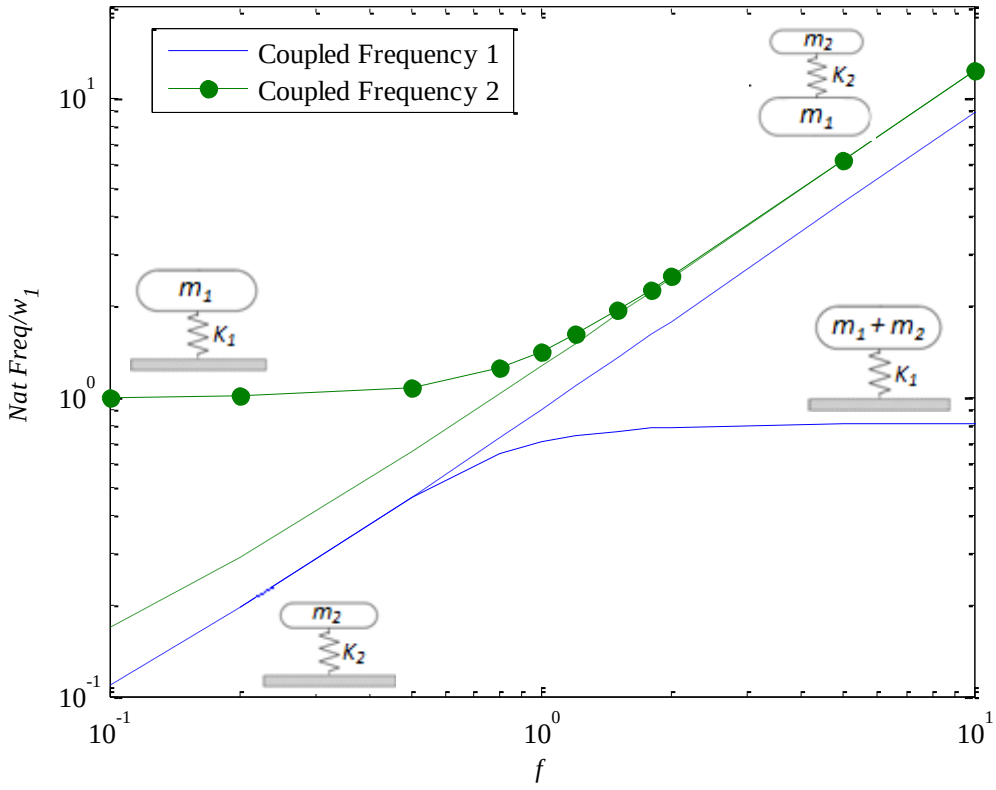

Source: Elaborated by the author.

Interesting factors that can be observed in this figure are that as the ratio f is close to zero the value of coupled frequency, $\omega_{2Coupled}$, approaches the value of the natural frequency of the base system without the DVA, ω_1, and when the value of f increases the system coupled frequency, $\omega_{1Coupled}$, approaches the value of the base frequency, ω_1, when the considered mass is the sum $(m_1 + m_2)$, considering $\mu = 0.1$.

The Figure 76 shows more one example for the coupled system in analysis in this work where the isolator acts as a dynamic vibration absorber, it occurs when the third flexural

mode of the beam with natural frequency of 334.4 Hz is coupled with the mass-isolator subsystem mode with frequency of 346.2 Hz, as the frequencies are close the mass-isolator subsystem act as a DVA to the beam. In this case, shown in Figure 76, the mass-isolator subsystem is coupled close to the end of the beam.

Figure 77 – Coupled modes for the third flexural mode of beam, with the isolator at ⅛ of the beam.

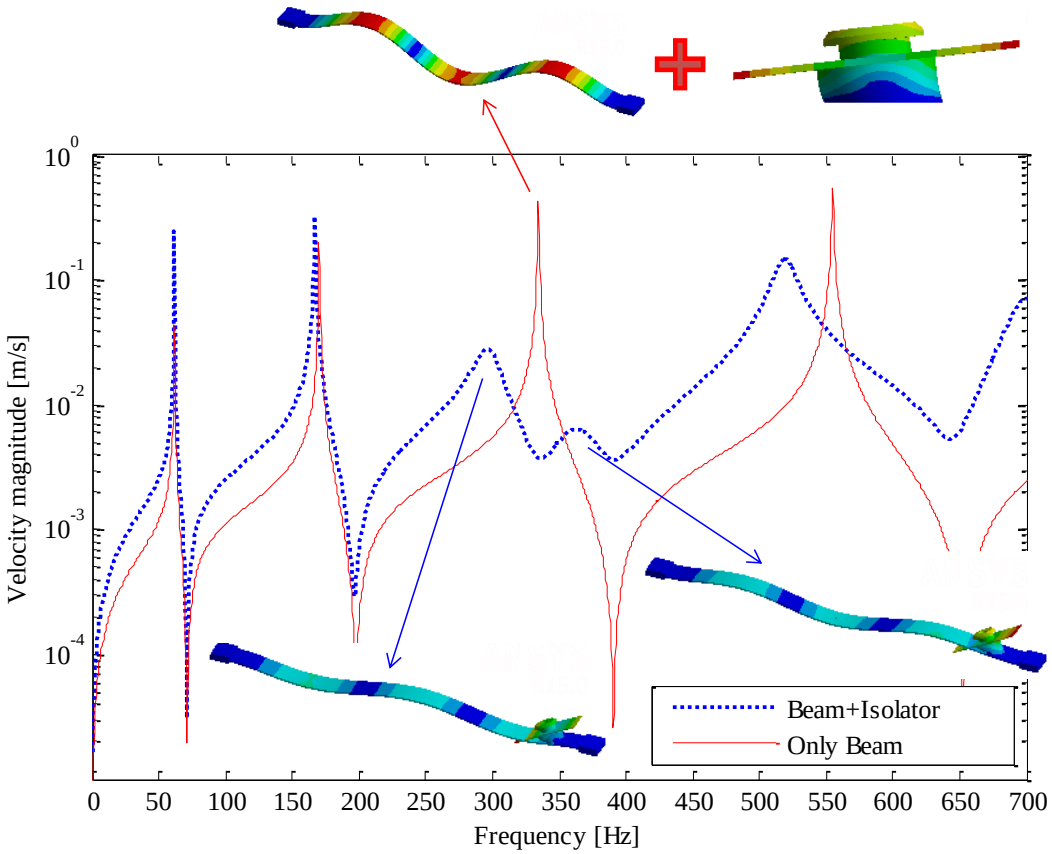

Source: Elaborated by the author.